"CFD Analysis of Wavy Micro-Channel Heat Sink with Hemispherical Obstruction"

Major project-II

Submitted to Delhi Technological University in partial fulfilment of the requirement for the award of Degree of

Master of Technology

In

Thermal Engineering

UNDER THE SUPERVISION OF

Mr. M. ZUNAID

Asst. Professor

Department Of Mechanical Engineering

Delhi Technological University

Delhi-110042

SUBMITTED BY-

RAJNISH KUMAR

2K14/THE/17

Department of Mechanical Engineering

Delhi Technological University

(Formerly DELHI COLLEGE OF ENGINEERING)

Bawana road, Delhi -110042

CERTIFICATE

DELHI TECHNOLOGICAL UNIVERSITY

(Formerly DELHI COLLEGE OF ENGINEERING)

Date:-_____

This is to certify that report entitled **"CFD Analysis of wavy microchannel heat sink with hemispherical obstructions"** by **RAJNISH KUMAR** in the requirement of the partial fulfilment for the award of Degree of **Master of Technology (M.Tech)** in **Thermal Engineering** at **Delhi Technological University**. This work was completed under my supervision and guidance. He has completed his work with utmost sincerity and diligence. The work embodied in this project has not been submitted for the award of any other degree to the best of my knowledge.

M. ZUNAID

(Assistant Professor)

Delhi technological university

Delhi

DECLARATION

I declare that the work presented in this thesis titled “CFD analysis of wavy micro-channel heat sink with hemispherical obstructions”, submitted to Department of Mechanical Engineering, is an authentic record of my own work carried out under the supervision of asst. prof. Mr. M. ZUNAID, Department of Mechanical Engineering, Delhi technological university, Delhi.

This report does not, to the best of my knowledge, contain part of my work which has been submitted for the award of any other degree either of this university or any other university without proper citation.

Date:

Place: DTU, Delhi Signature of candidate

ACKNOWLEDGEMENT

First of all, I would like to express my gratitude to God for giving me ideas and strengths to make my dreams true and accomplish this thesis.

To achieve success in any work, guidance plays an important role. It makes us put right amount of energy in the right direction and at right time to obtain the desired result. Express my sincere gratitude to my guide, **MR. M. ZUNAID**, Asst. Professor, Mechanical Engineering Department for giving valuable guidance during the course of this work, for his ever encouraging and timely moral support.

I am greatly thankful to **DR. R. S. MISHRA**, Professor and Head, Mechanical Engineering Department, Delhi Technological University, for his encouragement and inspiration for execution of the this work. I express my feelings of thanks to the entire faculty and staff, Department of Mechanical Engineering, Delhi Technological University, and Delhi for their help, inspiration and moral support, which went a long way in the successful completion of my report work.

RAJNISH KUMAR

(Roll No-2K14/THE/17)

ABSTRACT

In the present study of fluid flow, there are three cases. In first case, pressure drop and heat transfer characteristics of rectangular micro-channel heat sinks have been analysed and validation is done by comparing experimental results with numerical results using computational fluid dynamics. Water is taken as coolant and cooper is used as a sink material. In the second case, geometry of the channel has been changed, by making it wavy edge with hemispherical obstructions and the simulation results are obtained by taking all the parameters same as that of the first case. The main aim of changing the geometry of the straight channel to wavy channel with the inclusion of hemispherical obstructions is to increase the surface area and contact time of coolant with the heated surface to increase the temperature rise by decreasing thermal resistance. In the third case, Performance Fluid PF 5052 is taken as a coolant instead of water and cooper is taken as a sink material and rest of the parameters are same as that of second case and finally simulation results are obtained. At last comparative study of results all the three cases are done. Both the micro-channels have a width of 0.23mm and height of 0.71 mm. The aspect ratio (ɣ) and the length of both the channels is kept same as 0.32 and 44.7mm respectively. The diameter of hemispherical obstruction is taken as 0.22 mm. The analysis for both the micro-channels is done for five sets of Reynolds number which are 400, 600, 800, 1000 and 1200 respectively. The two values of heat flux used are $100W/cm^2$ and $200W/cm^2$.After constructing the geometry in solid works and partially in the Design Modular, the simulation is done on ANSYS CFX.

CONTENTS

LIST OF FIGURES

LIST OF TABLES

NOMENCLATURE

A_c	Cross-sectional area of channel (m^2)
C_p	Specific heat at constant pressure (J/kg-K)
D_h	Hydraulic diameter of channel perimeter (m)
H	Height of micro-channel heat sink (m)
H_{ch}	Height of micro-channel (m)
H_{w1}	Substrate thickness on insulated side of microchannel heat (m)
H_{w2}	Substrate thickness on heated side of microchannel heat sink(m)
K	Thermal conductivity (W/m-K)
L	Length of microchannel heat sink (m)
P	Pressure (Pa)
q	Heat flux (W/m^2)
Re	Reynolds number based on channel hydraulic diameter
R_{th}	Thermal resistance (m-K/W)
T	Temperature (K)
T_{in}	Fluid inlet temperature (K)
T_{bm}	Fluid bulk temperature (K)
W	Width of micro-channel heat sink unit cell (m)
W_{ch}	Width of micro-channel (m)
W_{w1}, W_{w2}	Half-thickness of wall separating micro-channels (m)
ɣ	aspect ratio

Greek symbols

μ	dynamic viscosity ($N\text{-}s/m^2$)
ρ	density (kg/m^3)

CHAPTER 1

INTRODUCTION

1.1 Micro-channel heat sink-

Micro-channels have become very popular in applications where very high heat transfer rates are necessary. Its development trend as electronics equipment becomes more advanced and smaller in size with continuing innovations. It faces thermal engineering challenges from the high level of heat generation and the reduction of available surface area for heat removal. In the absence of sufficient heat removal, the working temperature of this component may exceed a desired temperature level which then increases the critical failure rate of equipment. Therefore, advanced electronic equipment with high heat generation requires an efficient and compact device to provide proper cooling operation. In order to meet the cooling requirement, needs to increase the product of heat transfer coefficient (h) and heat transfer surface area (A) for a device. Since heat transfer coefficient is related to the channel hydraulic diameter. The heat transfer surface area can be increased by incorporating micro channels on the device surface. One promising solution to the problem is liquid cooling incorporating on micro-channels. Micro-channel heat transfer has the potential of cooling high power density microchips. One can expect that as the size of the channel decrease, the value of convective heat transfer coefficient(h) becomes increasing in order to maintain a constant value of the Nusselt number (hDh/kf). These chips have machined micro-channels through which cooling fluid like water is circulated. The cooling liquid removes heat by single phase forced convection. Flow within the micro-channel is considered as fully developed laminar flow with constant heat flux. Therefore, heat sinks with larger extended surfaces, highly conductive materials and more coolant flow are key parameters to reduce the base temperature.

1.2 Straight Microchannel

In Today's world the basic requirement in the field of heat transfer is compact heat exchanger, for cooling of electronic chips, micro level biological instruments etc. As we are having fixed surface area so, the solution is to vary the surface properties by having surface obstacles (delta-wings), surface indentation (dimples), surface channels (wavy, zigzag channel).

The major advantages of straight channels includes, increased surface area for heat flow, better flow mixing at curved portion results in better distribution of heat, and effective cooling . In normal heat flow as in straight channel same molecule remains in contact with the surface throughout the flow causes poor heat transfer, but in wavy or zig-zag channel, due to the phenomenon known as boundary layer regeneration fluid particle from free layer gets chance to come in contact with the surface which enhances the heat transfer characteristics. But its disadvantage is that it causes pressure drop. But the value of effectiveness of channel is greater than one which shows that heat transfer enhancement is more as compared to pressure drop.

1.3 Wavy Microchannel

In Today's world the basic requirement in the field of heat transfer is compact heat exchanger, for cooling of electronic chips, micro level biological instruments etc. As we are having fixed surface area so, the solution is to vary the surface properties by having surface obstacles (delta-wings), surface indentation (dimples), surface channels (wavy, zigzag channel).

The major advantages of wavy channels includes, increased surface area for heat flow, better flow mixing at curved portion results in better distribution of heat, and effective cooling . In normal heat flow as in straight channel same molecule remains in contact with the surface throughout the flow causes poor heat transfer, but in wavy or wavy channel, due to the phenomenon known as boundary layer regeneration fluid particle from free layer gets chance to come in contact with the surface which enhances the heat transfer characteristics. But its disadvantage is that it causes pressure drop. But the value of effectiveness of channel is greater than one which shows that heat transfer enhancement is more as compared to pressure drop.

1.4 Requirement of micro-channels

The flow section measurements in convective exchange of heat applications have been moving towards littler measurements for the accompanying three main reasons:

1. Heat transfer enhancement.
2. Increased heat flux dissemination in microelectronic gadgets.

3. Rise of micro-scale gadgets that support cooling utilizing littler direct measurements brings about higher heat exchange execution.

Micro-channel coolers comprise of a very powerful way for dissipating very large amounts of heat from small surfaces. The heat sinks possess several features that make them very prime devices which can be used for the next generation of cooling technology in various high performance supercomputer chips and diodes of laser. The construction of a typical micro-cooler comprise of very large number coolant channels. Heat sinks can be classified as single-phase or two-phase depending as to whether the fluid or liquid boils inside the micro–channels or not.

The study on single phase micro-channel heat sink has a very extensive coverage since the last two decades. Since the last two decades, micro-channel coolers having different dimensions and and different material of substrate have been fabricated and tested with numerous cooling liquids. Test results have demonstrated several technical merits of single-phase micro-channel heat sinks, namely, the ability to produce very large heat transfer coefficients, small size and volume per heat load, and small coolant inventory requirements. The main objective of these studies is to develop heat transfer modelling tools that are essential to the design and optimization of heat sink geometry.

1.5 Coolants used in micro-channel heat sink

Numerous coolants are available in the market that can be employed in the heat sink for the removal of heat energy. A commonly used coolant in a heat sink is water, because of its better thermal properties. However, for better cooling performance of the micro-channel cooler nano-fluids can be used. But in the recent trend, it has been seen that cooling performances of performance fluids like PF5052, PF5060 etc. are quite superior to their counterparts.

1.6 Materials used for the heat sink

Generally the thermal property which a heat sink material should possess is high thermal conductivity for better heat dissipation. A lot of materials are available in the market such as silicon, copper, aluminium etc. that can be used for heat sink.

Table 1.1: Thermal properties of some metals used as a sink material

Material	Thermal Conductivity	Thermal Expansion
Aluminium	237 (W/m-K)	23.1 (µm/m-K)
Silicon	149 (W/m-K)	2.60 (µm/m-K)
Copper	401 (W/m-K)	17.1 (µm/m-K)

1.7 Solid works-

Solid works is a computer aided design (CAD) and solid modelling software program which runs on windows. The Solid Works is product of the Dassault systems. Solid Works is a solid modeller, and in turn uses a parametric element based way to deal with assemblies, parts and models. Parameters allude to imperatives whose qualities focus the shape or geometry of the parts or assemblies. Parameters can be either numeric parameters, for example, line lengths or circle measurements, or geometric parameters, for example, parallel, tangent, vertical etc.

1.8 ANSYS CFX package-

ANSYS CFX software is a high performance and elite, fluid dynamics software package. The package has been in use for solving fluid flow and heat transfer problems since the last 20 years. Application of ANSYS CFX includes-

1. Fluid flow problems.

2. Conjugate heat transfer problems, involving heat transfer between a solid and a fluid.

The ANSYS CFX solver uses a finite elements (cell vertex numeric), similar to those used in mechanical analysis, to discretize the domain. ANSYS CFX software package involves only one approach for solving the necessary governing equations. Major advantage of using ANSYS CFX is seen in problems on conjugate heat transfer where selection of interface is the main criteria. ANSYS CFX sets a default interface and hence is more user friendly in comparison to other software packages for problems on heat transfer and fluid flow.

1.9 Computational Fluid Dynamics (CFD)

Computational system dynamics is the analysis of the systems involving fluid flow, heat transfer and associated phenomenon such as chemical reactions by means of computer-based simulation. The technique is very powerful and spans a wide range of industrial and non-industrial applications areas. Some examples are: aerodynamics of aircrafts and vehicles, hydrodynamics of ships, combustion, turbo machinery, electrical and electronic engineering, chemical process engineering, external and internal environment of buildings, marine engineering, environmental engineering, hydrology and oceanography, metrology, biomedical engineering etc. More recently the methods have been applied to the design of microchannels, multiphase analysis. Increasingly CFD is becoming a vital component in the design of industrial products and processes. The ultimate aim of development in the CFD field is to provide a capability comparable to other CAE (Computer-Aided Engineering) tools such as stress analysis codes. The main reason why CFD has lagged behind is the tremendous complexity of the underlying behaviour, which precludes a description of the fluid flows this is at the same time economical and sufficiently complete. The availability of affordable high performance computing hardware and the introduction of user friendly interference have led to a recent upsurge of interest and CFD is poised to make an entry into the wider industrial community in the 1990s. Clearly the investment costs of a CFD capability are not small, but the total expense is not normally as great as that of a high quality experimental facility. Moreover, there are several unique advantages of CFD over experimental-based approaches to fluid systems design.

1. Substantial reduction of lead times and costs of new design.
2. Ability to study systems where controlled experimental are difficult or impossible to perform. (e.g. very large systems)
3. Ability to study systems under hazardous conditions at and beyond their normal performance limits. (e.g. safety studies and accident scenarios)
4. Practically unlimited level of detail of results.

In contrast CFD codes can produce extremely large volumes of results at virtually no added expense and it is very cheap to perform parametric studies, for instance to optimize equipment performance.

Advantages of Computational Fluid Dynamics (CFD)

1. CFD compliments EFD (Experimental Fluid Dynamics) and theoretical fluid dynamics.
2. Alternative cost effective means of simulating real fluid flow (lower energy consumption also).
3. Significant reduction of lead-time in design and development.
4. Simulate flow conditions not reproducible in model tests (weather forecasts, extremely high pressure and temperature etc.).
5. Provide more detailed and comprehensive information.
6. CFD is increasing more cost effective than wind tunnel testing.

1.10 Heat Transfer

In the simplest terms, the discipline of heat transfer is concerned with only two things, namely temperature and flow of heat. Temperature is the thermodynamic property which represents the amount of thermal energy available, whereas heat flow represents the movement of thermal energy from place to place. On microscopic scale, thermal energy is related to kinetic energy of molecules. The greater a material's temperature, the greater the thermal agitation of its constituent molecules (manifested both in linear motion and vibration modes). It is natural for regions containing greater molecular kinetic energy to pass this energy to regions with less kinetic energy.

Several material properties serve to modulate the heat transferred between two regions at different temperatures. Examples include thermal conductivities, specific heat, material densities, fluid velocities, fluid viscosities, surface emissivity and more. Taken together, these properties serve to make the solution of many heat transfer problems an involved process.

The transfer of heat is normally from a high temperature object to a lower temperature object. Heat transfer changes the internal energy of both systems involved according to First law of Thermodynamics.

1.11 Conjugate heat transfer-

The term conjugate heat transfer is used to describe processes which involve variations of temperature within solids and fluids, due to thermal interaction between the solids and fluids. Most common example of a conjugate heat transfer problem is a micro-channel heat sink.

Conjugate heat transfer in fluids and solids is the key to designing effective coolers, heaters, or heat exchangers. The fluid usually plays the role of energy carrier on large distances. Forced convection is the most common way to achieve high heat transfer rate. In some applications, the performances are further improved by combining convection with phase change.

1.12 Applications-

1. Laser diodes

2. Micro-chips.

3. Soldering circuit boards.

CHAPTER 2

LITERATURE REVIEW

2.1 Experimental studies-

Peng and Peterson (1996) investigated experimentally the single-phase forced convective heat transfer micro-channel structures with small rectangular channels having hydraulic diameters of 0.133–0.367 mm for different types of geometric configurations. The results shows heat transfer and flow characteristics. The laminar heat transfer found to be dependent upon the aspect ratio i.e. the ratio of hydraulic diameter to the centre to centre distance of micro-channels.

Fedorov and Viskanta (2000) developed a three dimensional model to investigate the conjugate heat transfer in a micro channel heat sink with the same channel geometry used in the experimental work done. This investigation indicated that the average channel wall temperature along the flow direction was nearly uniform except in the region close to the channel inlet, where very large temperature gradients were observed. This allowed them to conclude that the thermo–properties are temperature dependent.

Jiang et al. (2001) performed an experimental comparison of microchannel heat exchanger with microchannel and porous media. The effect of the dimensions on heat transfer was analyzed numerically. It was emphasized that the heat transfer performance of the microchannel heat exchanger using porous media is better than using of microchannels, but the pressure drop of the former is much larger.

Qu and Mudawar (2002) have performed experimental and numerical investigations of pressure drop and heat transfer characteristics of single-phase laminar flow in 0.231 mm by 0.713 mm channels. Deionized water was employed as the cooling liquid and two heat flux levels, 100 W/cm^2 and 200 W/cm^2. Good agreement was found between the measurements and numerical predictions, validating the use of conventional Navier–Stokes equations for micro channels. For the channel bottom wall, much higher heat flux and Nusselt number values are encountered near the channel inlet.

Lee and Mudawar (2007) have done experimental work to explore the micro-channel cooling benefits of water-based nano-fluids containing small concentrations of Al2O3. It was observed that the presence of nano-particles enhances the single-phase heat transfer coefficient, especially for laminar flow. For two-phase cooling, nanoparticles caused catastrophic failure by depositing into large clusters near the channel exit due to localized evaporation once boiling commenced.

Chein and Chuang (2007) have addressed micro-channel heat sink (MCHS) performance using nanofluids as coolants. They have carried out a simple theoretical analysis that indicated more energy and lower micro-channel wall temperature could be obtained under the assumption that heat transfer could be enhanced by the presence of nano-particles. It was observed that nano fluid cooled MCHS could absorb more energy than water-cooled MCHS.

2.2 Numerical studies-

Liu and Garimella (2004) have studied numerically on fluid flow and heat transfer in micro channels and confirmed that the behaviour of micro channels is quite similar to that of conventional channels. And their analysis showed that conventional correlations offer reliable predictions for the laminar flow characteristics in rectangular micro channels over a hydraulic diameter in the range of 244–974 μm.

Roy et al. (2004) has studied a steady, laminar flow and heat transfer of a nanofluid flowing inside a radial channel between two coaxial and parallel discs. The non-dimensional governing equations of mass, momentum and energy were solved by computational fluid dynamics method. Results have shown that the inclusion of nanoparticles in a traditional coolant can provide considerable improvement in heat transfer rates, even at small particle volume fractions. Increases in the resulting wall shear stresses were also noticed.

Hetsroni et al. (2005) has further verified the capacity of conventional theory to predict the hydrodynamic and thermal features of laminar Newtonian incompressible flows in micro channels in the range of hydraulic diameter from D_h =15 μm to D_h = 401 μm . They have compared their results with the data available in open literature. The theoretical models were subdivided in two groups depending on the degree of correctness of the assumptions. The first group includes the

simplest one-dimensional models assuming uniform heat flux, constant heat ransfer coefficient, etc. The comparison of these models with experiment shows significant discrepancy between the measurements and the theoretical predictions.

Khanafer et al. (2003) has investigated heat transfer enhancement in a two-dimensional rectangular enclosure using nanofluids. The material used is water/copper. The transport equations were solved numerically using the finite-volume approach along with the alternating direct implicit procedure. The effect of suspended ultrafine metallic nanoparticles on the fluid flow and heat transfer processes within the enclosure was analyzed. The heat transfer correlation of the average Nusselt number for various Grashof numbers and volume fractions was also presented.

Jou and Tzeng (2006) have used the Khanafer's model to analyze heat transfer performance of nanofluids inside an enclosure taking into account the solid particle dispersion. Transport equations were modeled by a stream function-vorticity formulation and solved numerically by finite difference approach. Based upon the numerical predictions, the effects of Rayleigh number (Ra) and aspect ratio on the flow pattern and energy transport within the thermal boundary layer were presented. It was observed that increasing the buoyancy parameter and volume fraction of nanofluids cause an increase in the average heat transfer coefficient. Finally, the empirical equation was built between average Nusselt number and volume fraction.

Allen (2007) had investigated fluid flow and heat transfer in microchannels experimentally and numerically. Fluid flow and heat transfer experiments were conducted on a copper micro channel heat exchanger with constant surface temperature. The experimentally obtained friction factor were found fairly well agreement with theoretical correlations and moreover the experimental Nusselt number results agreed with theory very well in the transition and turbulent regime, but the results show a higher Nusselt number in the laminar regime than predicted by theoretical correlations. Philips created a CFD model to simulate the fluid in the inlet plenum and the micro-channels. The results from these simulations showed good agreement with the experimental data in the transition/turbulent regime as well as with theoretical correlations for laminar and turbulent flow.

Sabbah et al. (2008) observed that the prediction of heat transfer in micro-channels becomes difficult with increase in complicacy of the geometry of the micro-channels, requiring three dimensional analysis of heat transfer in both solid and liquid phases. Computational Fluid Dynamics (CFD) models were implemented in order to study and optimize the thermal and hydraulic performance of micro channel heat sinks. Despite the small width of the channels, the conventional Navier Stokes and energy conservation equations still apply to the flow due to the continuum of the working fluid where the channel width is many times larger than the mean free path of liquid molecules (water). The micro-channel is characterized by the laminar flow in it, due to the small hydraulic diameter of the channel which results in low Reynolds numbers.

Mokrani et al. (2009) developed a reliable experimental device and adequate methodology to characterize the flow and convective heat transfer in flat micro channels. The study was concerned with measurement of pressure drop and heat transfer by a Newtonian fluid flow inside a flat micro channel of rectangular cross-section whose aspect ratio is sufficiently high that the flow can be considered two dimensional They considered the hydraulic diameter as twice of the channel height. The mathematical model used to describe the convective heat transfer between the walls and the fluid takes into account the whole field (solid wall and fluid layer) and the coupling between the conduction and the convection modes. Finally they concluded that the conventional laws and correlations describing the flow and convective heat transfer in ducts of large dimension are directly applicable to the micro channels of heights between 500 and 50 microns

Mathew and Hegab (2009) theoretically analyzed the thermal performance of parallel flow micro heat exchanger subjected to constant external heat transfer. The model equations predicts temperature distributions as well as effectiveness of the heat exchanger. Moreover, the model can be used when the individual fluids are subjected to either equal or unequal amounts of external heat transfer.

Rebrov et al. (2011) has reviewed the experimental and numerical results on fluid flow distribution, heat transfer and combination thereof, available in the open literature. They have found that the experiments with single channels are in good agreement with predictions using the published correlations. The review consists of two parts. In the first, the main methods to

control flow distribution were reviewed. Several different designs of inlet/outlet chambers were presented together with corresponding models used for optimization of flow distribution.

Zhang et al. (2013) has made a special kind of micro-channel heat sink by using lotus-type porous (also named Gasar) metals with long cylindrical pores formed during unidirectional solidification of metal–gas eutectic system. Copper was selected as the matrix metal because of its high heat conductivity. The heat transfer performance of lotus-type porous copper heat sink with a length of 20 mm along the axial direction of pores was studied on a testing platform designed and set up in this paper.

Salma Halelfad et al. (2014) have work on analytical optimization of a rectangular microchannel heat sink using aqueous carbon nanotubes based nano fluid as coolant. The particles weight concentration used in this study is 0.01%. The density, the thermal conductivity and the rheological behaviour of the nano fluid are experimentally investigated in order to evaluate the thermal resistance and the pumping power in microchannel under laminar flow. An analytical approach of optimization scheme was applied; it is compiled from a systematic thermal resistance model as an analysis method The effects of the temperature, the channel aspect ratio, the channel wall ratio and the use of aqueous carbon nanotubes based nano fluid on the thermal resistance and the pumping power are investigated.

S.M. Peyghambarzadeh et al. (2014) have experimentally investigated single phase forced convective heat transfer and fluid flow of CuO/water andAl2O3/water nano fluids have been experimentally investigated in a microchannel heat sink (MCHS). The heat sink consisted of 17 rectangular cross section microchannels with the dimensions of 400lm * 560 lm. All the experiments have been performed at constant heat flux of 19 W/cm2 and at the laminar flow regime $500 < Re < 2000$. Heat transfer coefficient, Nu number, and also pressure drop in the MCHS have been measured and compared with the conventional correlations.

M. Rahimi-Gorji et al. (2015) have done an analytical investigation of the heat transfer for the microchannel heat sink (MCHS) cooled by different nanofluids (Cu, Al2O3, Ag, TiO2 in water and ethylene glycol as base fluids) is studied by the porous media approach and the Galerkin

method and results are compared with numerical procedure. Response surface methodology (RSM) is applied to obtain the desirability of the optimum design of the channel geometry.

PX Jiang et al. (2001) have experimentally investigated fluid flow and forced convection heat transfer in micro-heat-exchangers with either micro-channels or porous media. The influence of the dimensions of the micro-channels on the heat transfer performance was first analysed numerically. Based on these computations, deep micro-channels were used for the experimental studies reported here. The measured performance of both micro-channel and porous-media micro-heat-exchangers are compared with those of similar heat-exchangers tested by other researchers.

Afzal Husain and Kwang Yong Kim (2009) have been performed microchannel heat sink shape optimization using response surface approximation. Three design variables related to microchannel width, depth, and fin width are selected for optimization, and thermal resistance has been taken as objective function. Design points are chosen through a three-level fractional factorial design of sampling methods. Navier–Stokes and energy equations for steady, incompressible, and laminar flow and conjugate heat transfer are solved at these design points using a finite volume solver. Solutions are carefully validated with the analytical and experimental results and the values of objective function are calculated at the specified design points.

CHAPTER 3

MATHEMATICAL FORMULATION

In the present study the single phase model of computational fluid dynamics is used for the purpose of computing and solving the problem of particular category. This single phase model will solve and calculate one transport equation for continuity and one for momentum for each phase, and after this the energy equations are solved for studying the fluid and thermal performance of the system. The simulation for this single phase model is done using ANSYS CFX.

The equations used in this model include the equation of momentum, equation of continuity and energy equation (ANSYS CFX). The use of energy equation is done for finding out temperature distribution on the wall. The equation for conservation of mass, continuity equation, can be written as follows:

Mass conservation equation

The equation for conservation of mass, or continuity equation, can be written as follows:

$$\frac{\partial \rho}{\partial t} + \nabla.(\rho \vec{v}) = S_m$$

The equation written above is a general equation for conservation of mass. Here S_m is the mass added from any user defined sources.

Momentum conservation equation

Momentum conservation in a reference frame which is non accelerating can be written as

$$\frac{\partial}{\partial t}(\rho \vec{v}) + \nabla.(\rho \vec{v}\vec{v}) = -\nabla p + \nabla.(\bar{\bar{\tau}}) + \rho g + \vec{F}$$

Where,

p is the static pressure ,τ is the stress tensor

F and ρg are the external forces on body and gravitational force on body.

Energy equation-

ANSYS CFX solves the energy equation in the following form:

$$\frac{\partial}{\partial t}(\rho E) + \nabla.(\vec{v}\,(\rho E + p)\,) = \nabla.\left(k_{eff}\nabla T + \sum_{J} h_j \overrightarrow{J_J} + \overline{\overline{\tau_{eff}}}.\vec{v} \right) + S_h$$

Where,

k_{eff} is the effective conductivity ($k+k_t$), where k_t is the turbulent thermal conductivity, defined on the basis of turbulence model being used, and J_j is the diffusion flux of species J . On the right-hand side of the equation the first three terms represents energy transfer due to species diffusion, conduction, and viscous dissipation, respectively, S_h denotes the chemical reaction heat, and some other sources of heat.

Standard relations and associated equations

The bulk mean temperature, T_{bm} and the wall temperature, T_{wx} with distance x from the micro-channel entrance can be obtained by doing the thermal energy balance around the micro-channel which is given by the following equations.

$$T_{bm} = T_{in} + \frac{q\pi Dhx}{mCp}$$

Where,

T_{bm} is the bulk mean temperature.

T_{in} is inlet temperature.

q is the heat flux.

D_h is hydraulic diameter of channel.

m is mass flow rate across channel.

The relation between the hydraulic diameter and Reynolds number in a channel is given by

$$Re=\rho v D_h/\ \mu$$

Where,

ρ is density

v is average velocity.

μ is dynamic viscocity.

D_h is hydraulic diameter of channel

CHAPTER 4

METHODOLOGY

Problem 1

4.1 Straight rectangular micro-channel heat sink

In this chapter a three dimensional CFD simulation is done for the heat transfer and pressure drop characteristics of rectangular micro-channel. Material used for heat sink construction is copper. The experimental set up shown in figure was developed by Mudawar and Qu (2002).

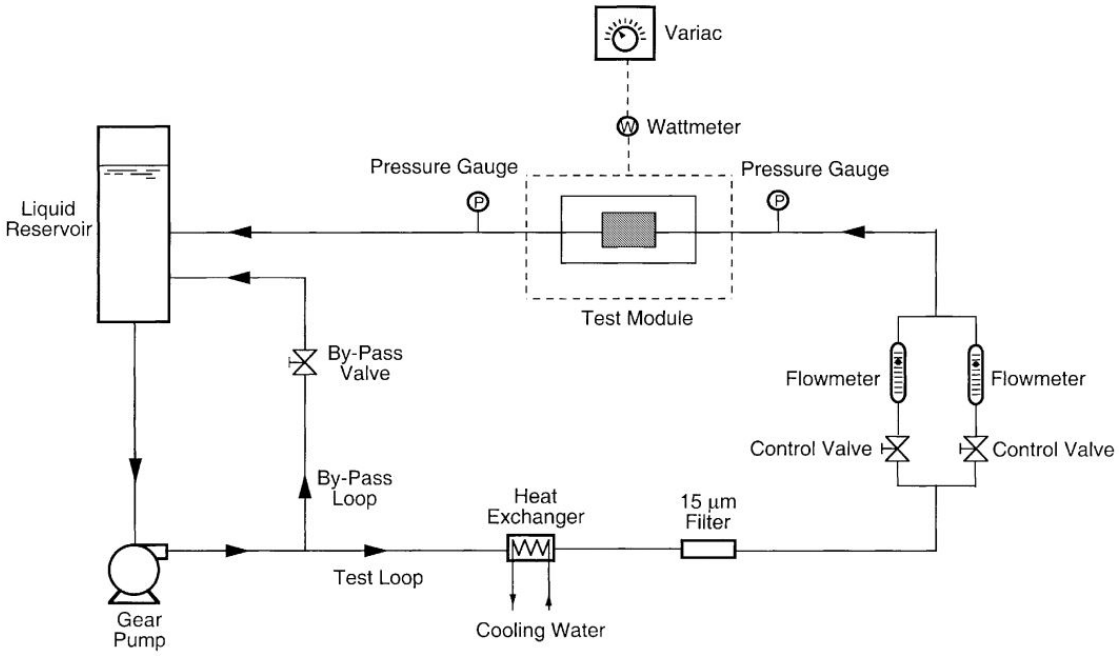

Figure 4.1: Schematic diagrams of flow loop [1]

Description of problem

The experimental work done by Qu and Mudawar, (2001) on the test apparatus is modelled and simulated in this present study. Water is moving through a straight rectangular smaller scale channel implanted in a test module. 21 rectangular smaller scale openings were machined into micro- channel surface by an accuracy machining procedure. The miniaturized scale openings

were equidistantly divided inside of the 1-cm heat sink width and had the cross-sectional measurements of 231 µ m wide and 712 µm profound. There are 21 parallel rectangular small scale directs in the module.

4.2 Geometry of the heat sink

In the present analysis, only one micro channel of the remaining 21 micro-channels is considered as a computational domain. Figure shows the micro-channel heat sink with single unit cell used for simulation.

Table 4.1: Dimensions of the rectangular channel unit cell used for simulation

W_w(µm)	$W_{channel}$(µm)	H_{w1}(µm)	H_{ch}(µm)	H_{w2}(µm)	L(mm)
118	231	12700	713	5637	44.7

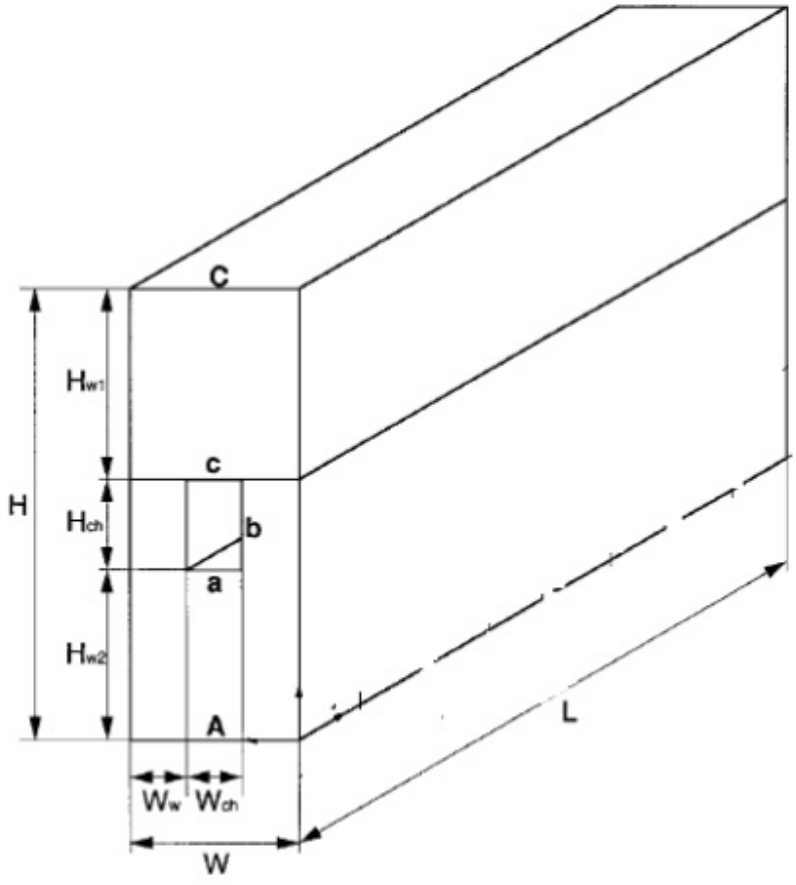

Figure 4.2: Schematic diagram of rectangular microchannel unit cell [1]

Geometry construction

For this computational fluid dynamics problem, the geometry of the heat sink was constructed using solid works, and was imported to ANSYS workbench CFX for further meshing and CFD simulations.

For creating geometry, first the heat sink was made in solid works as per the dimensions given in table 1 and was named as solid part while fluid channel was created of the same dimensions as of the rectangular slot along the length of heat sink for proper mating and was given the name of fluid part.

Both parts were created separately using solid works and were later assembled by inserting fluid channel in solid heat sink using the insert components and mate option in solid works.

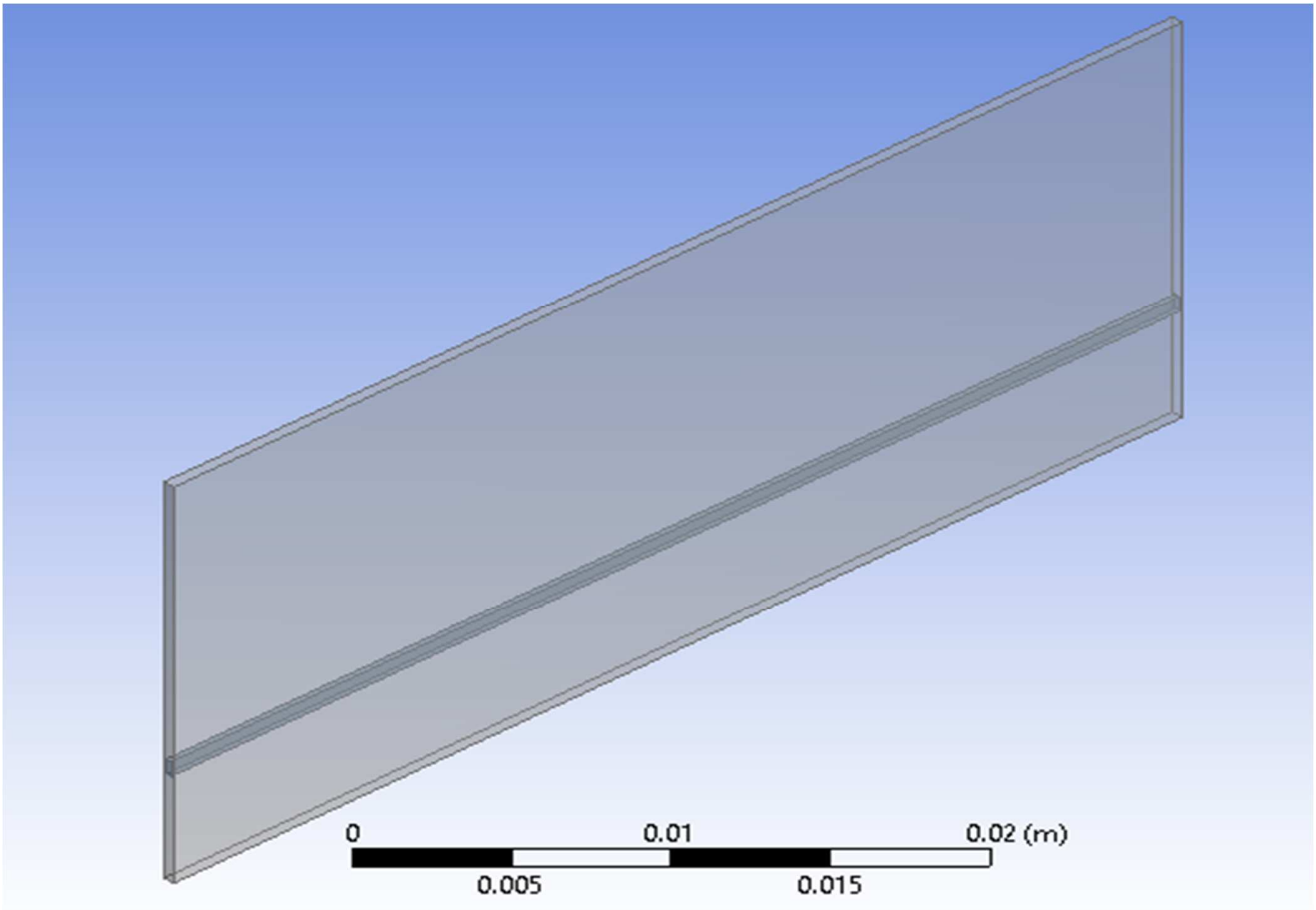

Figure 4.3: Geometry of straight micro-cannel heat sink used in simulation

4.3 Meshing

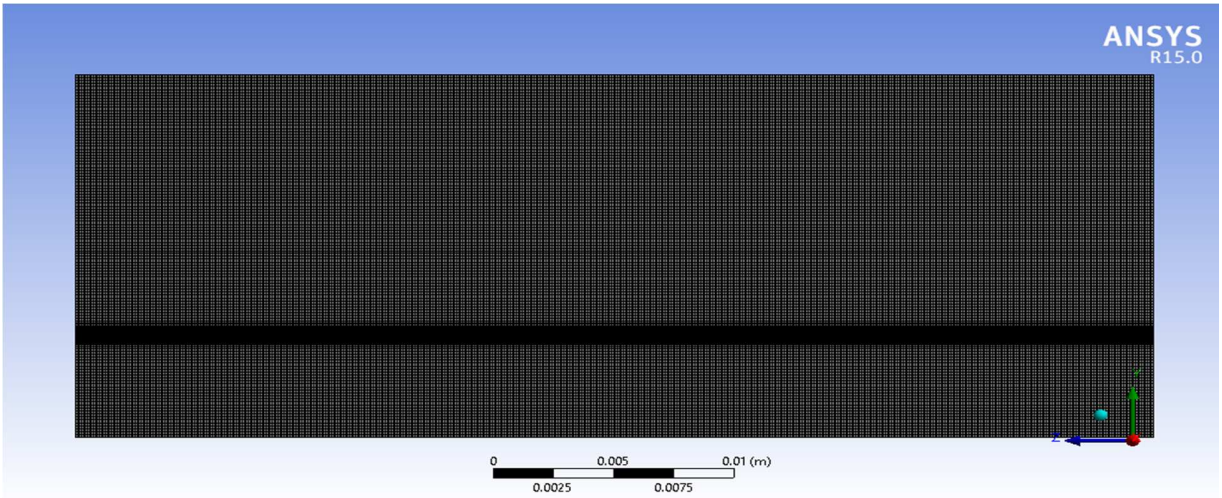

Figure 4.4: Meshing of the geometry in ANSYS CFX

Table 4.2: Mesh details

Physics preference	CFD
Solver preference	CFX
Smoothing	Medium
Transition	Slow
Transition ratio	0.77
Minimum size	2.42e-5
Maximum face size	2.42e-3
Maximum size	4.84e-3
Nodes	409520
Elements	309993

The mesh was generated using proximity on option. For the straight micro-channel the mesh was created as a structured mesh and for checking the solutions the mesh was made finer and the solutions obtained were mesh independent. After the meshing, the named selection were given, which are to be considered as boundary conditions.

4.4 Set up details

Before giving the boundary conditions two domains were created in the ANSYS CFX set up. Out of the two domains created one domain was given the name as fluid while the other domain was assigned the name as solid domain. The fluid channel constructed in solid works was given the name fluid domain while the heat sink constructed in solid works was given the name solid domain.

After making the domains in the set up the boundary conditions were created in the solid domain and the fluid domain. Inlet and outlet boundary conditions were given in the fluid domain whereas the bottom wall heat flux and adiabatic conditions for the remaining walls were given in the solid domain.

Boundary conditions

1. No slip on the surface.

2. Uniform inlet temperature and static pressure were given at the entry of the channel.

3. Outlet of the channel is based on mass flow rate.

4. A uniform heat flux of 100 W/cm^2 and 200 W/cm^2 at the bottom wall of the heat sink.

Table 4.3: Zone specification

Heat sink front wall	Wall
Heat sink top wall	Wall
Heat sink back wall	Wall
Heat sink bottom wall	Heat flux
Heat sink right wall	Wall
Heat sink left wall	Wall
Channel entry	Static pressure
Channel outlet	Mass flow outlet
Default Interface	Wall

Table 4.4: Solver settings

Following are the solver settings which are to be used in simulation.

Min. Iterations	1
Max. Iterations	250
Residual type	RMS
Residual target	1E-4
Time scale control	Auto time scale

Problem 2

4.5 Wavy edge type rectangular micro-channel heat sink with hemispherical obstructions by taking water as a coolant and cooper as a sink material

In this chapter a three dimensional CFD simulation is done for the heat transfer and pressure drop characteristics of wavy edge rectangular micro-channel heat sink. Material used for heat sink construction is copper.

Problem description-

Water is moving through a wavy edge rectangular smaller scale channel heat sink assembly. In this analysis a design for wavy edge type of micro-channel heat sink is constructed. The dimensions of the micro-channel assembly are same as that of the micro-channels simulated in chapter 4 the only difference being the length is made wavy along with hemispherical obstruction.

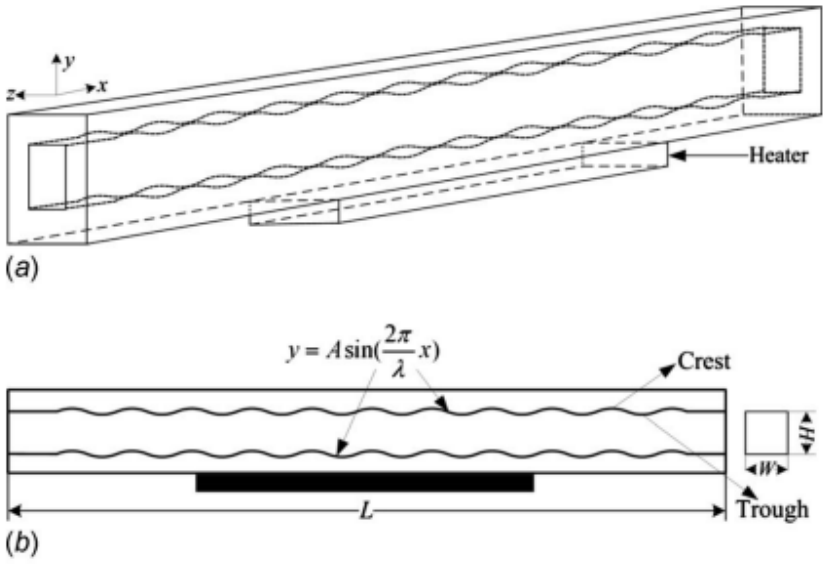

Figure 4.5: Schematic diagram of wavy microchannel heat sink. [18]

Table 4.5: Dimensions of the wavy channel unit cell used for simulation

W_{wall}(µm)	W(µm)	H_{wall2}(µm)	H(µm)	H_{wall1}(µm)	L(mm)
118	231	12700	713	5637	44.7

In this analysis the only the length of the micro-channel heat sink is made wavy and the pressure drop and heat transfer characteristics are simulated.

Wave equation used- In this analysis, for the construction of geometry a sine wave is used which has the following equation.

$$y = Asin(2\pi x/\lambda)$$

Here, A is wave amplitude and λ is the wavelength.

4.6 Geometry construction-

For the analysis of computational fluid dynamics problem, the geometry of the heat sink was constructed using solid works, and was imported to ANSYS workbench CFX for further meshing and CFD simulations (figure 4.5 and 4.6).

For creating geometry, first the heat sink was made in solid works as per the dimensions given in table 2. The wave dimensions were given according to the length of the channel which is 44.7 mm. A sinusoidal wave was assumed and constructed in the solid heat sink. The amplitude of the wave was taken as 0.15 mm while the wavelength was taken as 2 mm, and at a particular wavelength a hemispherical obstruction is made on the wavy edge and repeated to get fully along the channel (in figure 4.5 and 4.6). However, fluid channel was created in the design modular of Ansys CFX and not in the solid work as it was easy to make in the design modular and also it is made of the same dimensions as of the wavy rectangular slot along the length of heat sink with hemispherical depression for proper mating and was given the name of fluid part.

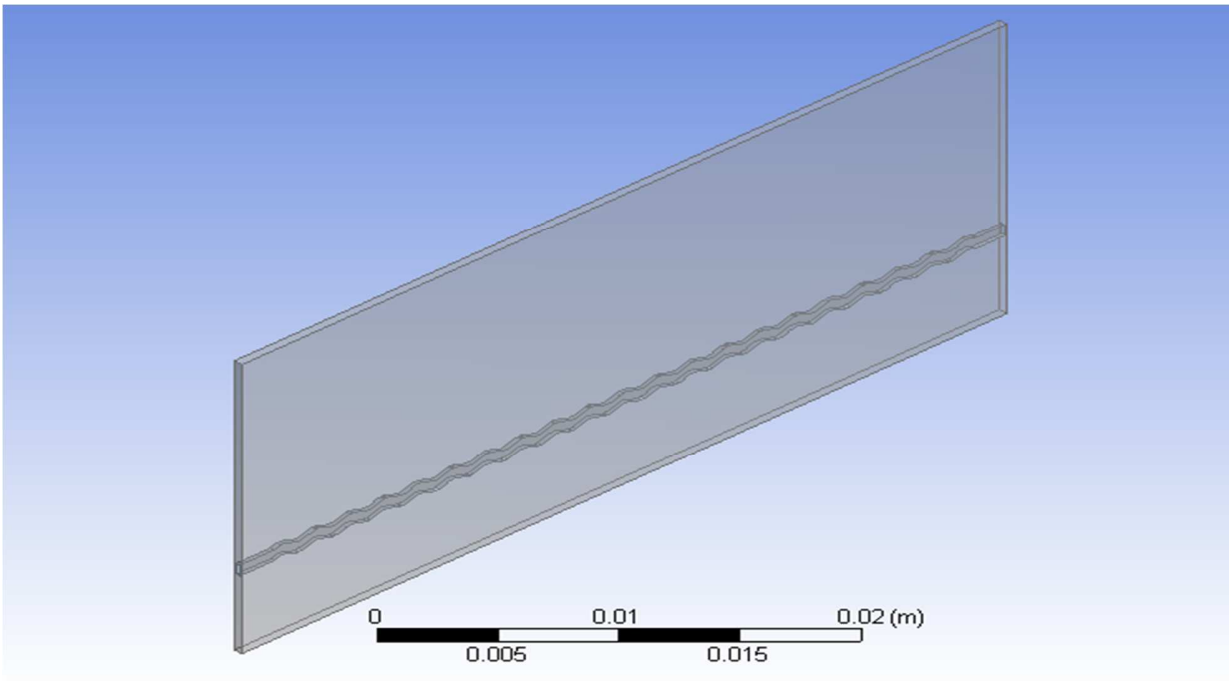

Figure 4.6: Geometry of wavy micro-cannel heat sink used in simulation

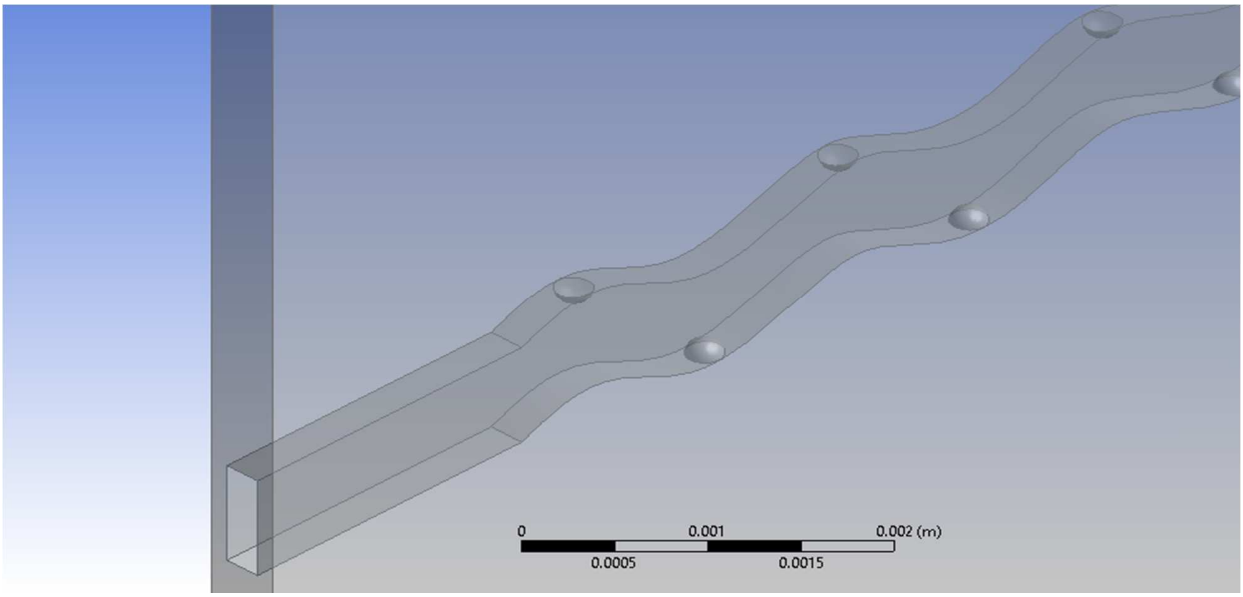

Figure 4.7: Detailed view of wavy micro-cannel heat sink with hemispherical obstructions

4.7 Meshing-

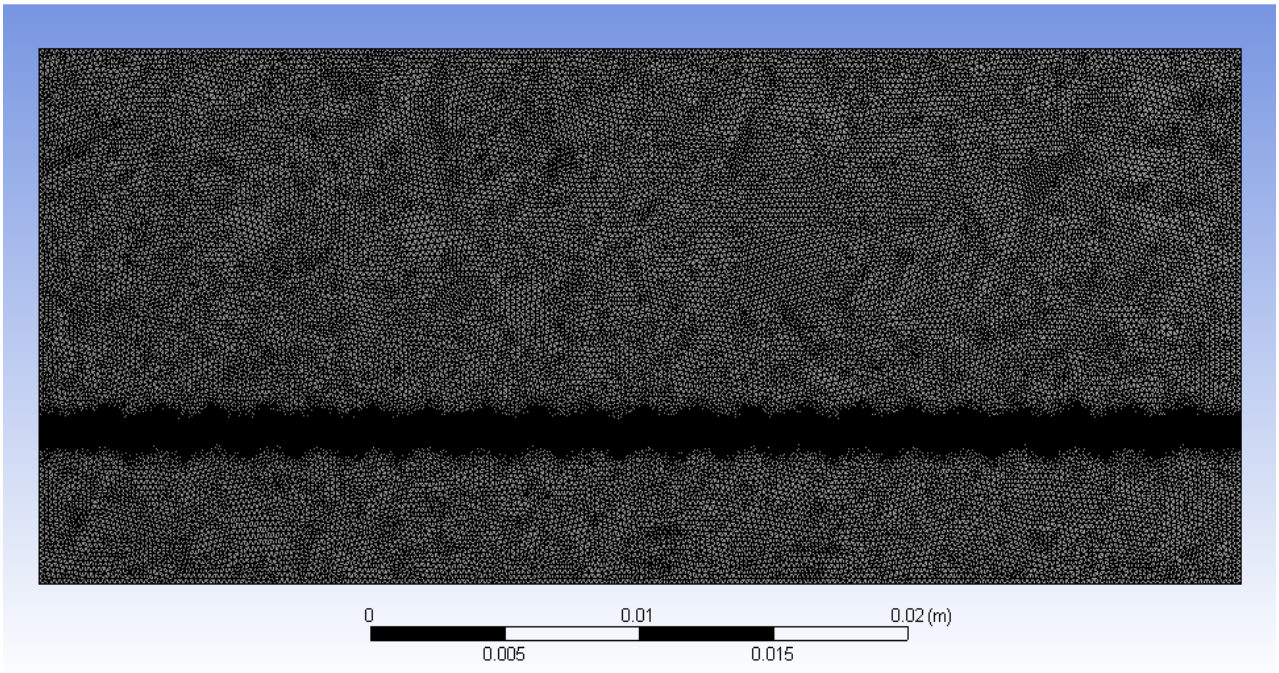

Figure 4.8: Meshing of geometry in ANSYS CFX

Table 4.6: Mesh details-

Physics preference	CFD
Solver preference	CFX
Smoothing	Medium
Transition	Slow
Transition ratio	0.77
Minimum size	1.2e-5
Maximum face size	1.21e-3
Maximum size	2.42e-3
Nodes	631403
Elements	3125145

The mesh was generated using proximity and curvature on option. For checking the solutions the mesh was made finer and the solutions obtained were mesh independent. After the meshing, the named selection were given, which are to be considered as boundary conditions.

4.8 Set up details

Before giving the boundary conditions two domains were created in the ANSYS CFX set up. Out of the two domains created, one domain was given the name as fluid while the other domain was assigned the name as solid domain. The fluid channel constructed in solid works 2013 was given the name fluid domain while the heat sink constructed in solid works 2013 was given the name solid domain.

After making the domains in the set up the boundary conditions were created in the solid domain and the fluid domain. Inlet and outlet boundary conditions were given in the fluid domain whereas the bottom wall heat flux and adiabatic conditions for the remaining walls were given in the solid domain.

Boundary conditions-

1. No slip on the surface.

2. Uniform inlet temperature and static pressure were given at the entry of the channel.

3. Outlet of the channel is based on mass flow rate.

4. A uniform heat flux of 100W/cm^2 and 200 W/cm^2 at the bottom wall of the heat sink for two separate cases was applied.

Table 4.7: Zone specification

Front wall of solid heat sink	Wall
Top wall of solid heat sink	Wall
Back wall of solid heat sink	Wall
Bottom wall of solid heat sink	Heat flux
Heat sink right wall	Wall
Heat sink left wall	Wall
Channel entry	Static pressure
Channel exit	Mass flow rate
Default Interface	Wall

Table 4.8: Solver settings

Following are the solver settings which are to be used in simulation.

Min. Iterations	1
Max. Iterations	250
Residual type	RMS
Residual target	1E-4
Time scale control	Auto time scale

Problem 3

4.9 Wavy edge type rectangular micro-channel heat sink with hemispherical obstructions by taking Performance Fluid PF5052 as a coolant and cooper as a sink material

In this chapter a three dimensional CFD simulation is done for the heat transfer of wavy edge rectangular micro-channel heat with hemispherical obstruction by taking performance fluid PF5052 as a coolant and copper as a sink material.

Problem description

Performance fluid PF5052 is moving through a wavy edge rectangular smaller scale channel heat sink assembly. In this analysis a design for wavy edge type of micro-channel heat sink along with hemispherical obstruction is constructed. The dimensions of the micro-channel assembly are same as that of the micro-channels simulated in chapter 4 the only difference being the length is made wavy along with hemispherical obstructions.

Geometry and all the parameters are same, except PF5052 as a coolant instead of water in the problem 2

Table 4.9: Thermal Properties of Performance Fluid PF5052

FLUID	ρ (kg/m3)	Cp(J/kg-K)	K(w/m-K)	μ(kg/m-s)
PF-5052	1776	1014	0.065	97.77

CHAPTER 5

VALIDATION

5.1 Straight rectangular micro-channel

In this computational analysis validation is done for straight rectangular micro-channel heat sink and the results are plotted for pressure drop and heat transfer in straight rectangular micro-channel for two different values of heat fluxes applied at the bottom of the heat sink for varying set of values of Reynolds number. The value of heat flux used in the analysis are 100 W/$cm^2$and 200 W/cm^2. Five values of Reynolds number are taken for the analysis which are 400, 600, 800, 1000, and 1200 respectively.

Results for bottom wall heat flux value of 100 W/cm^2 and different sets of Reynolds number-

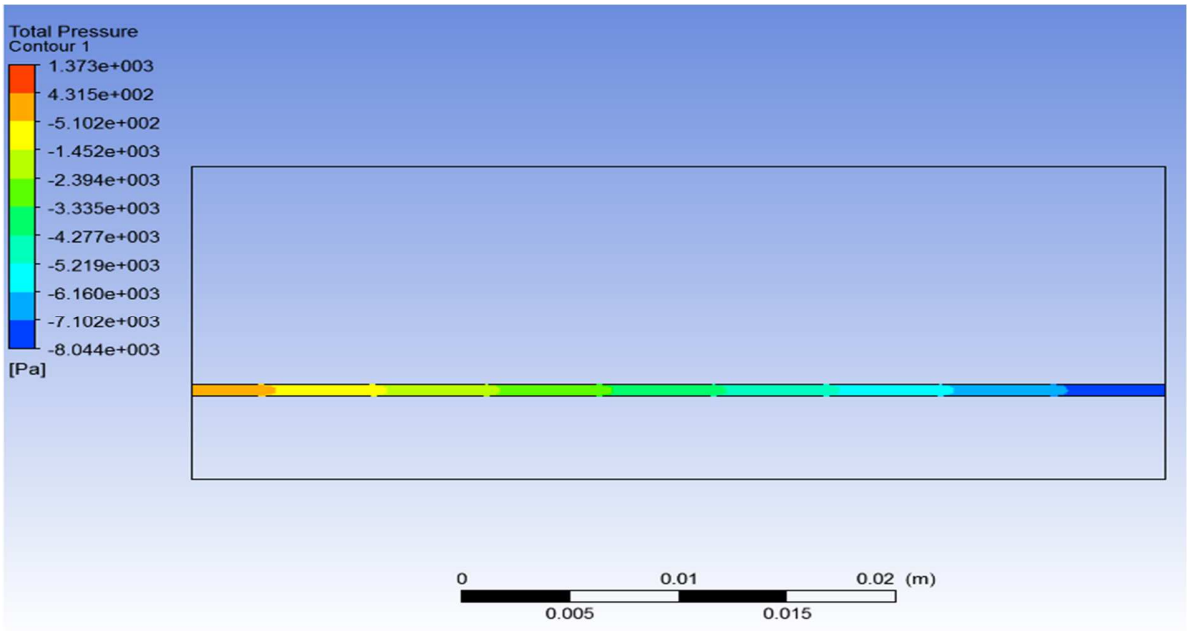

Figure 5.1: Pressure contours of water at Re=400

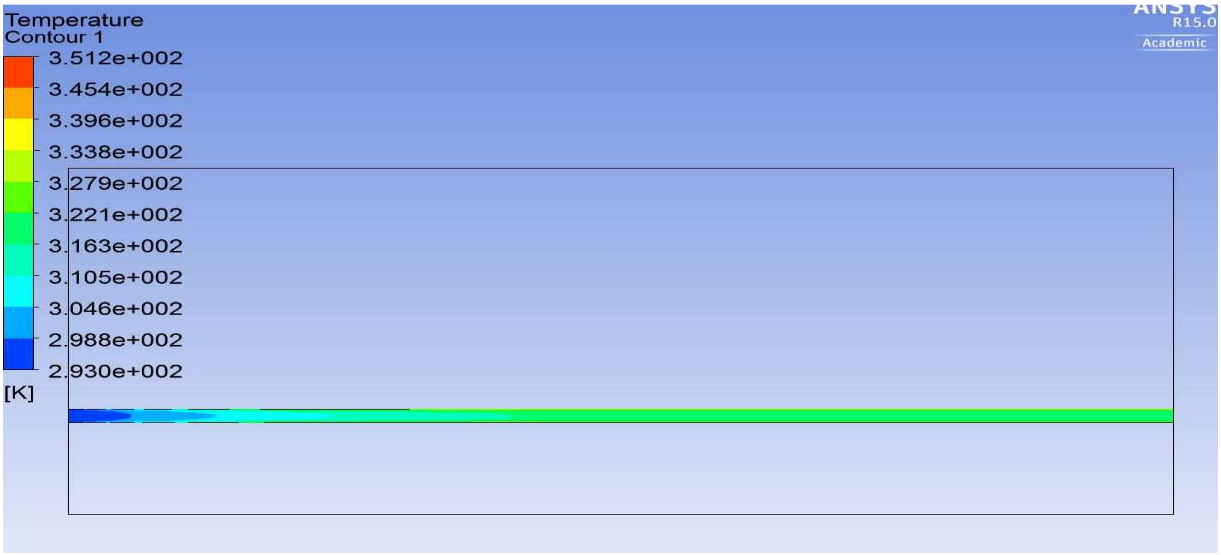

Figure 5.2: Temperature contours of water at Re=400

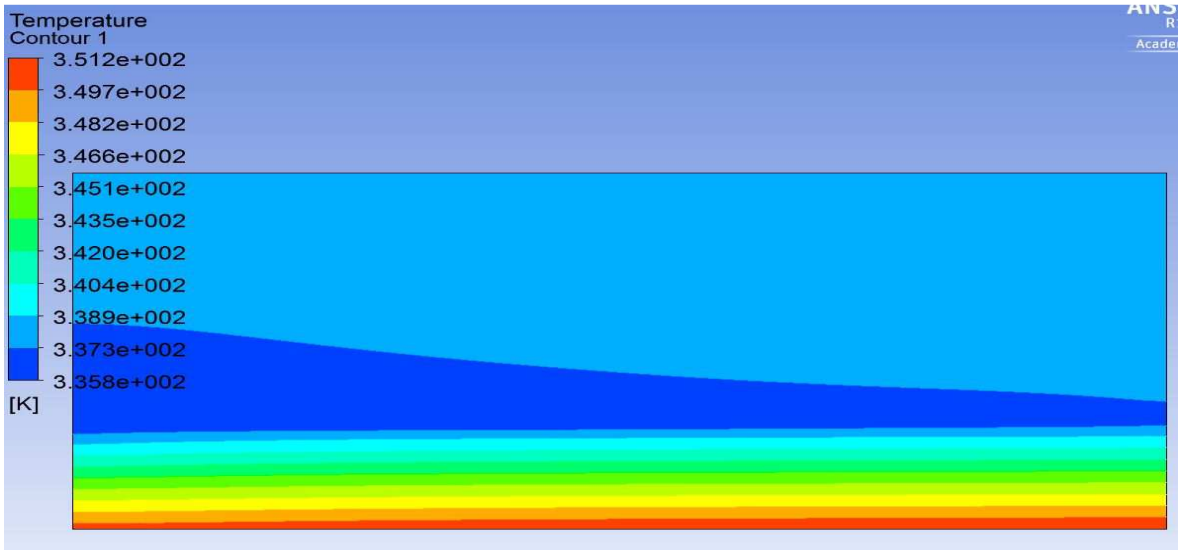

Figure 5.3: Temperature variation along the wall at Re=400

- In the figures 5.1 and 5.3, the contours for pressure and temperature in a straight rectangular channel for Reynolds number value equal to 400 are shown.
- In figure 5.1 pressure drop along the channel is found to be 0.09 bar.
- In figure 5.2 temperature at the outlet of the channel is found to be 314 K
- In figure 5.3 the maximum wall temperature is found to be 351 K at the bottom wall of the channel and wall temperature increases in the direction of flow.

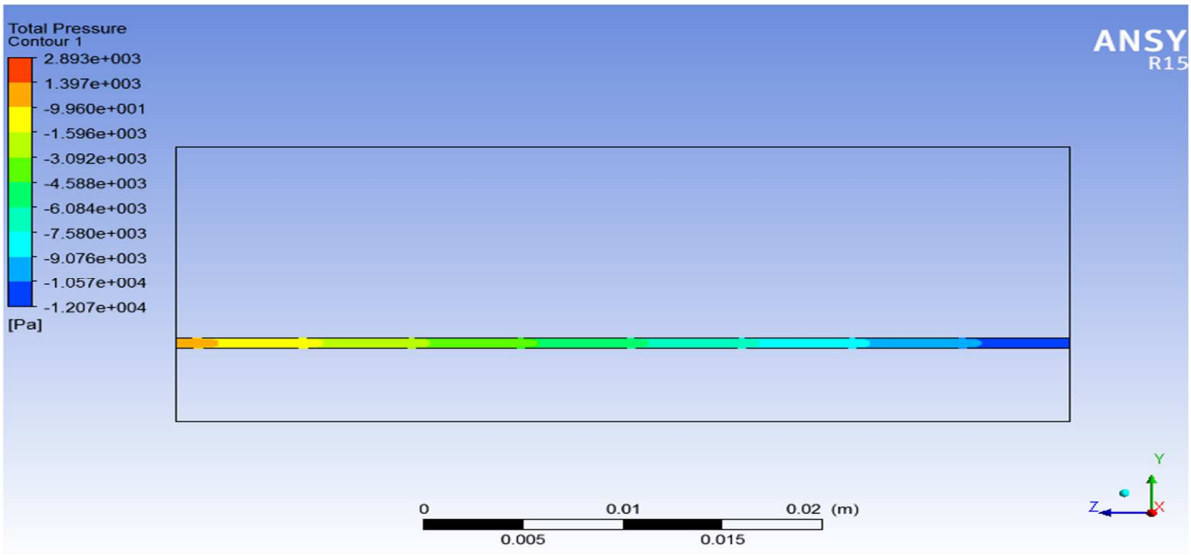

Figure 5.4: pressure contours for water at Re=600

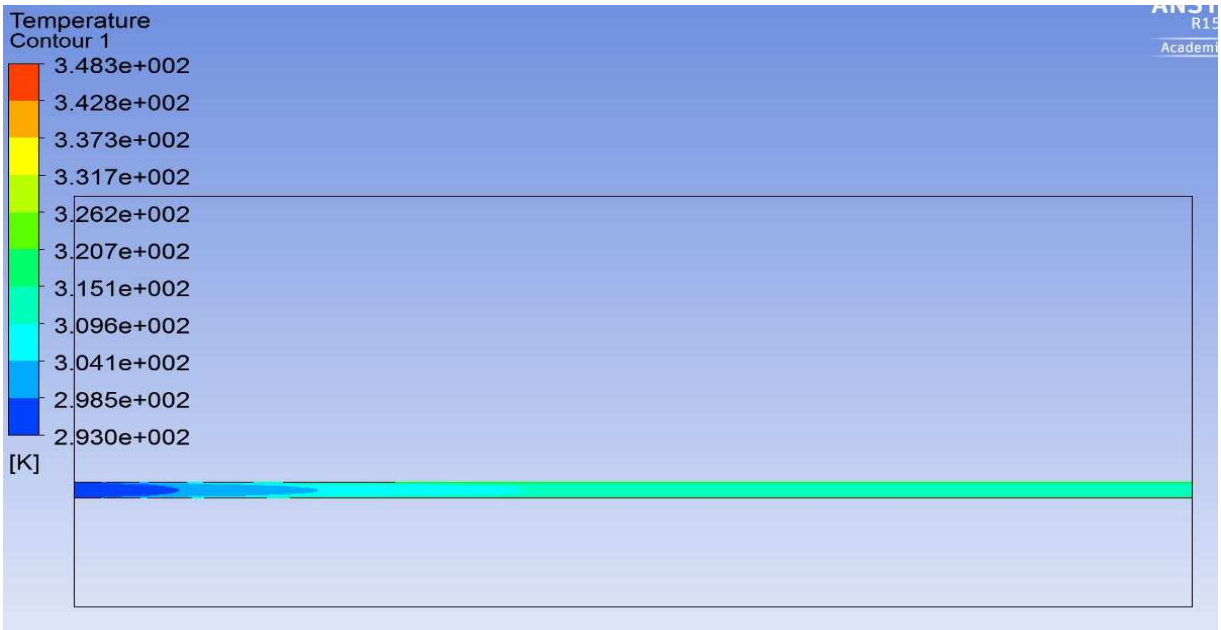

Figure 5.5: Temperature contours of water at Re=600

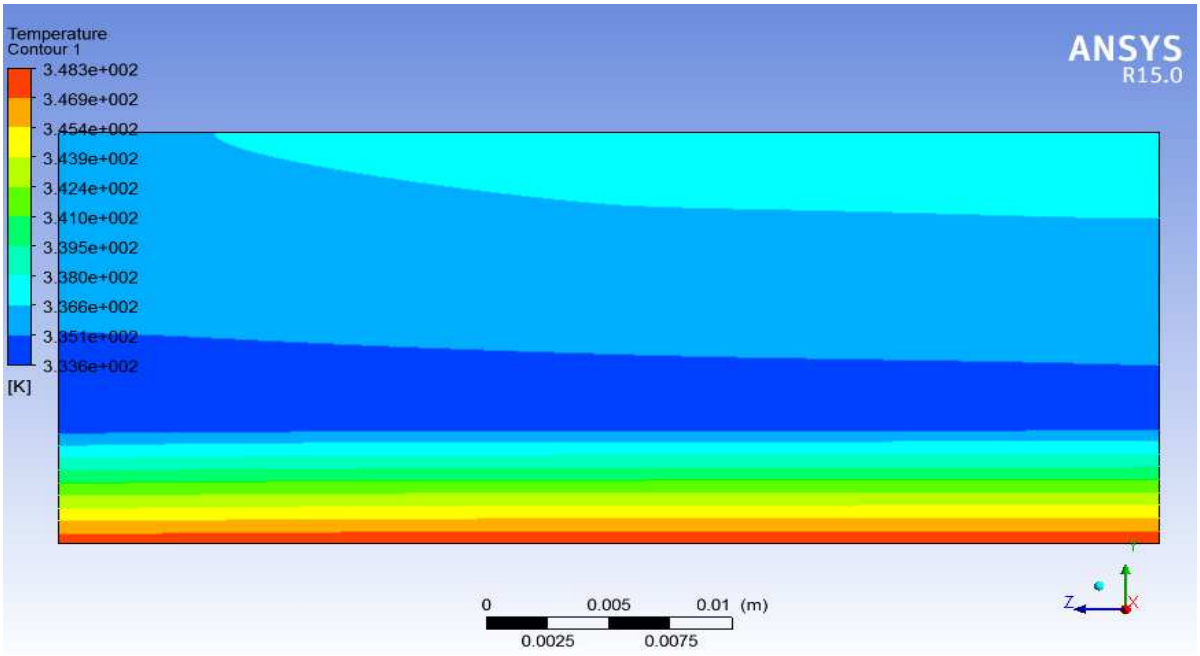

Figure 5.6: Temperature variation along the wall at Re=600

- In the figures 5.4 to 5.6, the contours for pressure and temperature in a straight rectangular channel for Reynolds number value equal to 600 are shown.
- In figure 5.4 pressure drop along the channel is found to be 0.15 bar.
- In figure 5.5 the temperature at the outlet of the channel is found to be 308.5 K.
- In figure 5.6 maximum wall temperature is found to be 348.5 K at the bottom wall of the channel and wall temperature increases in the direction of flow.

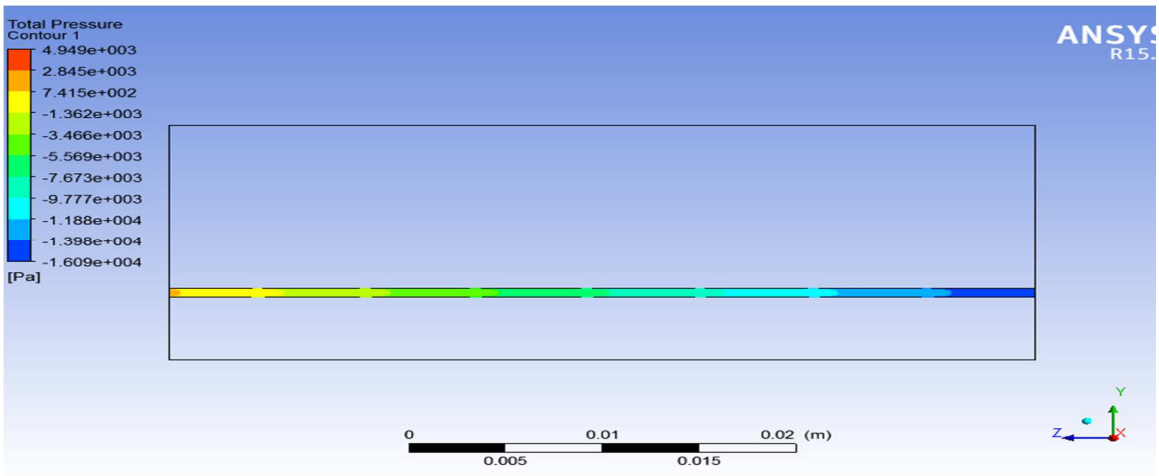

Figure 5.7: Pressure contours for water along channel at Re =800

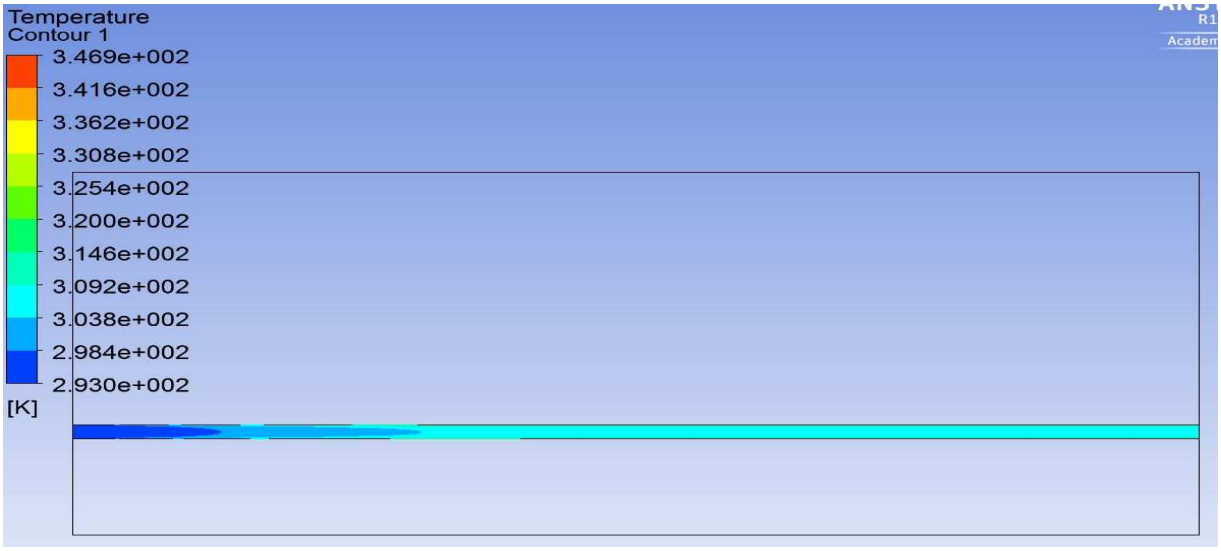

Figure 5.8: Temperature contour for water at channel outlet at Re=800

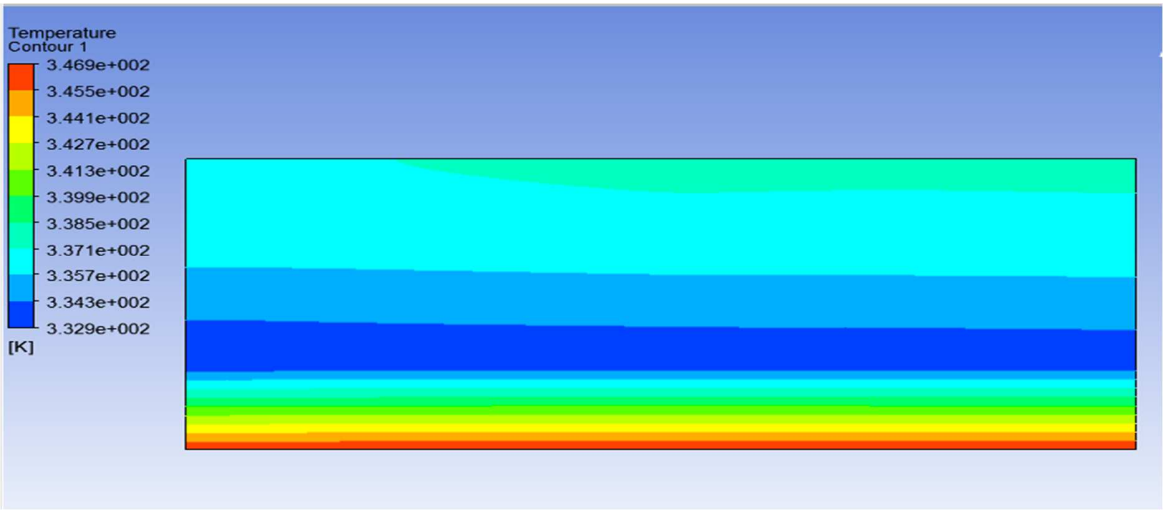

Figure 5.9: Temperature variation along the wall at Re=800

- In the figures 5.7 to 5.9, the contours for pressure and temperature in a straight rectangular channel for Reynolds number value equal to 800 are shown.
- In figure 5.7 the pressure drop along the channel is found to be 0.21 bar.
- In figure 5.8 the temperature at the outlet of the channel is found to be 306.5 K.
- In figure 5.9 maximum wall temperature is found to be 346 K at the bottom wall of the channel and wall temperature increases in the direction of flow.

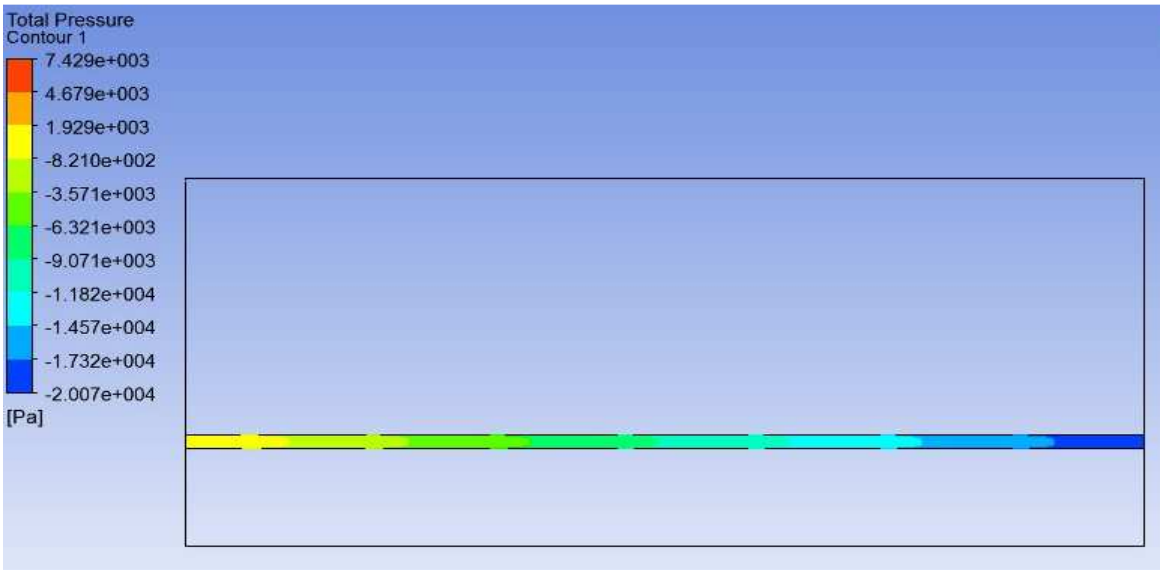

Figure 5.10: Pressure contour for water along the channel at Re=1000

Figure 5.11: Temperature variation along the wall at Re=1000

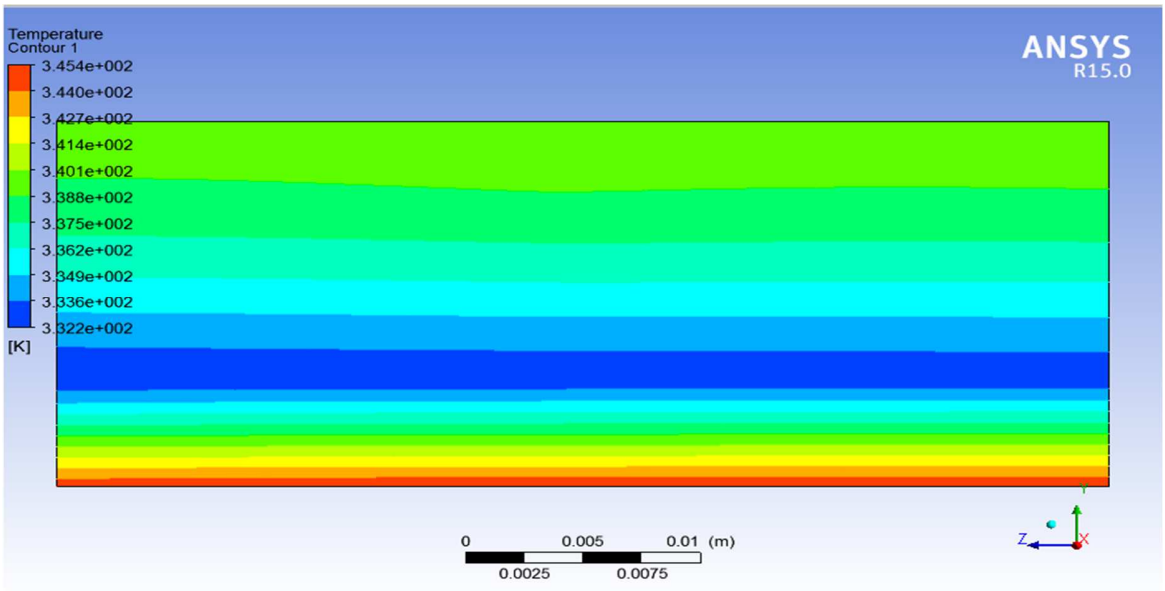

Figure 5.12: Temperature variation along the wall at Re=1000

- In the figures 5.10 to 5.12, the contours for pressure and temperature in a straight rectangular channel for Reynolds number value equal to 1000 are shown.
- In figure 5.10 pressure drop along the channel is found to be 0.275 bar.
- In figure 5.11 temperature at the outlet of the channel is found to be 303.04 K.
- In figure 5.12 maximum wall temperature is at the bottom wall of the heat sink and is found to be 345.35 K and further the wall temperature increases in the direction of flow.

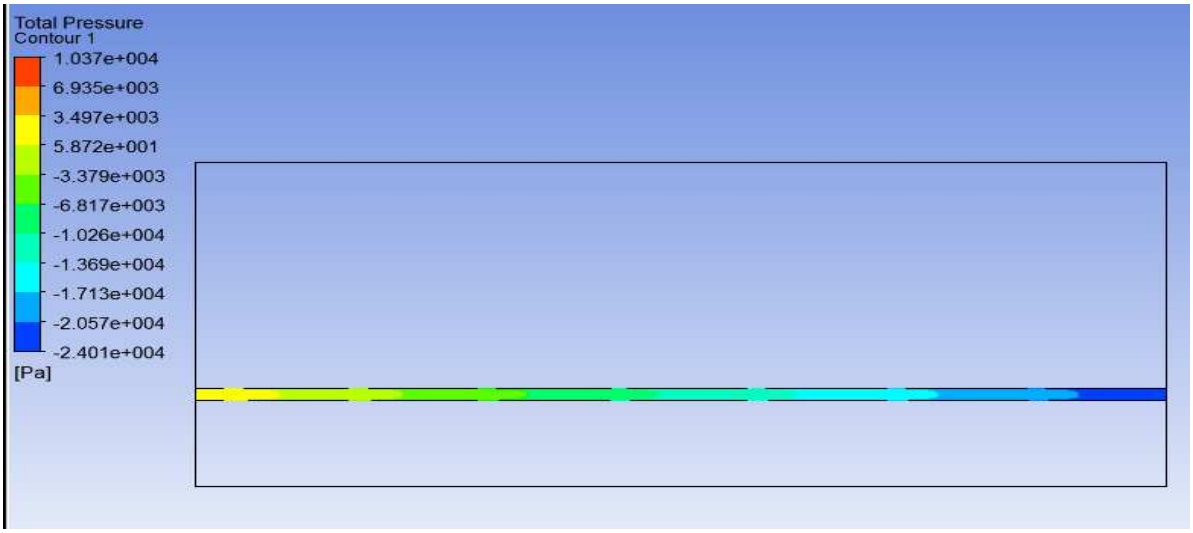

Figure 5.13: Pressure contour along channel at Re=1200.

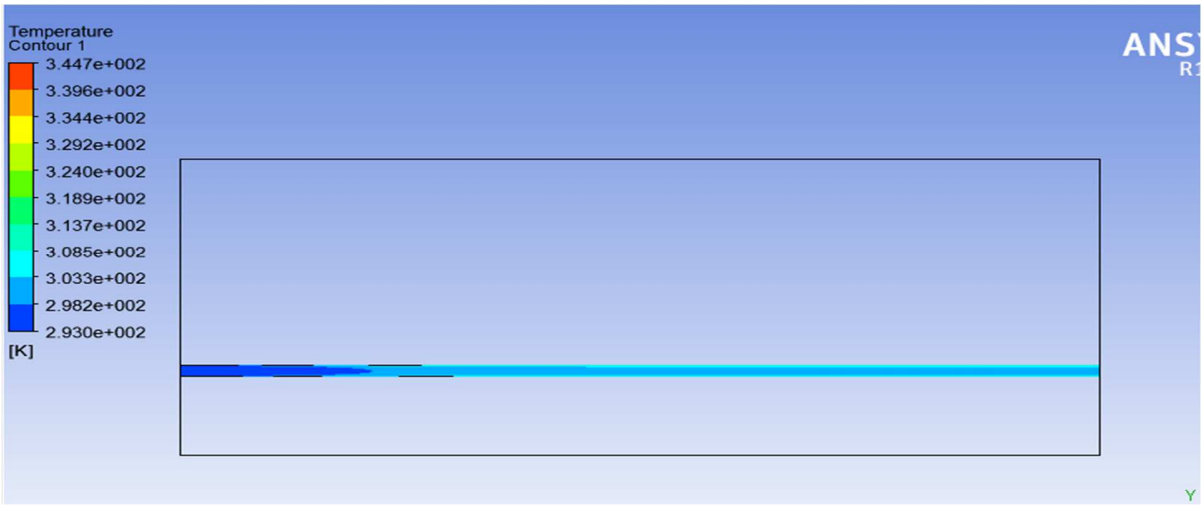

Figure 5.14: Temperature contour along channel at Re=1200

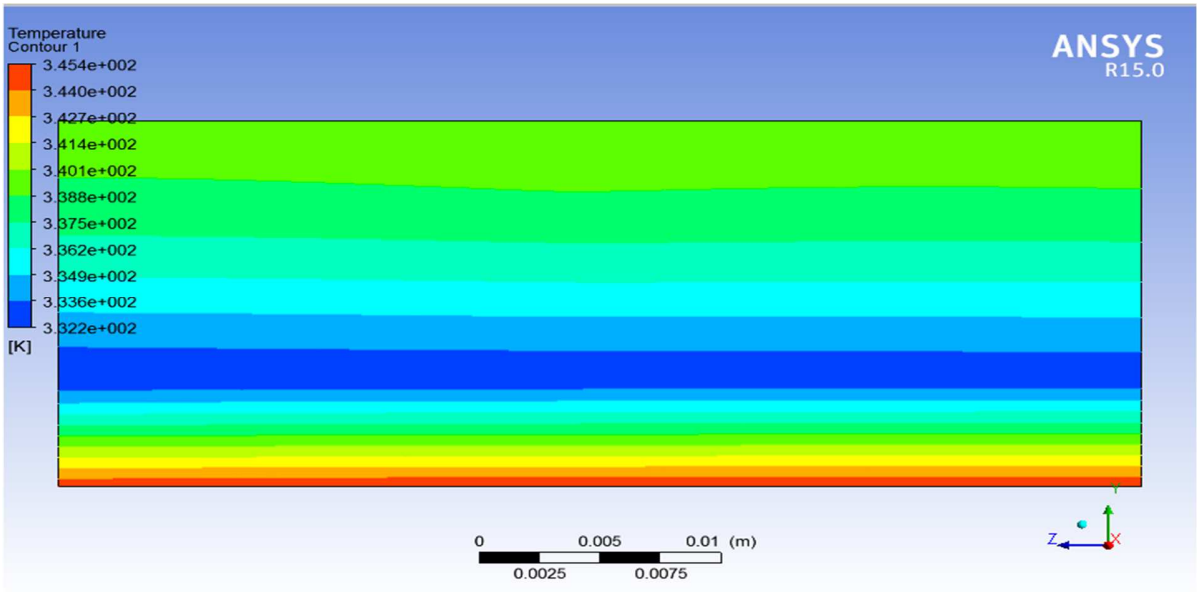

Figure 5.15: Temperature variation along the wall at Re=1200

- In the figures 5.13 to 5.15, the contours for pressure and temperature in a straight rectangular channel for Reynolds number value equal to 1200 are shown.
- In figure 5.13 pressure drop along the channel is found to be 0.343 bar.
- In figure 5.14 temperature at the outlet of the channel is found to be 301 K.
- In figure 5.15 maximum wall temperature is at the bottom wall of the heat sink and is found to be 344.74 K and further the wall temperature increases in the direction of flow.

Results for bottom wall heat flux value of 200W/$cm^2$and different sets of Reynolds number -

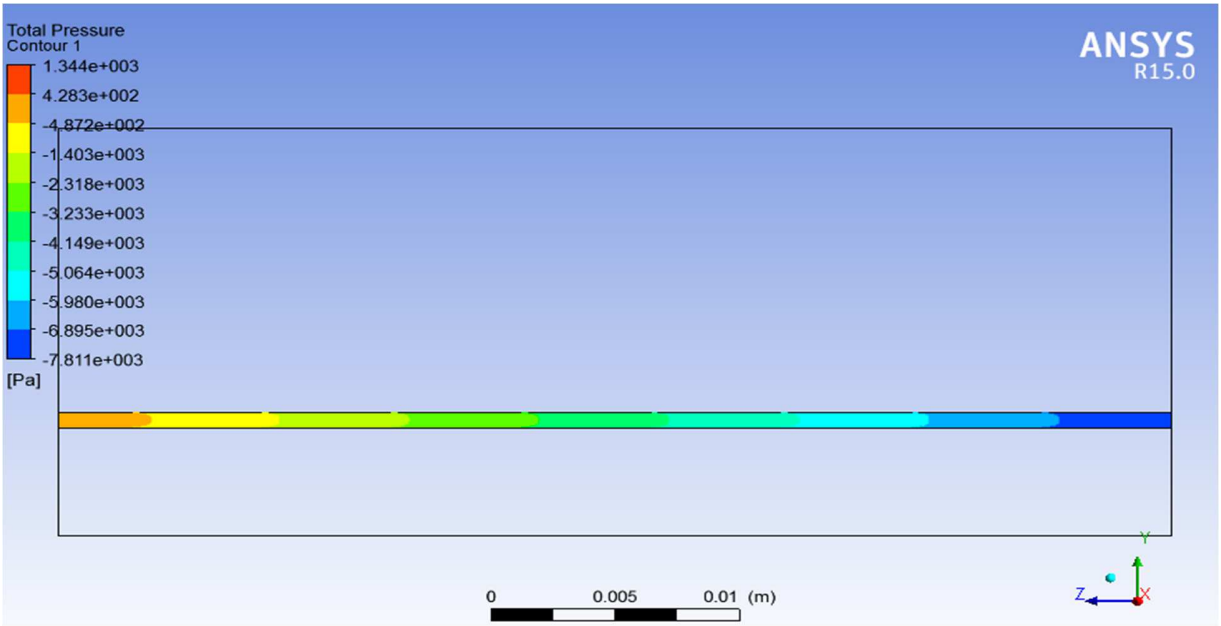

Figure 5.16: Pressure contours for water along channel at Re=400

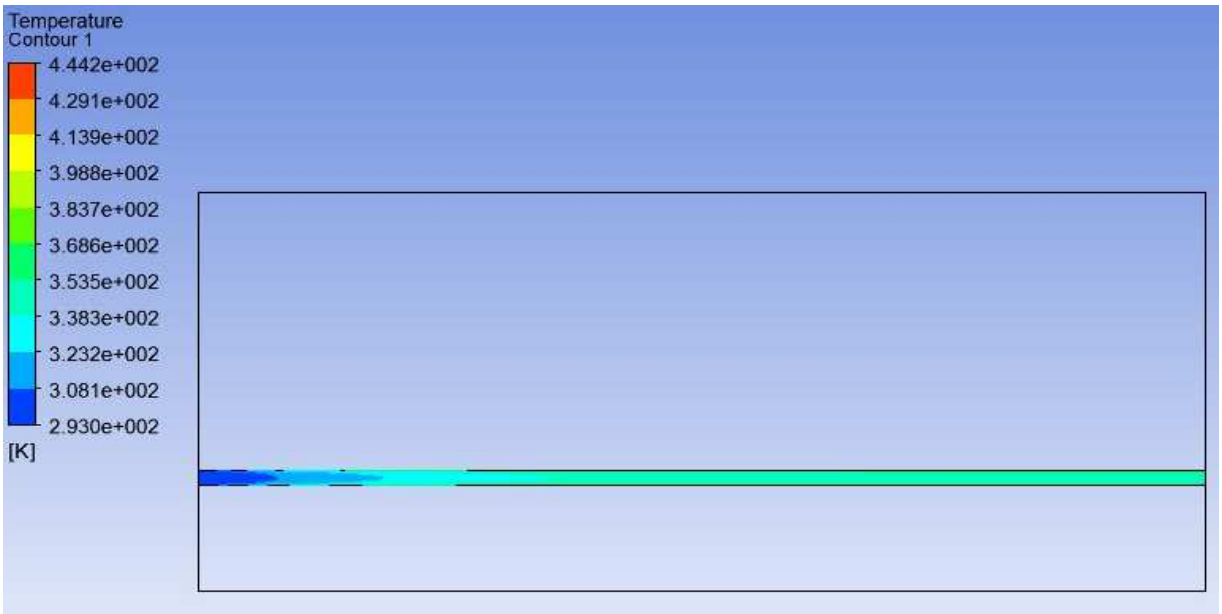

Figure 5.17: Temperature contour along the channel at Re=400

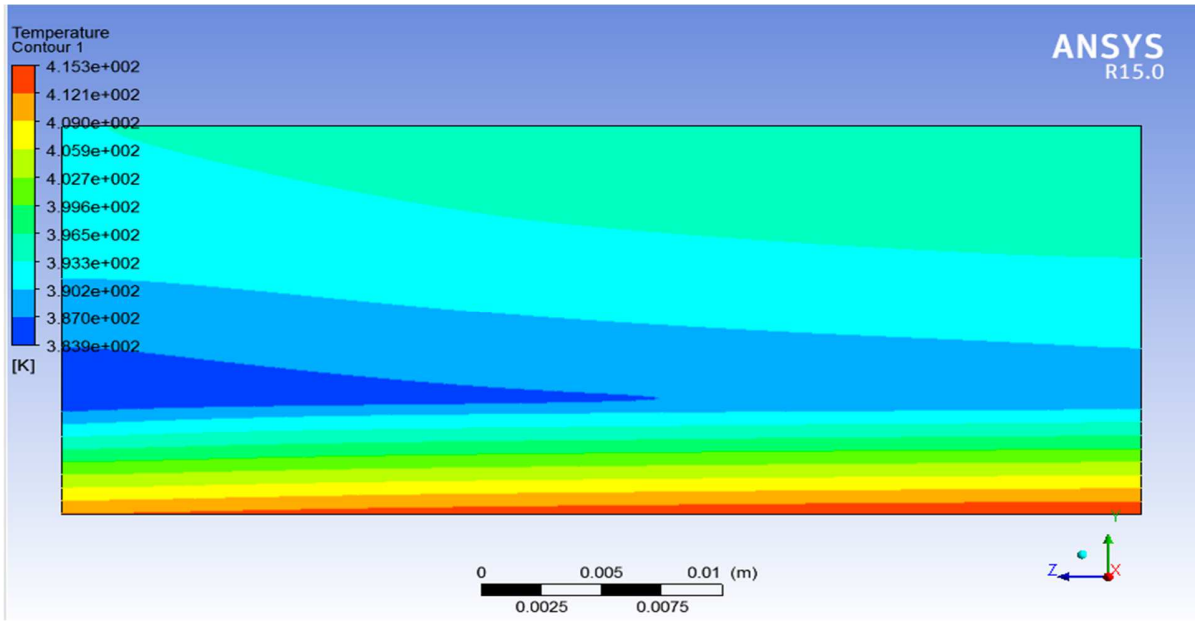

Figure 5.18: Temperature variation along the wall at Re=400

- In the figures 5.16 to 5.18, the contours for pressure and temperature in a straight rectangular channel for Reynolds number value equal to 400 are shown.
- In figure 5.16 pressure drop along the channel is found to be 0.091 bar.
- In figure 5.17 temperature at the outlet of the channel is found to be 341 K.
- In figure 5.18 maximum wall temperature is at the bottom wall of the heat sink and is found to be 415 K and further the wall temperature increases in the direction of flow.

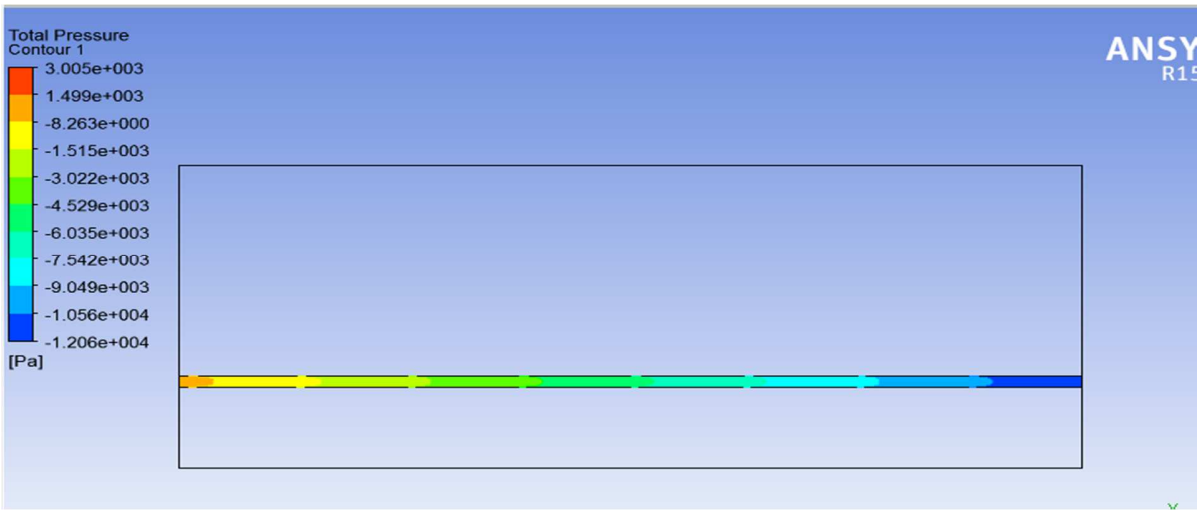

Figure 5.19: Pressure contours for water along the channel at Re=600

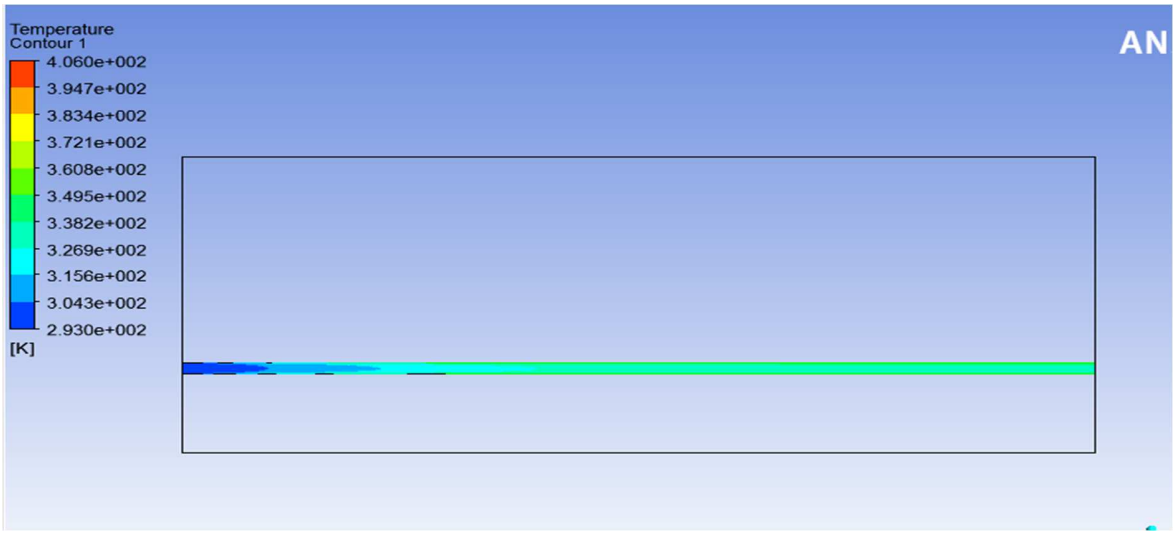

Figure 5.20: Temperature contour along the channel at Re=600

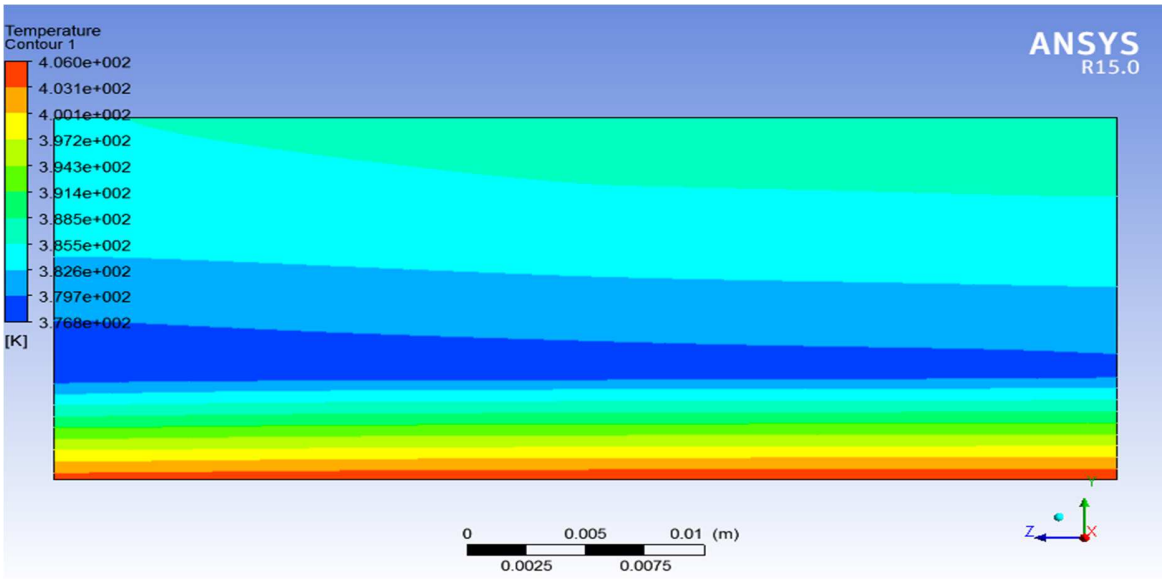

Figure 5.21: Temperature variation along the wall at Re=600

- In the figures 5.19 to 5.21, the contours for pressure and temperature in a straight rectangular channel for Reynolds number value equal to 600 are shown.
- In figure 5.19 pressure drop along the channel is found to be 0.15 bar.
- In figure 5.20 the temperature at the outlet of the channel is found to be 328 K.
- In figure 5.21 maximum wall temperature is at the bottom wall of the heat sink and is found to be 405 K and further the wall temperature increases in the direction of flow.

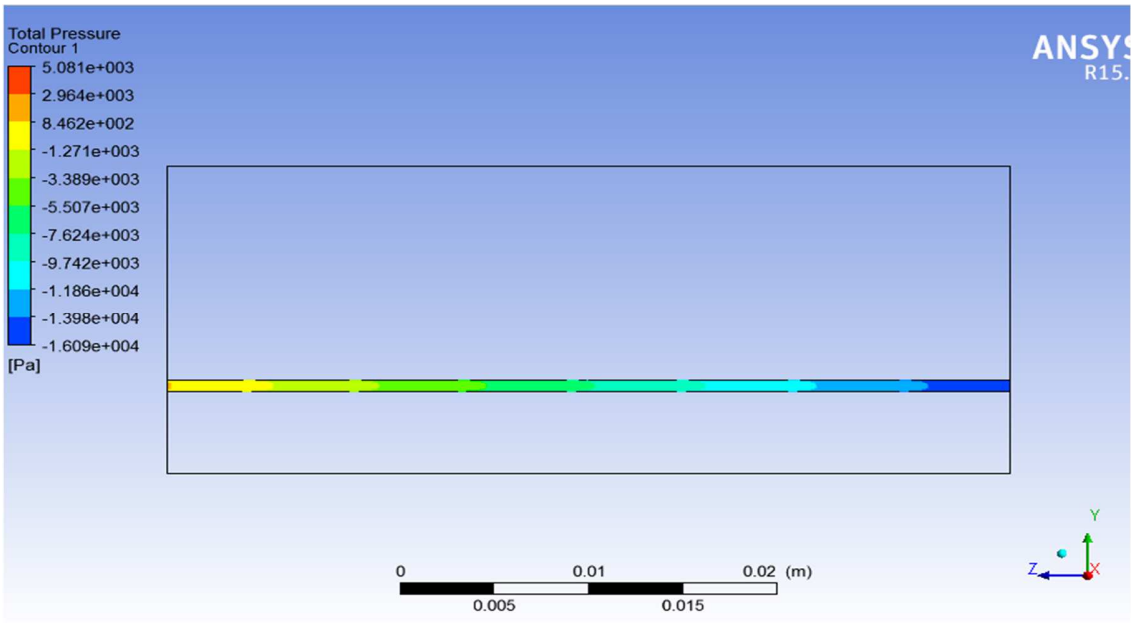

Figure 5.22: Pressure contours for water along channel at Re =800

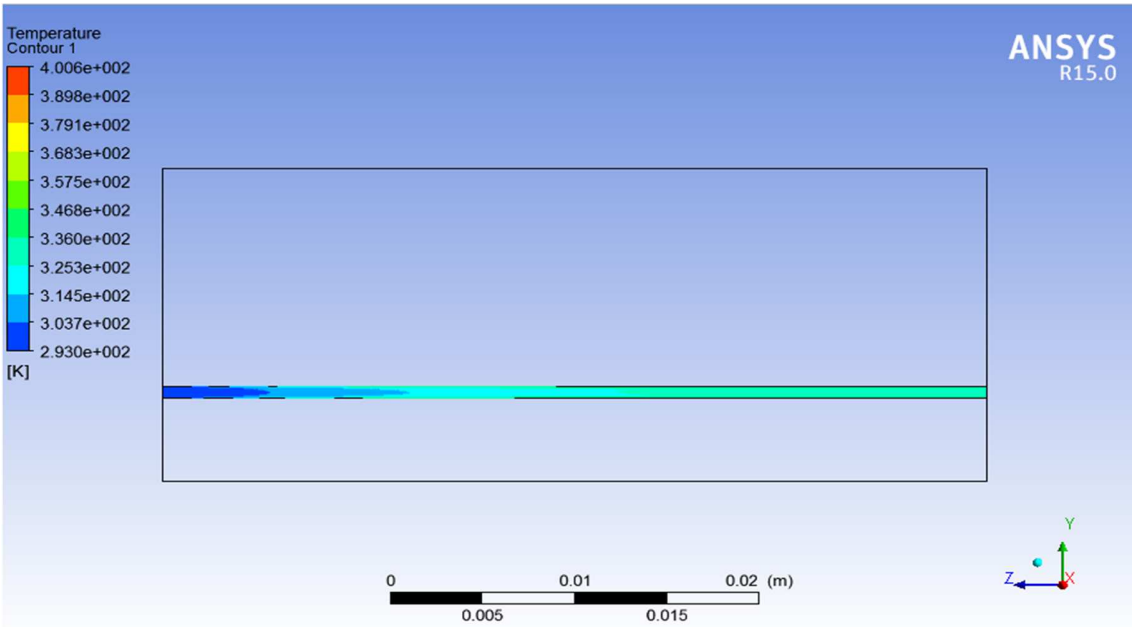

Figure 5.23: Temperature contour along the channel at Re=800

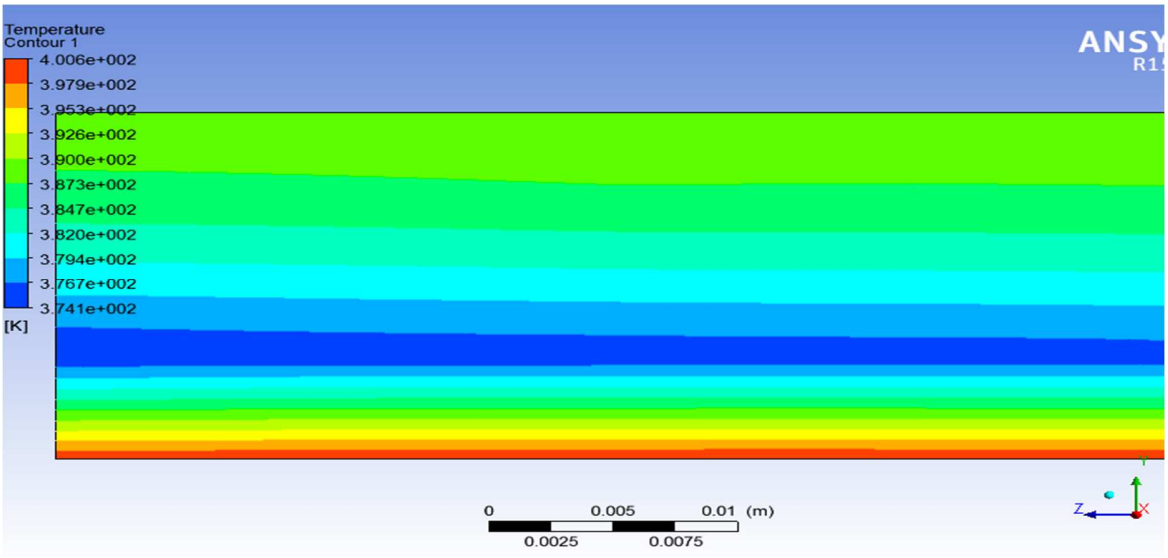

Figure 5.24: Temperature variation along the wall at Re=800

- In the figures 5.22 to 5.24, the contours for pressure and temperature in a straight rectangular channel for Reynolds number value equal to 800 are shown.
- In figure 5.22 pressure drop along the channel is found to be 0.21 bar.
- In figure 5.23 the temperature at the outlet of the channel is found to be 320 K.
- In figure 5.24 maximum wall temperature is at the bottom wall of the heat sink and is found to be 400 K and further the wall temperature increases in the direction of flow.

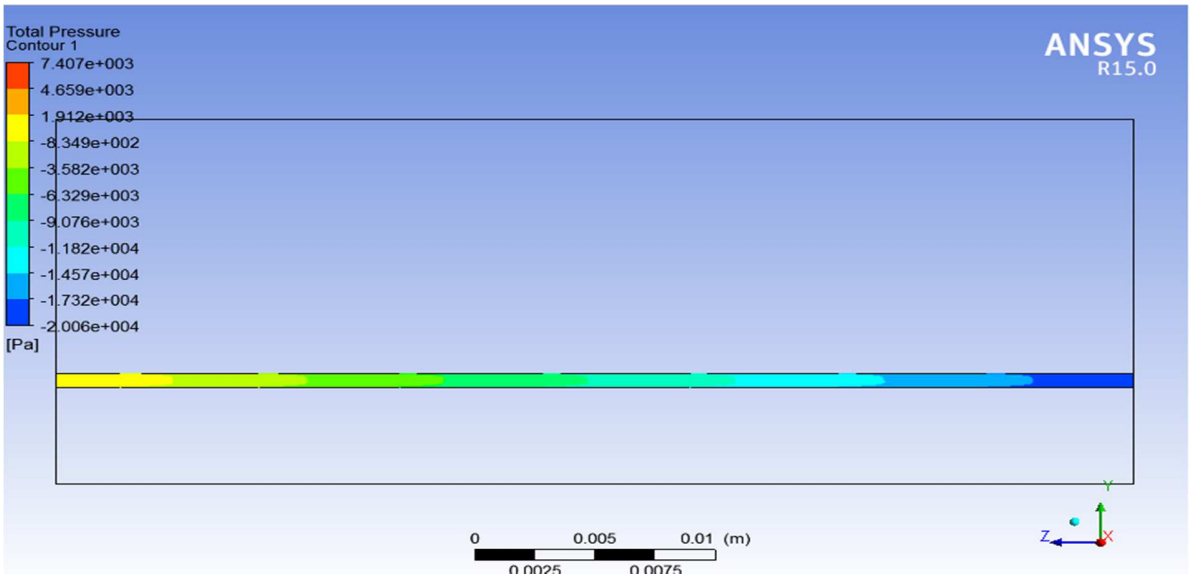

Figure 5.25: Pressure contour for water along the channel at Re=1000

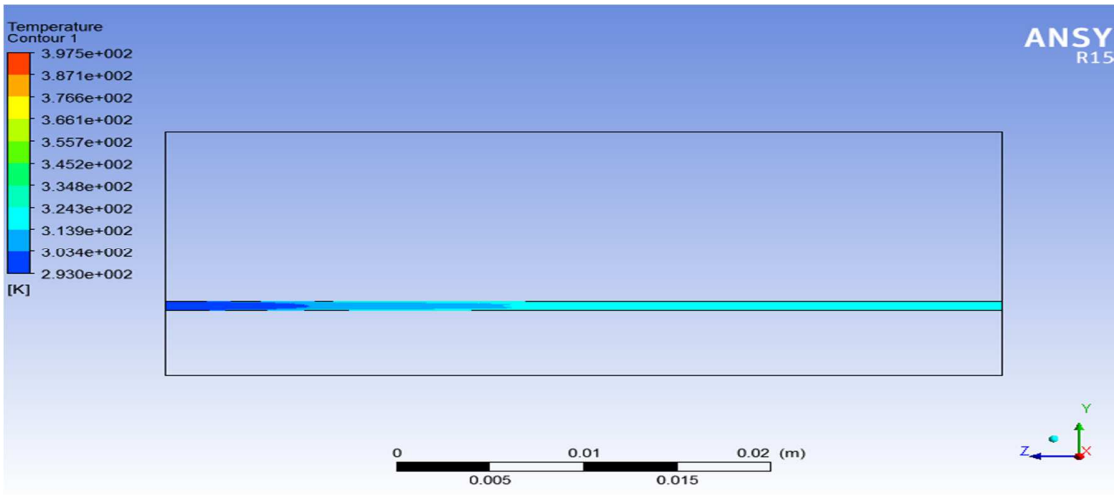

Figure 5.26: Temperature contour along the channel at Re=1000

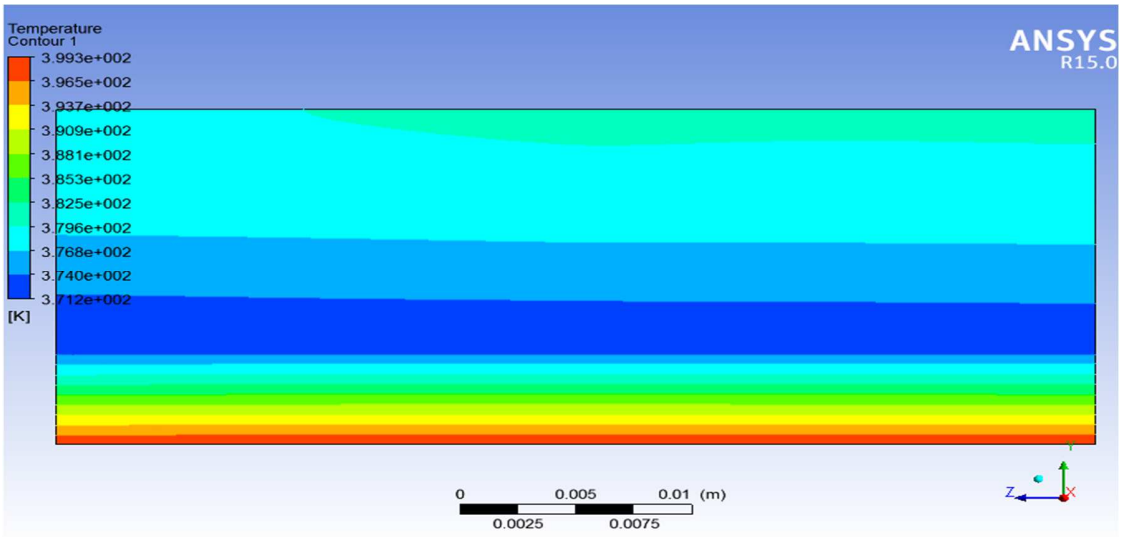

Figure 5.27: Temperature variation along the wall at Re=1000

- In the figures 5.25 to 5.27, the contours for pressure and temperature in a straight rectangular channel for Reynolds number value equal to 1000 are shown.
- In figure 5.25 pressure drop along the channel is found to be 0.27 bar.
- In figure 5.26 the temperature at the outlet of the channel is found to be 313 K.
- In figure 5.27 maximum wall temperature is at the bottom wall of the heat sink and is found to be 397 K and further the wall temperature increases in the direction of flow.

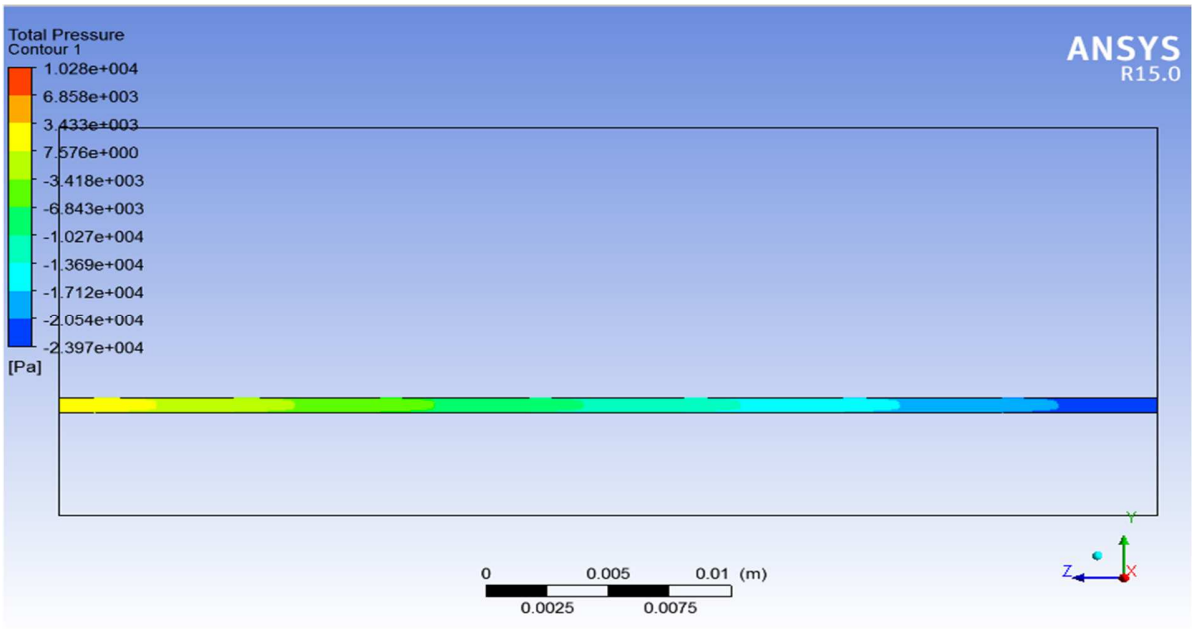

Figure 5.28: Pressure contour along channel at Re=1200

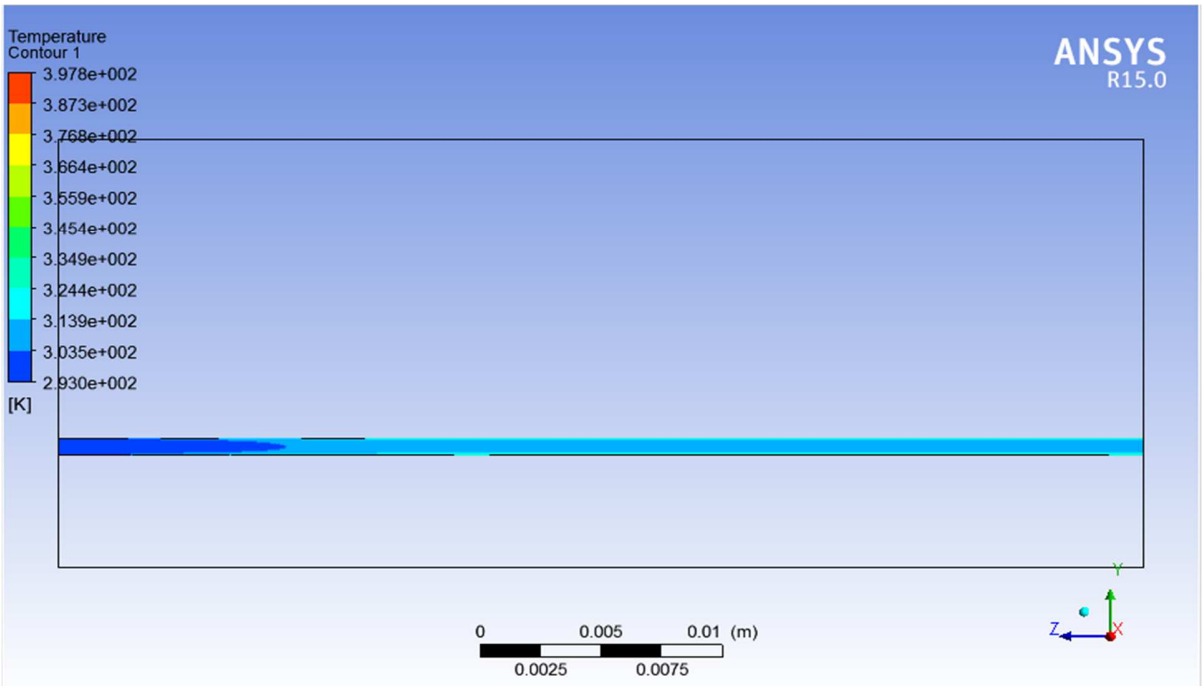

Figure 5.29: Temperature contour along the channel at Re=1200

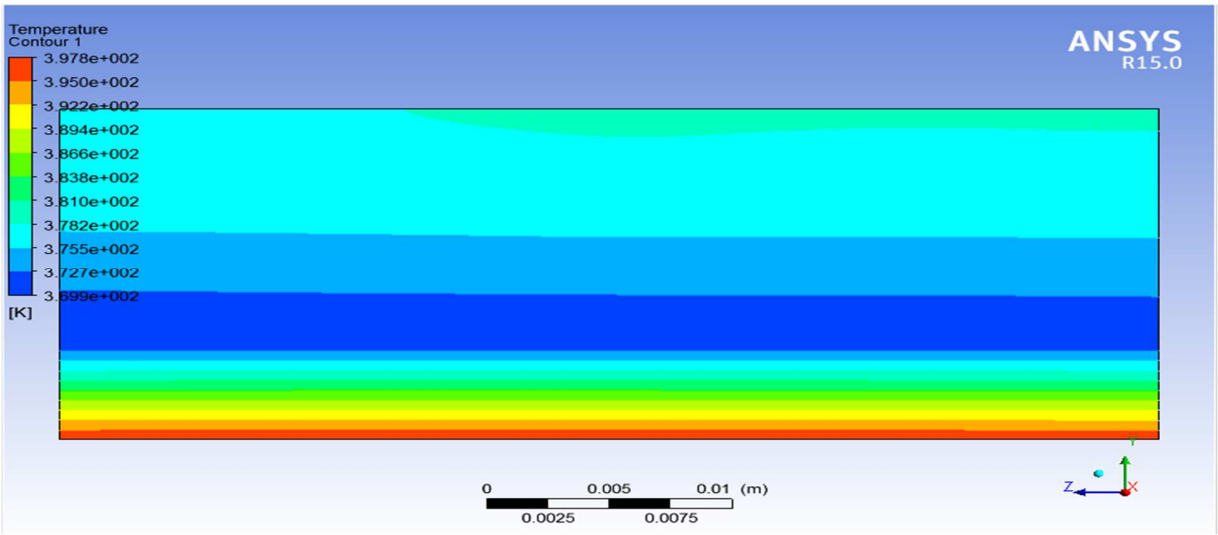

Figure 5.30: Temperature variation along the wall at Re=1200

In the figures 5.28 to 5.30, the contours for pressure and temperature in a straight rectangular channel for Reynolds number value equal to 1200 are shown.

- In figure 5.28 pressure drop along the channel is found to be 0.342 bar.
- In figure 5.29 the temperature at the outlet of the channel is found to be 310 K.
- In figure 5.30 maximum wall temperature is at the bottom wall of the heat sink and is found to be 396.5 K and further the wall temperature increases in the direction of flow.

5.2 Problem validation

Case 1

For the validation of the problem, the experimental pressure drop along the channel is compared with the computational pressure drop. The computational pressure drop from the pressure contours generated for different values of Reynolds number for 100W/cm^2 bottom wall heat flux are taken from figures 5.1, 5.4, 5.7, 5.10 and 5.13 respectively and for 200W/cm^2 bottom wall heat flux are taken form figures 5.16, 5.19, 5.22, 5.25, 5.28 respectively.

Table 5.1: Pressure drop for bottom wall heat flux value=100W/cm^2

Reynolds number	Experimental pressure drop (bar)	Computational pressure drop (bar)
400	0.10	0.09
600	0.17	0.15
800	0.23	0.21
1000	0.32	0.27
1200	0.41	0.34

Table 5.2: Pressure drop for bottom wall heat flux value=200W/cm^2

Reynolds number	Experimental pressure drop(bar)	Computational pressure drop (bar)
400	0.08	0.09
600	0.15	0.15
800	0.21	0.21
1000	0.30	0.27
1200	0.40	0.35

From table 5.1 and table 5.2 the values of computational pressure drop for heat flux values of 100W/cm^2 and 200W/cm^2 are found to be in close agreement with the experimental pressure

drop. Hence, the computational model is successfully validated on the basis of pressure drop along the channel length.

Case 2- For further validation the experimental temperature rise is compared with the computational temperature rise. The computational temperature rise taken from temperature contours generated for different values of Reynolds number for 100W/cm^2 bottom wall heat flux are taken from figures 5.2, 5.5, 5.8, 5.11 and 5.14 respectively and for 200W/cm^2 are taken from figures 5.17, 5.20, 5.23, 5.26, 5.29 respectively.

Table 5.3: Temperature rise for bottom wall heat flux value=100W/cm^2

Reynolds number	Experimental temperature rise (°C)	Computational temperature rise (°C)
400	22	21
600	16	15.5
800	10	12
1000	8	10
1200	6	8

Table 5.4: Temperature rise for bottom wall heat flux of 200 W/cm^2

Reynolds number	Experimental temperature rise (°C)	Computational temperature rise (°C)
400	44	48
600	31	35
800	22	27
1000	18	20
1200	15	17

From table 5.3 and table 5.4 the values of computational temperature rise for heat flux values of 100W/cm^2 and 200W/cm^2 are found to be in close agreement with the experimental temperature

rise. Hence, the computational model is successfully validated on the basis of temperature rise along the length of channel.

5.3 Graphical validation

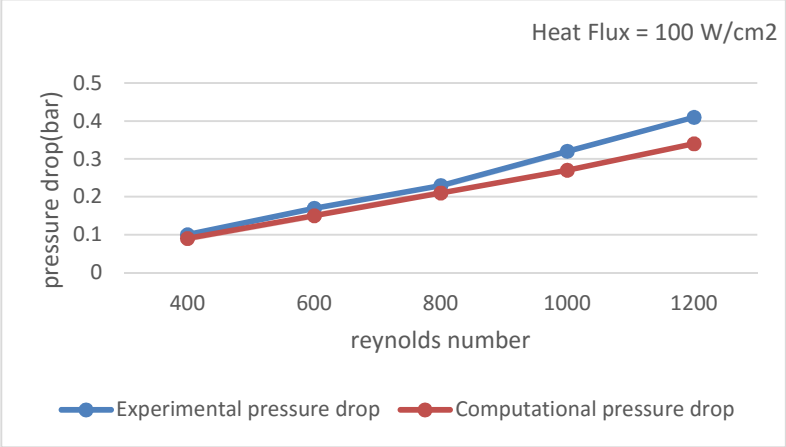

Figure 5.31: Pressure drop vs Reynolds number

Figure 5.31 shows comparison of experimental and numerical pressure drop results for varying sets of Reynolds number for heat flux=100W/cm^2.

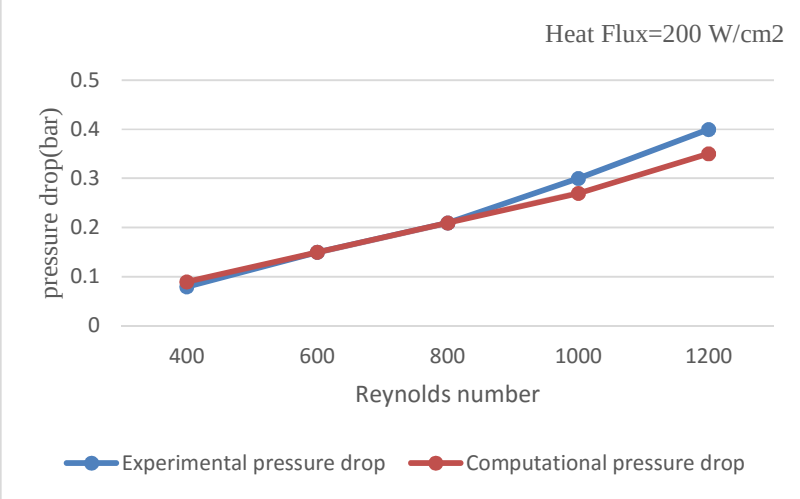

Figure 5.32: pressure drop vs Reynolds number

Figure 5.32 shows comparison of experimental and numerical pressure drop results for varying sets of Reynolds number for heat flux=200W/cm^2.

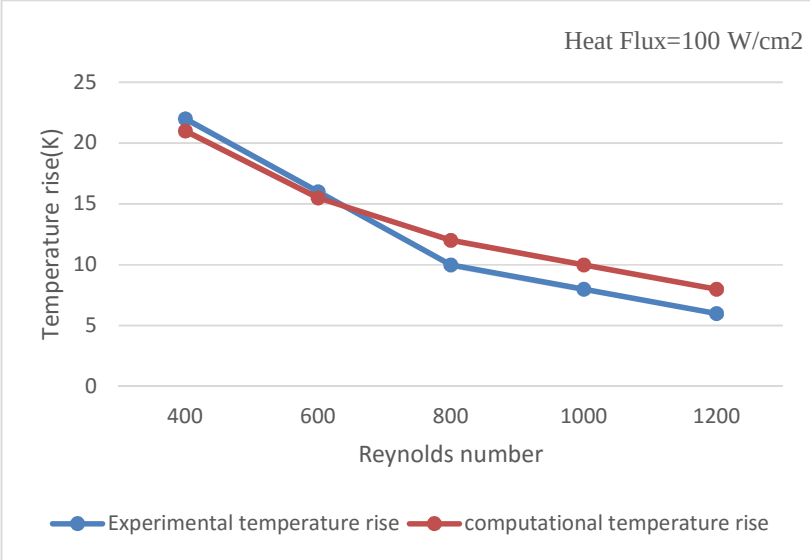

Figure 5.33: Temperature rise vs Reynolds number

Figure 5.33 shows the comparison of experimental and numerical temperature rise results for varying sets of Reynolds number for heat flux =100W/cm^2

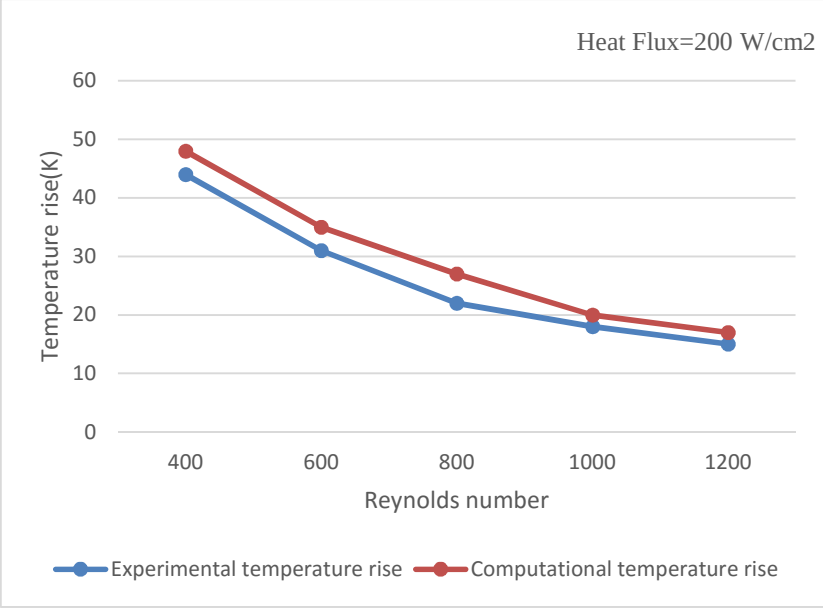

Figure 5.34: Temperature rise vs Reynolds number

Figure 5.34 shows the comparison of experimental and numerical temperature rise results for varying sets of Reynolds number for heat flux =200W/cm^2

CHAPTER 6

SIMULATION RESULTS

6.1 Simulation results for wavy edge rectangular microchannel heat sink with hemispherical obstructions-

In the following computational fluid dynamics analysis the results are plotted for temperature rise and heat transfer in wavy edge type rectangular microchannel for two different values of heat fluxes applied at the bottom of the heat sink for varying set of values of Reynolds number. The value of heat flux used in the analysis are 100W/$cm^2$and 200W/cm^2. Five values of Reynolds number are taken for the analysis which are 400, 600, 800, 1000 and 1200 respectively.

Results for heat flux= 100W/$cm^2$for different sets of Reynolds number

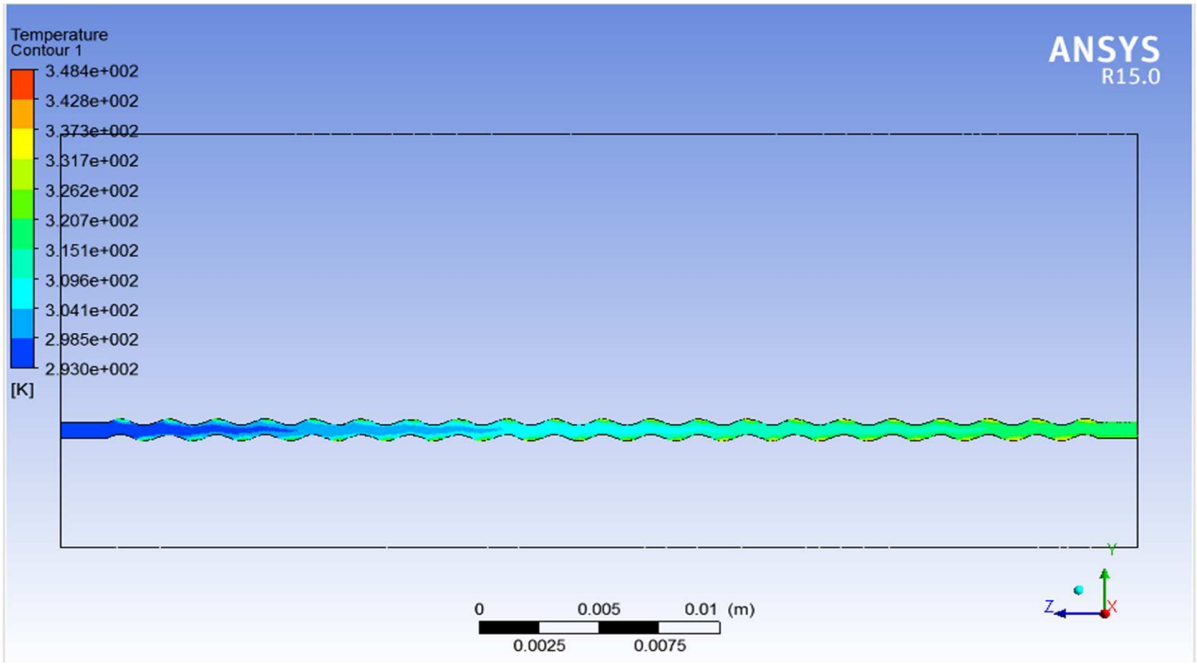

Figure 6.1: Temperature contour of water along wavy channel at Re=400

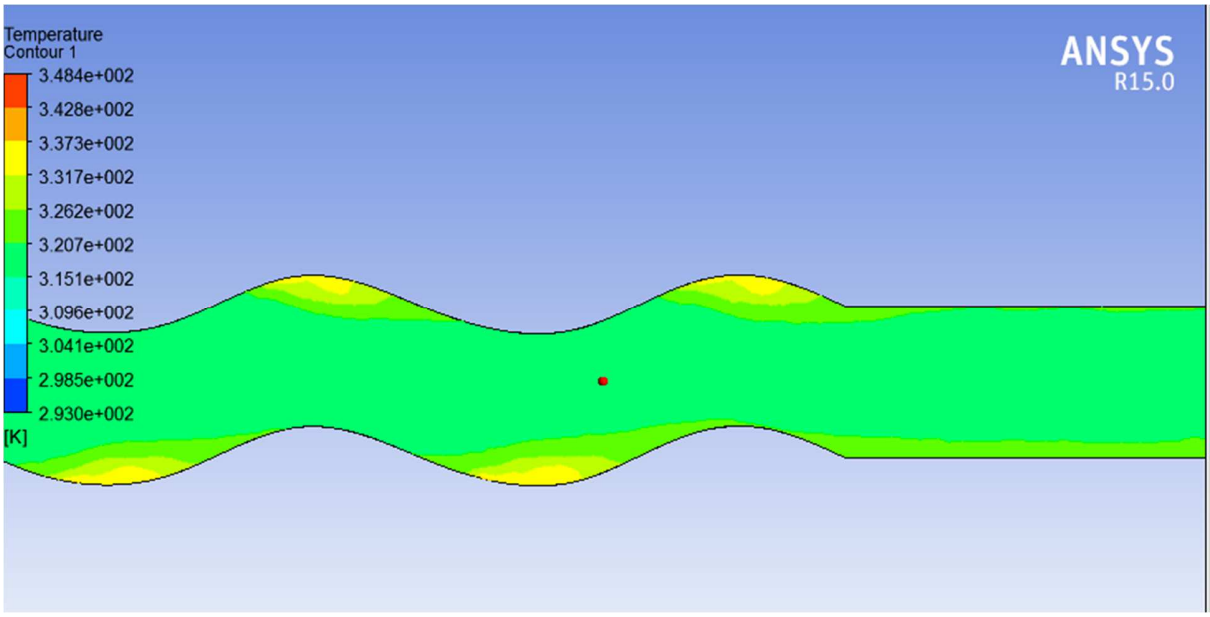

Figure 6.2: Temperature contour at the outlet of wavy channel at Re=400

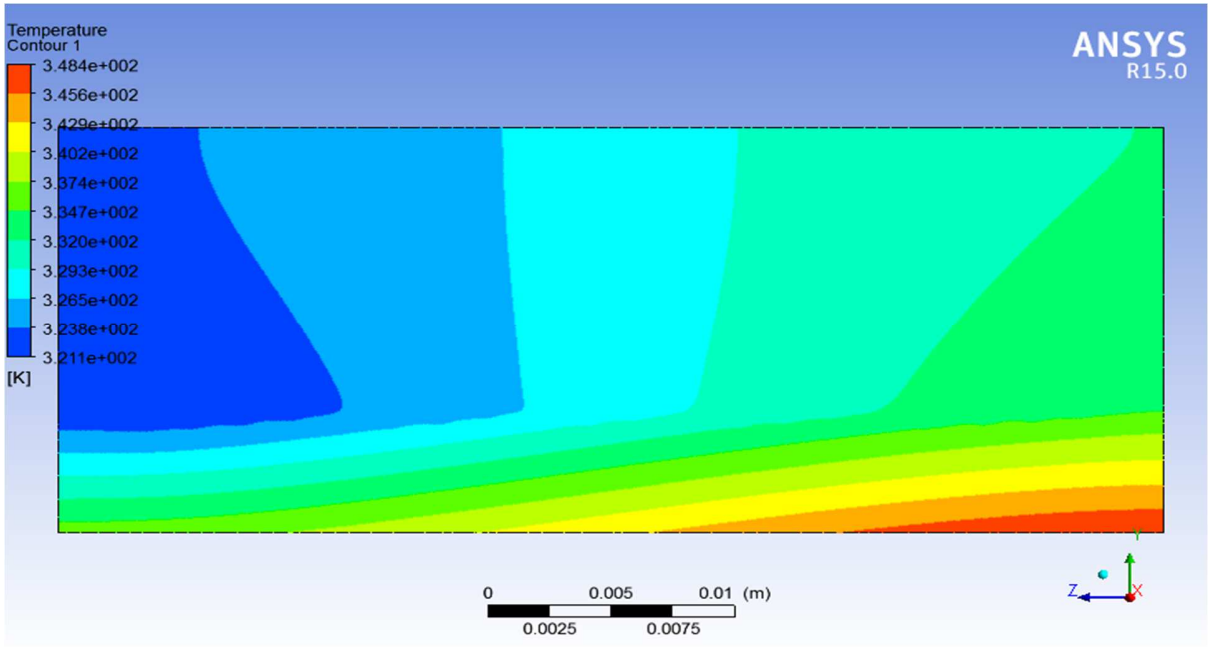

Figure 6.3: Temperature variation along the wall at Re=400

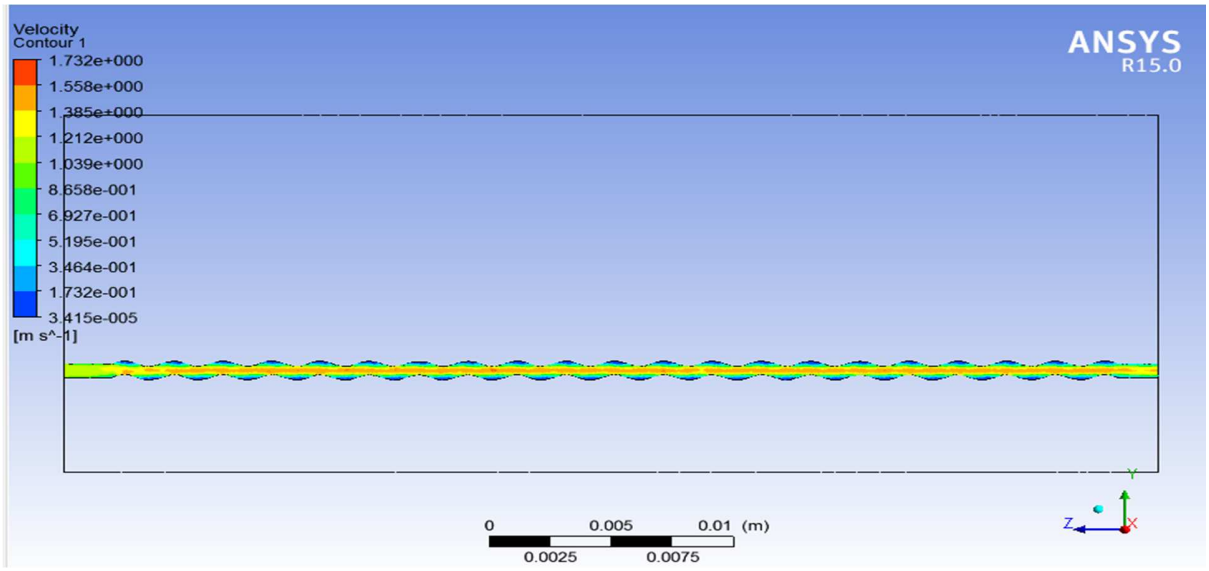

Figure 6.4: velocity contour along wavy channel at Re= 400

In the figures 6.1 to 6.4, the contours for temperature and velocity in a wavy edge rectangular channel for Reynolds number value equal to 400 are shown.

- In figure 6.2 temperature at the outlet of the channel is found to be 326 K.
- In figure 6.3 Maximum wall temperature is at the bottom wall of the heat sink and is found to be 348 K and further the wall temperature increases in the direction of flow.

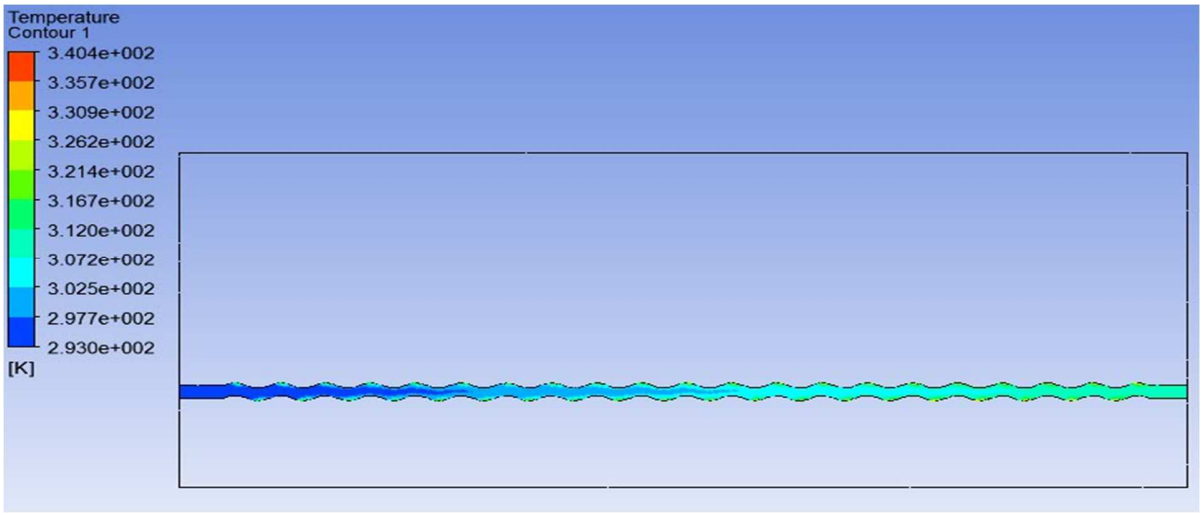

Figure 6.5: Temperature contour of water along wavy channel at Re= 600

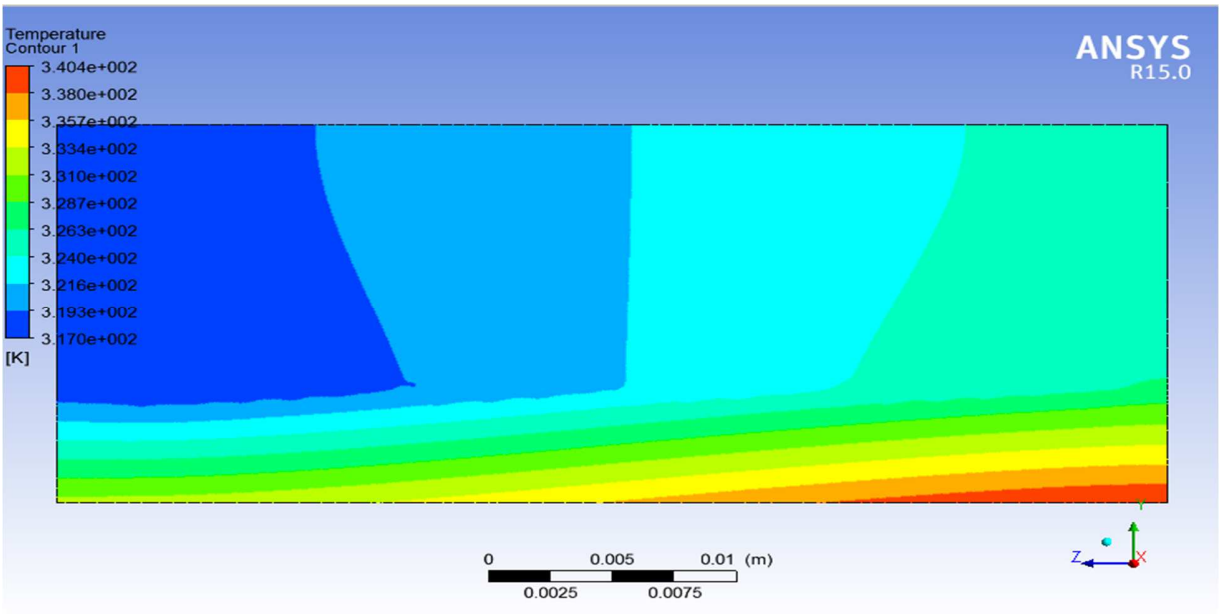

Figure 6.6: Temperature variation along the wall at Re=600

In the figures 6.5 to 6.6, the contours for temperature in a wavy edge rectangular channel for Reynolds number value equal to 600 are shown.

- In figure 6.5 Temperature at the outlet of the channel is found to be 318 K.
- In figure 6.6 Maximum wall temperature is at the bottom wall of the heat sink and is found to be 340 K and further the wall temperature increases in the direction of flow.

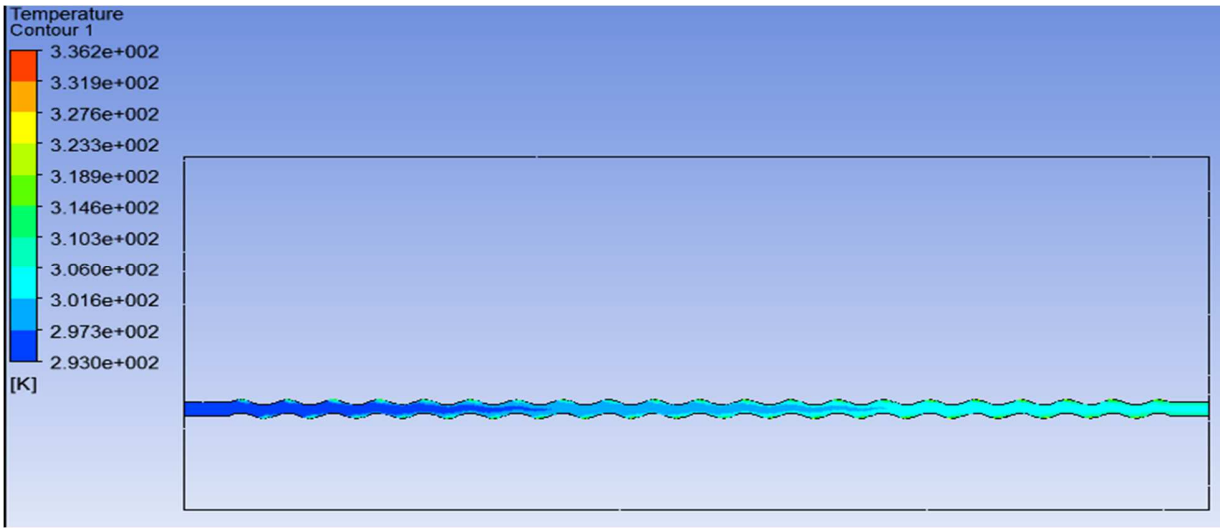

Figure 6.7: Temperature contour of water along wavy channel at Re=800

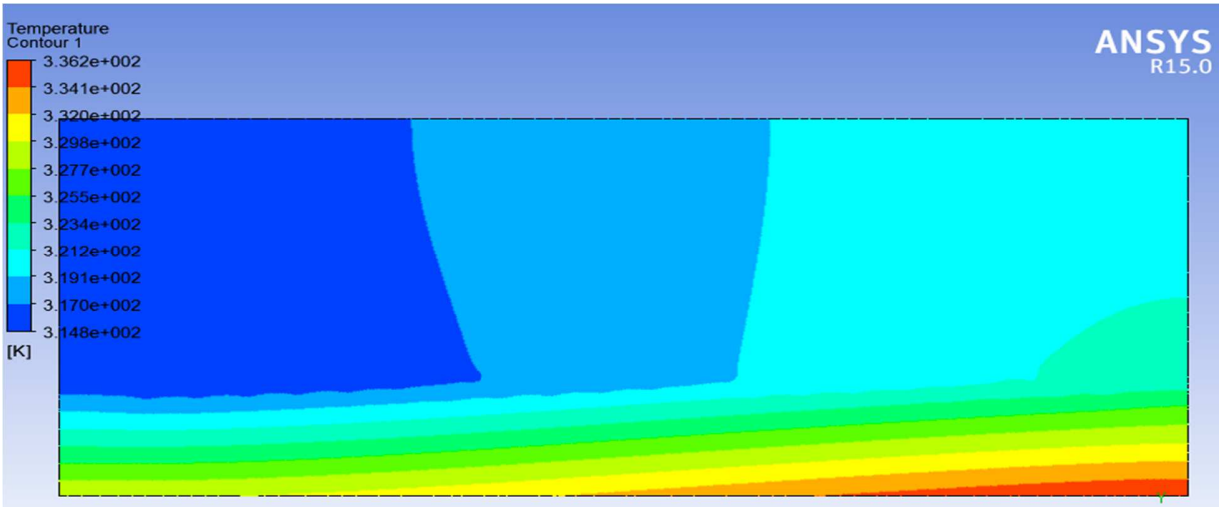

Figure 6.8: Temperature variation along the wall at Re=800

In the figures 6.7 to 6.8, the contours for temperature and in a wavy edge rectangular channel for Reynolds number value equal to 800 are shown.

- In figure 6.7 Temperature at the outlet of the channel is found to be 314 K.
- In figure 6.8 Maximum wall temperature is at the bottom wall of the heat sink and is found to be 336 K and further the wall temperature increases in the direction of flow.

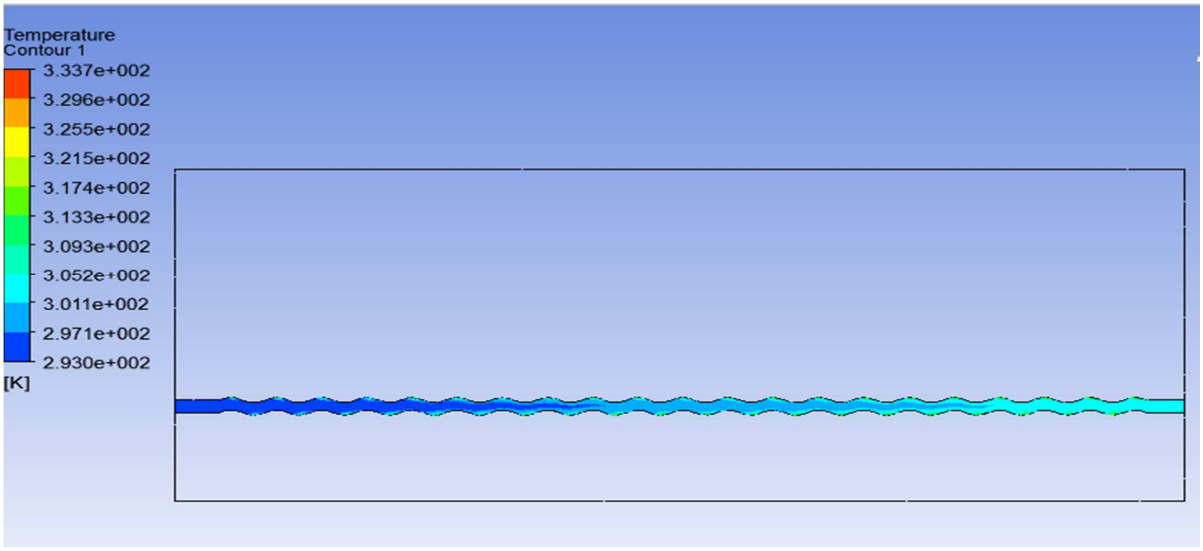

Figure 6.9: Temperature contour of water along wavy channel at Re=1000

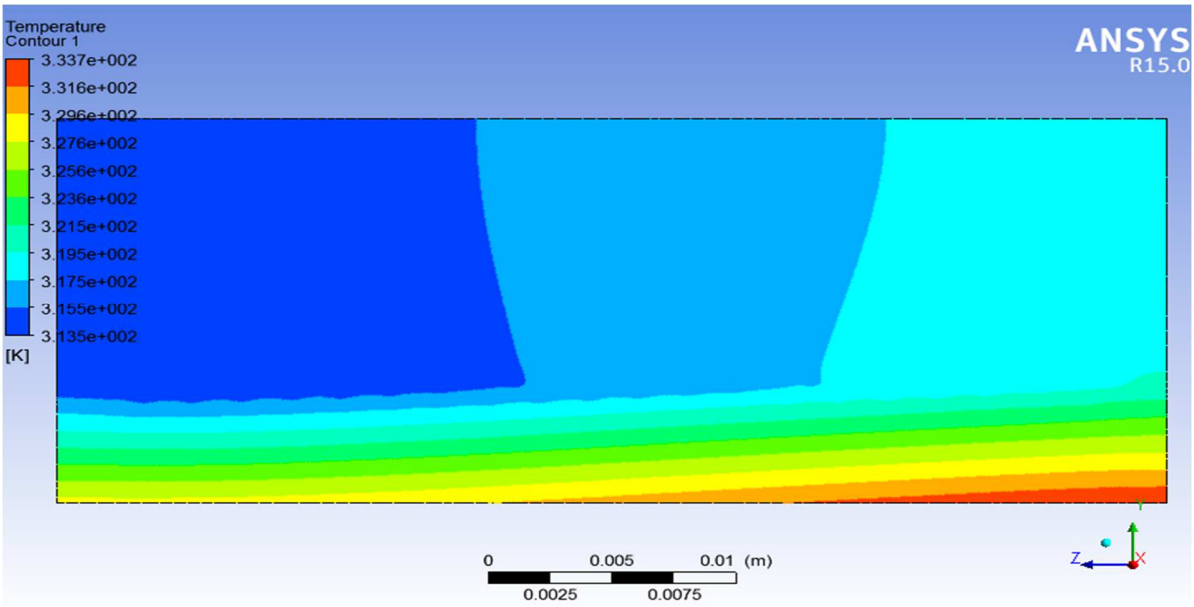

Figure 6.10: Temperature variation along the wall at Re=1000

In the figures 6.9 to 6.10, the contours for temperature in a wavy edge rectangular channel for Reynolds number value equal to 1000 are shown.

- In figure 6.9 Temperature at the outlet of the channel is found to be 311 K.
- In figure 6.10 Maximum wall temperature is at the bottom wall of the heat sink and is found to be 333 K and further the wall temperature increases in the direction of flow.

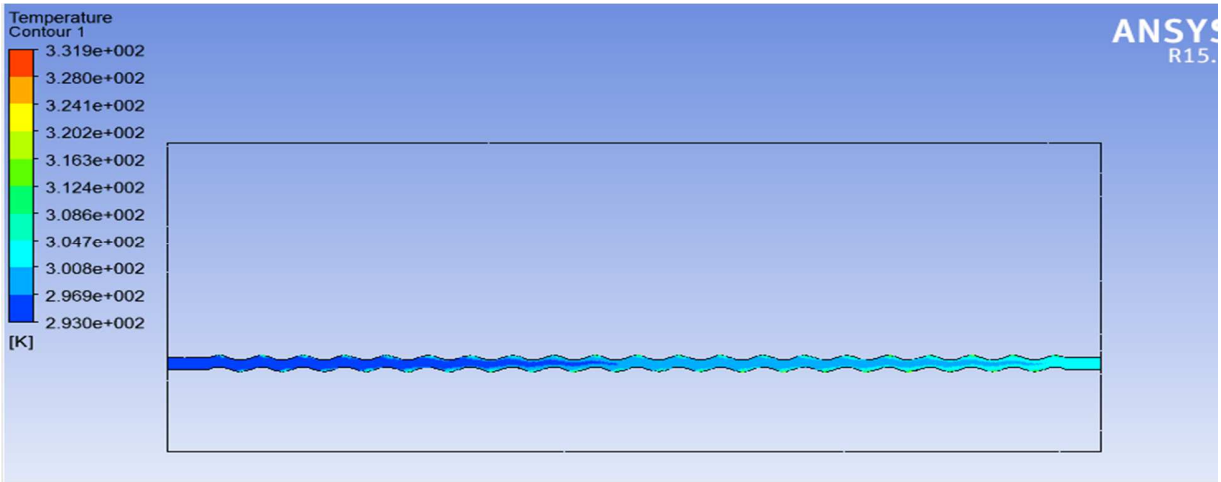

Figure 6.11: Temperature contour of water along wavy channel at Re=1200

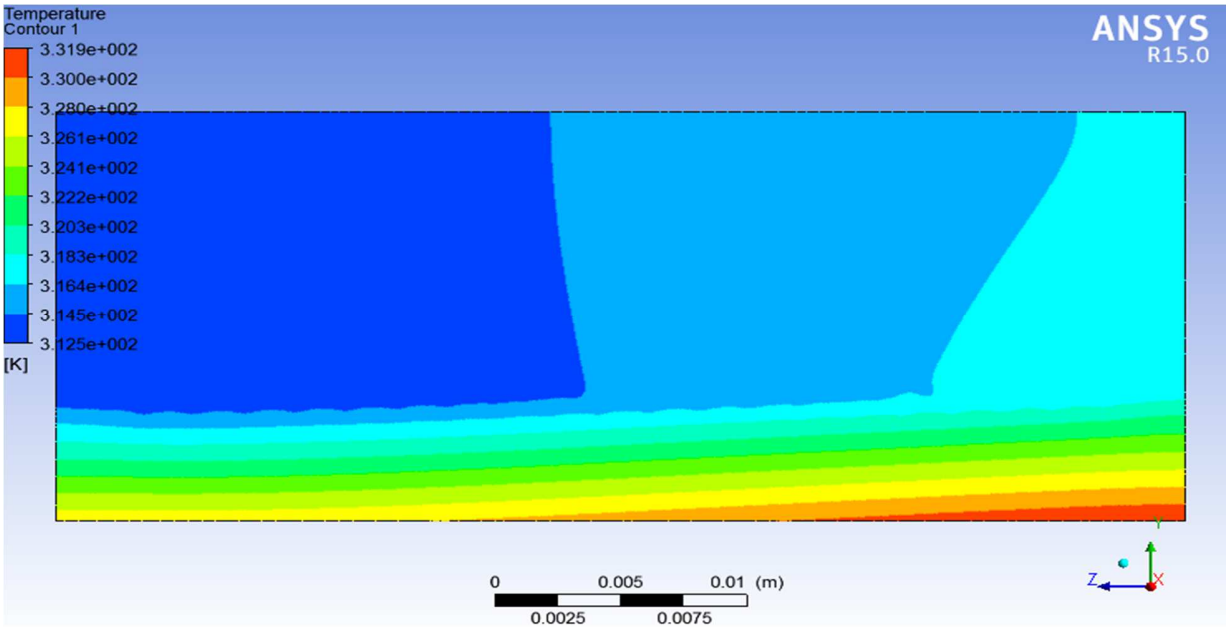

Figure 6.12: Temperature variation along the wall at Re=1200

In the figures 6.11 to 6.12 the contours for temperature in a wavy edge rectangular channel for Reynolds number value equal to 1200 are shown.

- In figure 6.11 Temperature at the outlet of the channel is found to be 310 K.
- In figure 6.12 Maximum wall temperature is at the bottom wall of the heat sink and is found to be 331 K and further the wall temperature increases in the direction of flow.

Results for heat flux of 200 W/cm^2 and different sets of Reynolds number

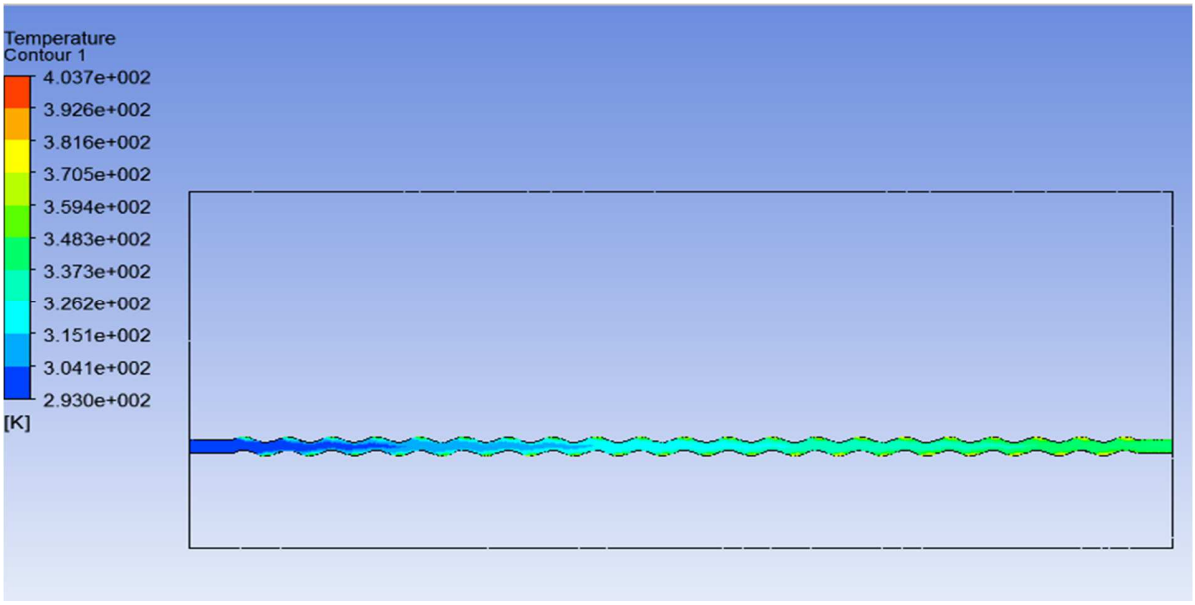

Figure 6.13: Temperature contour along wavy channel at Re=400.

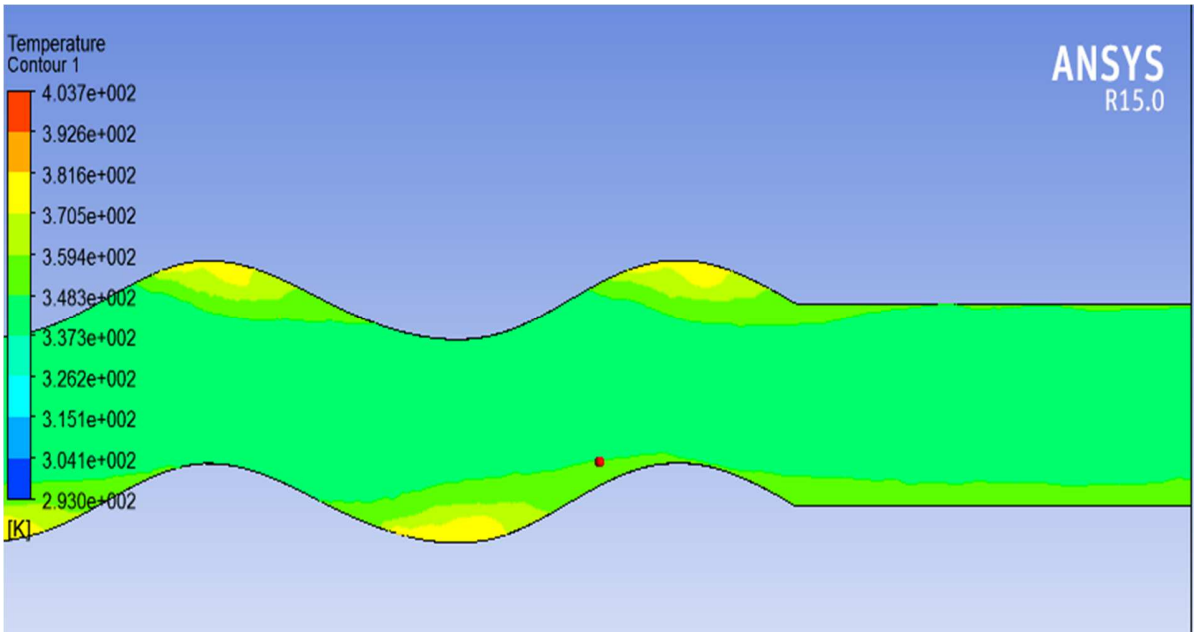

Figure 6.14: Temperature contour closer to outlet of wavy channel at Re=400

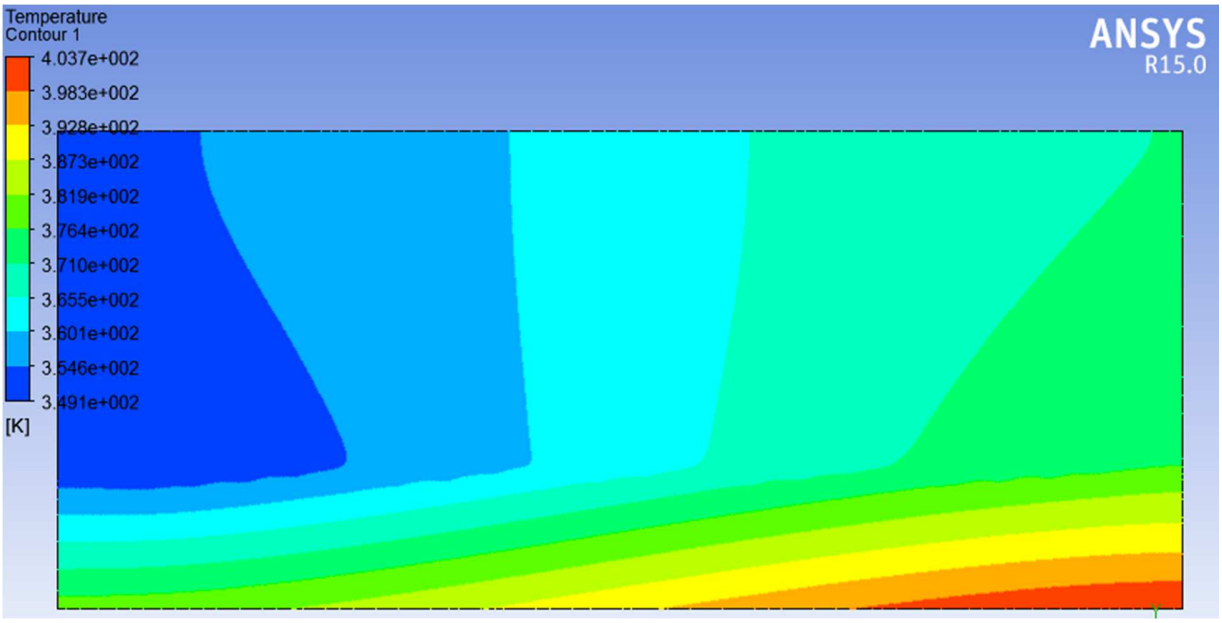

Figure 6.15: Temperature variation along the wall at Re=400

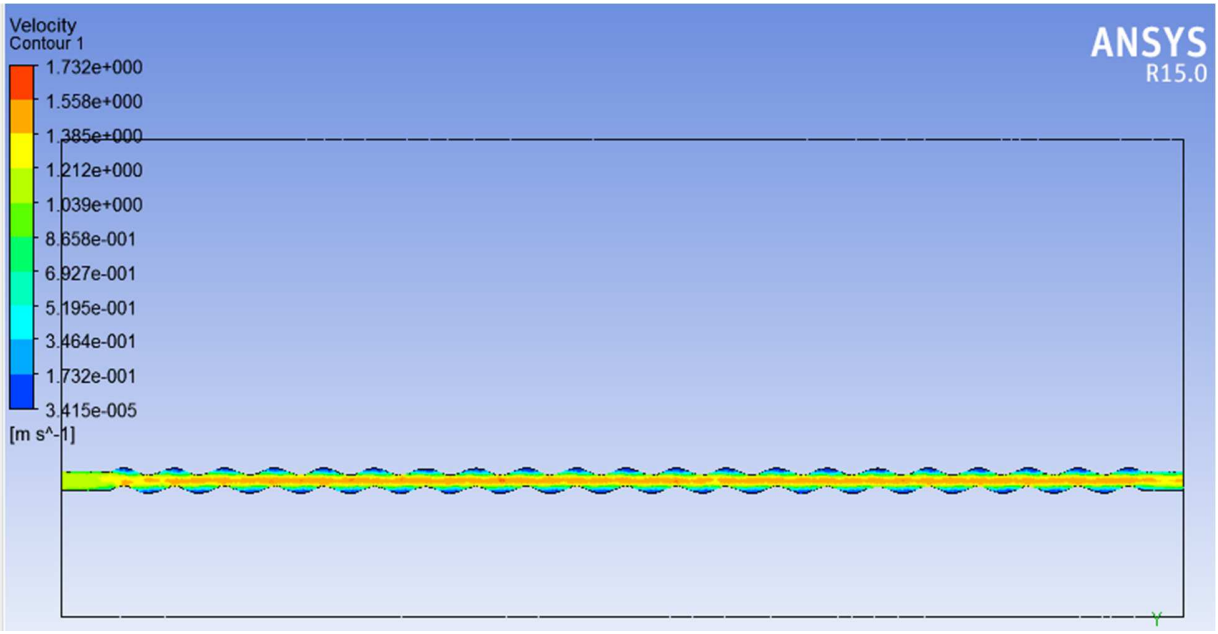

Figure 6.16: velocity contour along wavy channel at Re=400.

In the figures 6.13 to 6.16, the contours for temperature in a wavy edge rectangular channel for Reynolds number value equal to 400 are shown.

- In figure 6.14 temperature at the outlet of the channel is found to be 361 K.
- In figure 6.15 maximum wall temperature is at the bottom wall of the heat sink and is found to be 403 K and further the wall temperature increases in the direction of flow.

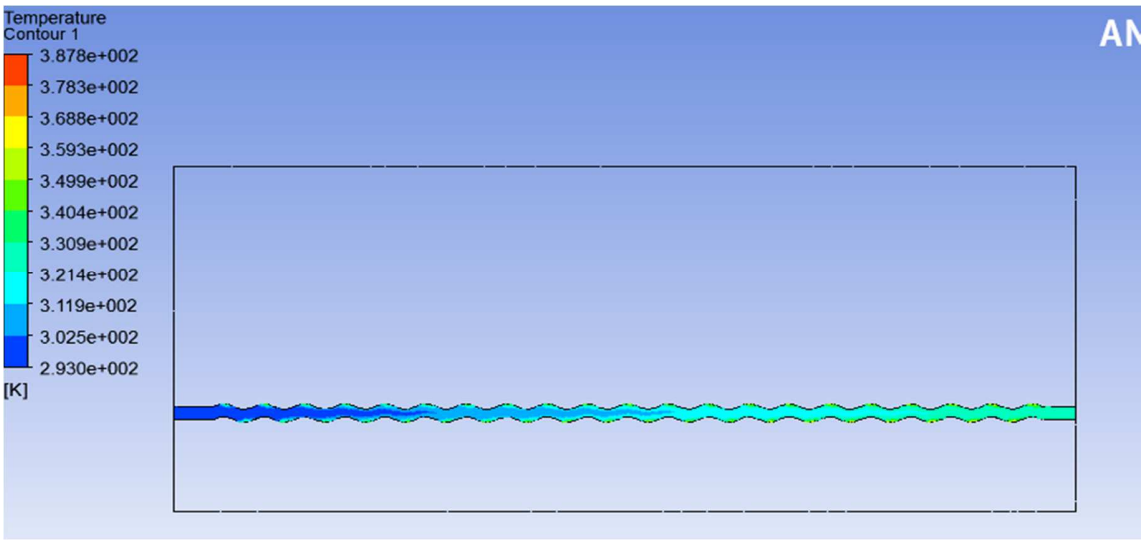

Figure 6.17: Temperature contour along wavy channel at Re=600

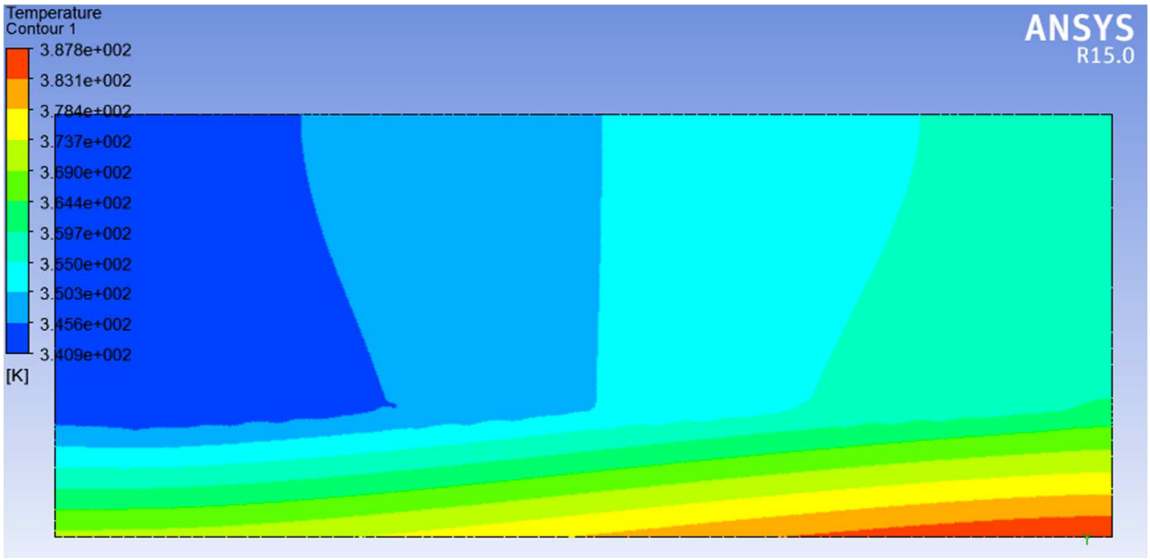

Figure 6.18: Temperature variation along the wall at Re=600

In the figures 6.17 to 6.18, the contours for temperature in a wavy edge rectangular channel for Reynolds number value equal to 600 are shown.

- In figure 6.17 temperature at the outlet of the channel is found to be 344 K.
- In figure 6.18 maximum wall temperature is at the bottom wall of the heat sink and is found to be 387 K and further the wall temperature increases in the direction of flow.

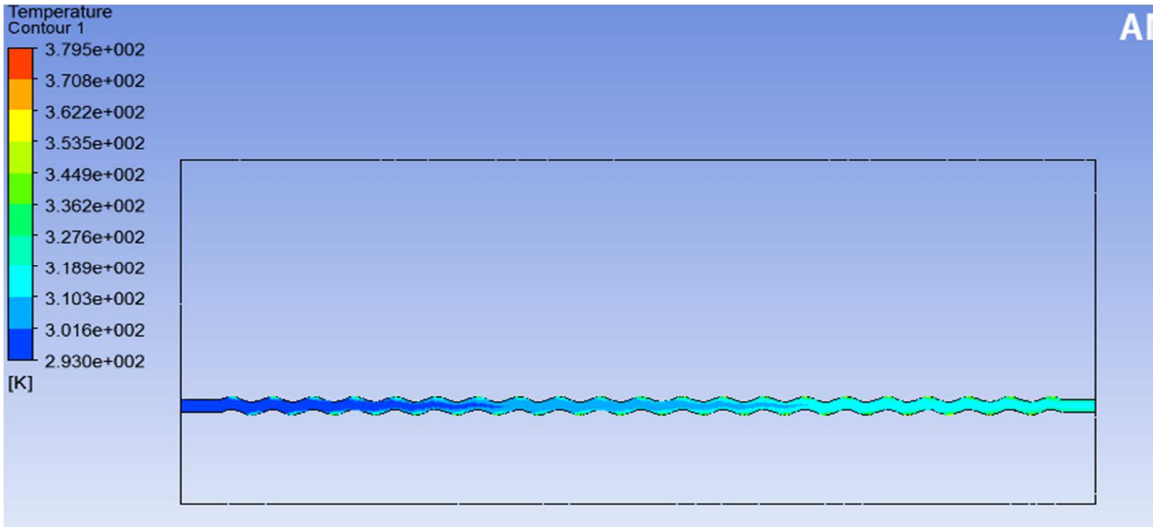

Figure 6.19: Temperature contour along wavy channel at Re=800

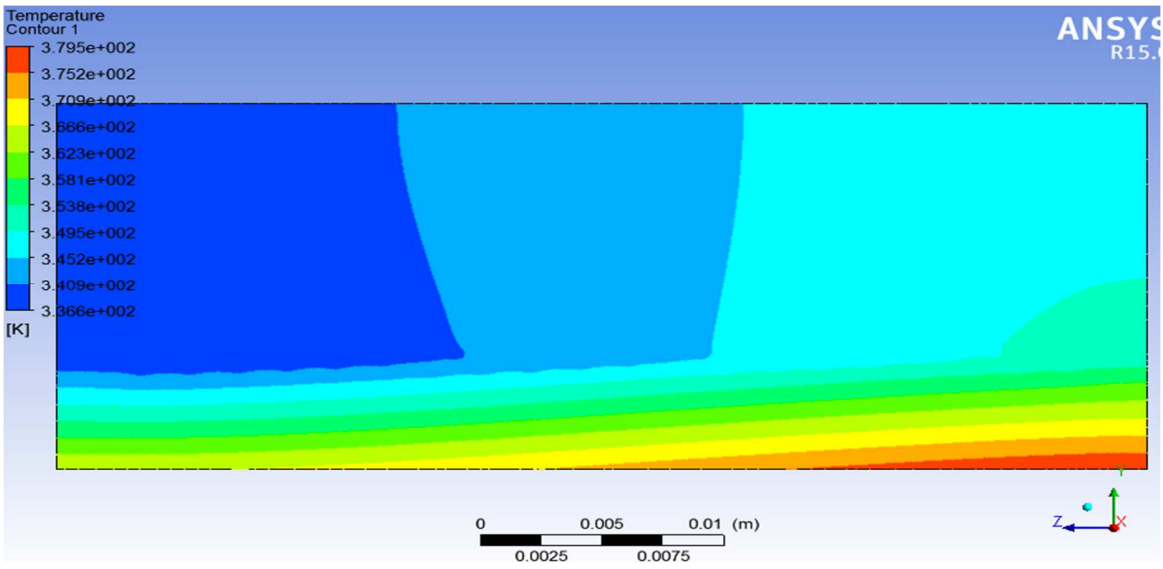

Figure 6.20: Temperature variation along the wall at Re=800

In the figures 6.19 to 6.20, the contours for temperature in a wavy edge rectangular channel for Reynolds number value equal to 800 are shown.

- In figure 6.19 Temperature at the outlet of the channel is found to be 324 K.
- In figure 6.20 Maximum wall temperature is at the bottom wall of the heat sink and is found to be 379 K and further the wall temperature increases in the direction of flow.

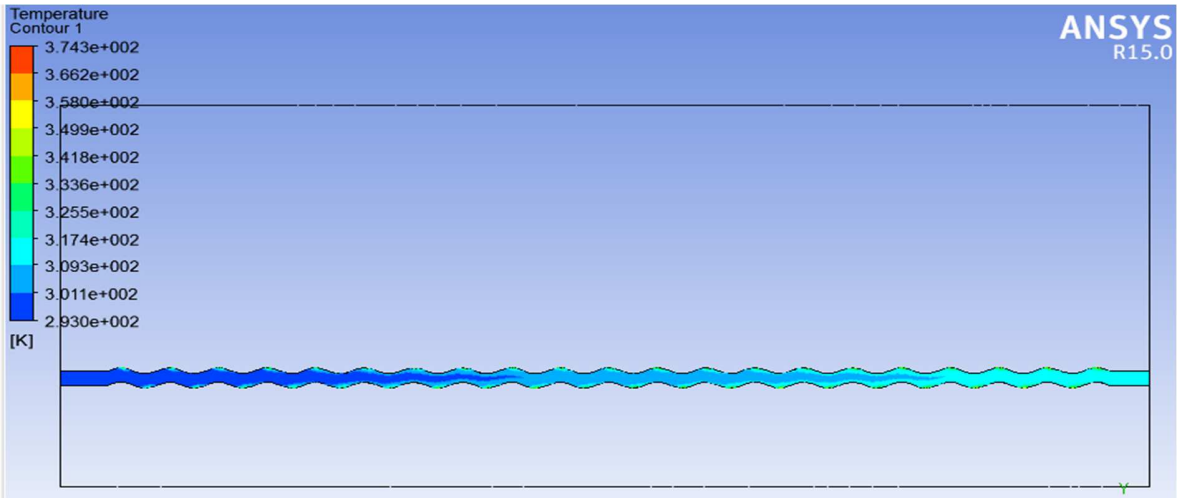

Figure 6.21: Temperature contour along wavy channel at Re=1000

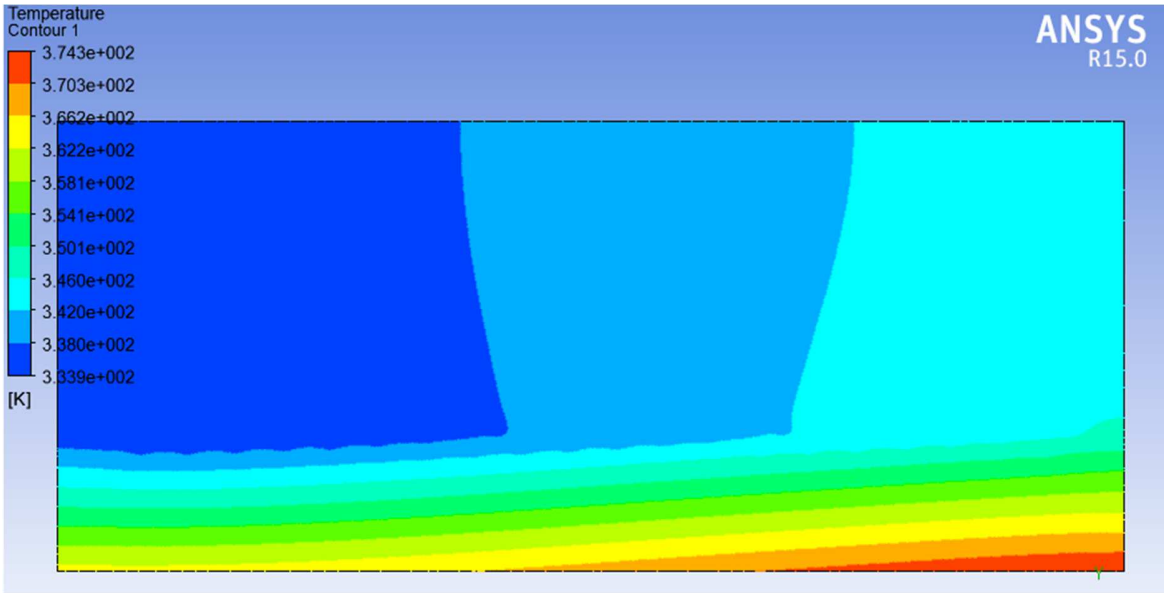

Figure 6.22: Temperature variation along the wall at Re=1000

In the figures 6.21 to 6.22, the contours for temperature in a wavy edge rectangular channel for Reynolds number value equal to 1000 are shown.

- In figure 6.21 temperature at the outlet of the channel is found to be 331 K.
- In figure 6.22 Maximum wall temperature is at the bottom wall of the heat sink and is found to be 374 K and the wall temperature increases in the direction of flow.

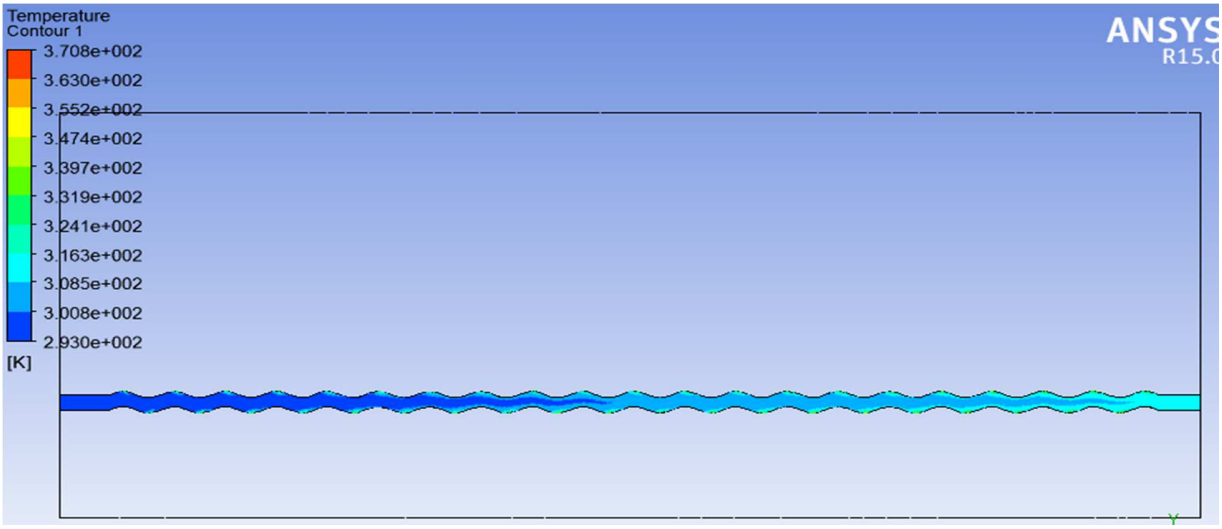

Figure 6.23: Temperature contour along wavy channel at Re=1200

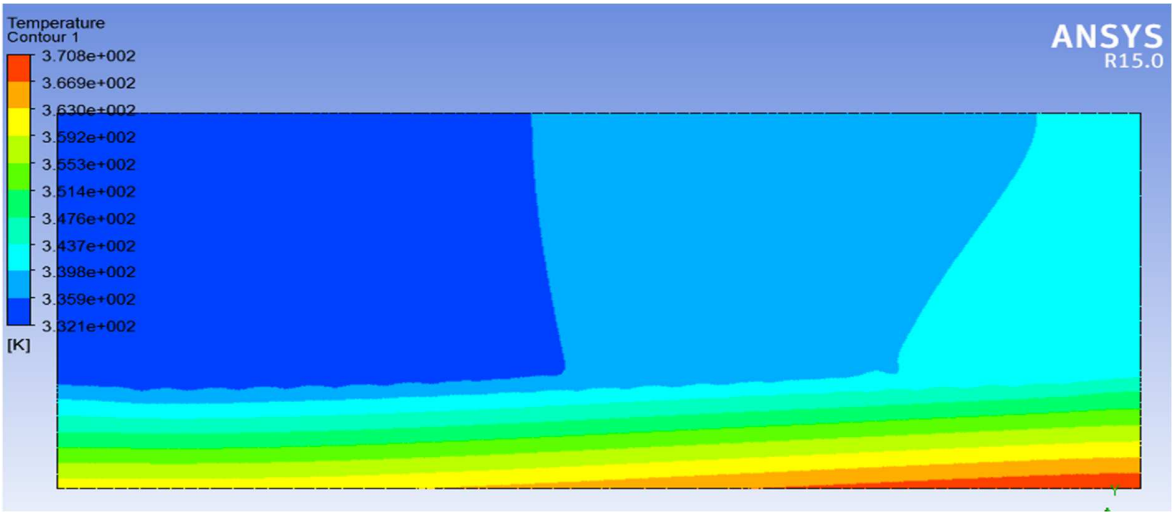

Figure 6.24: Temperature variation along the wall at Re=1200

In the figures 6.23 to 6.24, the contours for temperature in a wavy edge rectangular channel for Reynolds number value equal to 1200 are shown.

- In figure 6.23 Temperature at the outlet of the channel is found to be 328 K.
- In figure 6.24 Maximum wall temperature is at the bottom wall of the heat sink and is found to be 370 K and further the wall temperature increases in the direction of flow.

The computational temperature rise taken from the temperature contours generated for different sets of Reynolds number for 100W/cm^2 bottom wall heat flux are taken from figures 6.1, 6.5, 6.7, 6.9 and 6.11 respectively.

Table 6.1: Temperature rise for different Reynolds number for heat flux=100W/cm^2

Reynolds number	Computational temperature rise(°C)
400	27
600	23
800	21
1000	19
1200	18

The computational temperature rise taken from the temperature contours generated for different sets of Reynolds number for 200W/cm^2 bottom wall heat flux are taken from figures 6.13, 6.17, 6.19, 6.21 and 6.23 respectively.

Table 6.2: Temperature rise for different Reynolds number for heat flux =200W/cm^2

Reynolds number	Computational temperature rise (°C)
400	55
600	47
800	43
1000	40
1200	38

The maximum computational velocity taken from velocity contours generated for different sets of Reynolds number for 100W/cm^2 bottom wall heat flux are

Table 6.3: Maximum velocity for different Reynolds number for heat flux =100W/cm^2

Reynolds number	Maximum computational velocity(m/s)
400	1.731
600	2.534
800	3.325
1000	4.100
1200	4.890

The maximum computational velocity taken from velocity contours generated for different sets of Reynolds number for 200W/cm^2 bottom wall heat flux are

Table 6.4: maximum velocity for different Reynolds number for heat flux =200W/cm^2

Reynolds number	Maximum computational velocity(m/s)
400	1.731
600	2.534
800	3.325
1000	4.100
1200	4.890

6.2 Graphical result

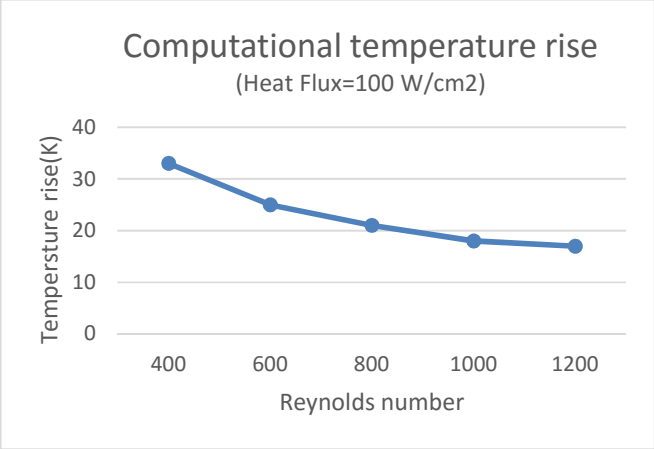

Figure 6.25: Temperature rise vs Reynolds number

Figure 6.25 shows the computational temperature rise results for varying sets of Reynolds number for heat flux =100W/cm^2

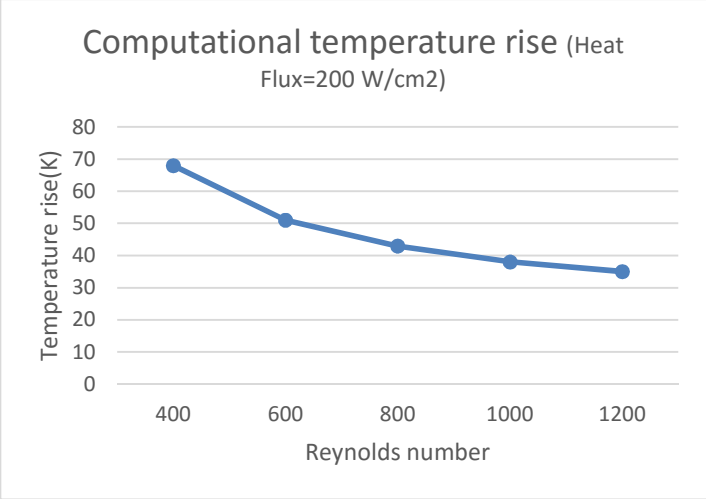

Figure 6.26: Temperature rise vs Reynolds number

Figure 6.26 shows the computational temperature rise results for varying sets of Reynolds number for heat flux =100W/cm^2

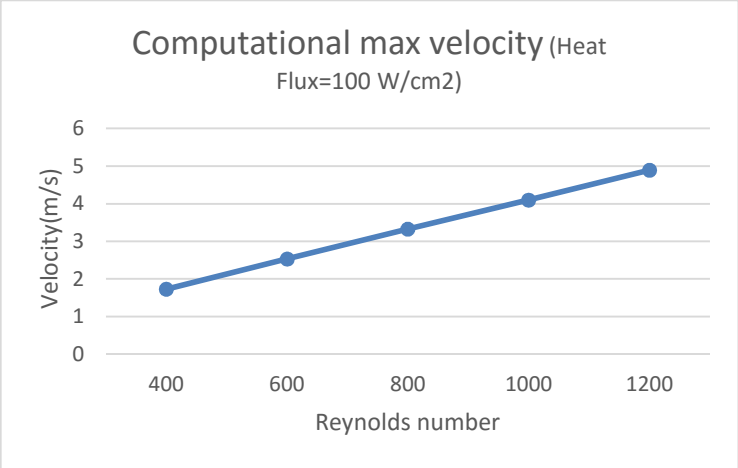

Figure 6.27: Maximum velocity vs Reynolds number

Figure 6.27 shows the computational maximum velocity results for varying sets of Reynolds number for heat flux =100W/cm^2

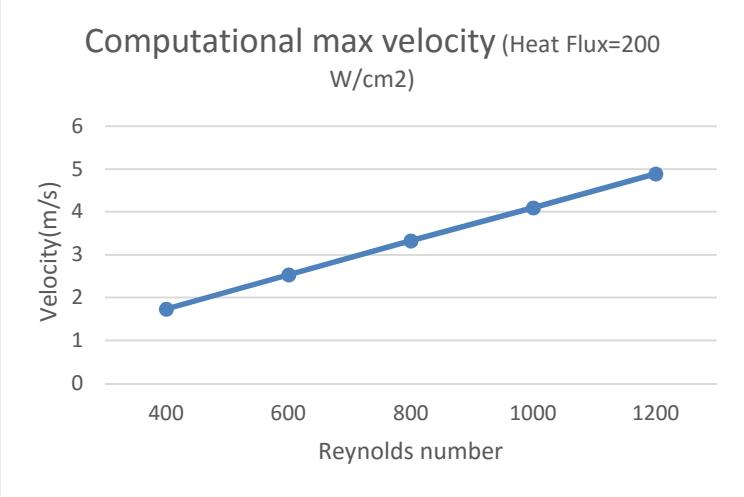

Figure 6.28: Maximum velocity vs Reynolds number

Figure 6.28 shows the computational maximum velocity results for varying sets of Reynolds number for heat flux =200W/cm^2

CHAPTER 7

SIMULATION RESULTS

7.1 Simulation results for wavy microchannel channel with hemispherical obstruction using performance fluid PF5052 as a coolant-

In the following computational fluid dynamics analysis, the simulation the done by using performance fluid PF5052, and the results are plotted for temperature rise heat in wavy edge micro-channel for two different values of heat fluxes applied at the bottom of the heat sink for varying set of values of Reynolds number. The value of heat flux used in the analysis are 100W/$cm^2$and 200W/cm^2. Five values of Reynolds number are taken for the analysis which are 400, 600, 800, 1000 and 1200 respectively.

Performance fluid PF5052-

Performance Fluid PF-5052 is a clear, colourless, fully-fluorinated liquid ideal for use in medium temperature range heat transfer applications. Like other 3M Performance Fluids, PF-5052 fluid is chemically and thermally stable, practically non-toxic, and non-flammable. The unique solvent properties of PF-5052 fluid also make this an ideal solvent for depositing or removing fluorinated oils and lubricants.

Table 7.1: Thermal Properties of Performance Fluid PF5052

FLUID	ρ (kg/m3)	Cp(J/kg-K)	K(w/m-K)	μ(kg/m-s)
PF-5052	1776	1014	0.065	97.77×10^{-5}

Results for heat flux= 100W/$cm^2$for different sets of Reynolds number

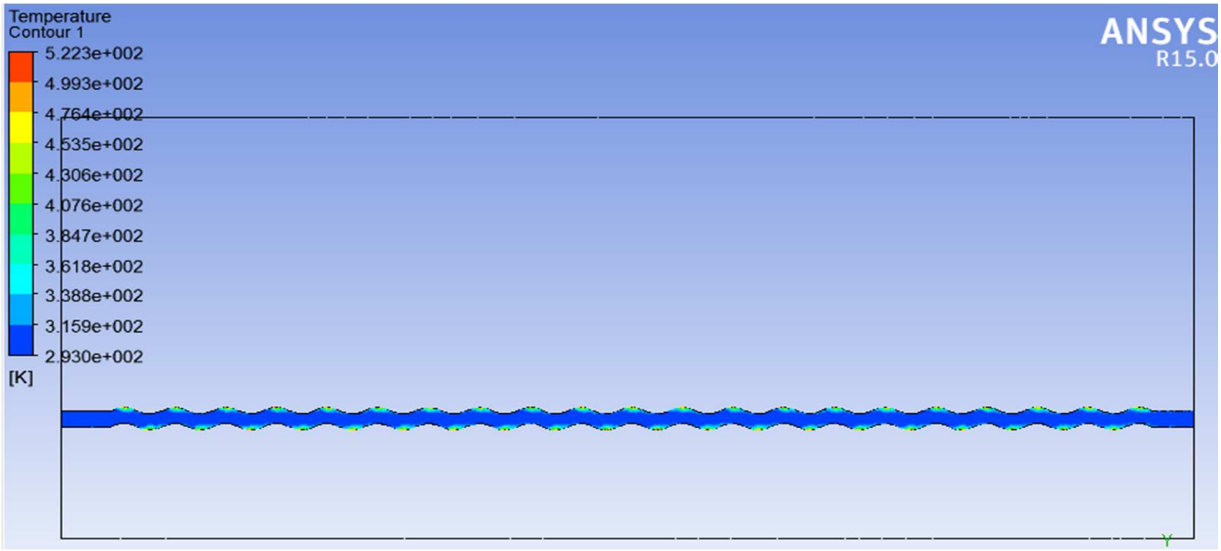

Figure 7.1: Temperature contour along wavy channel at Re=400

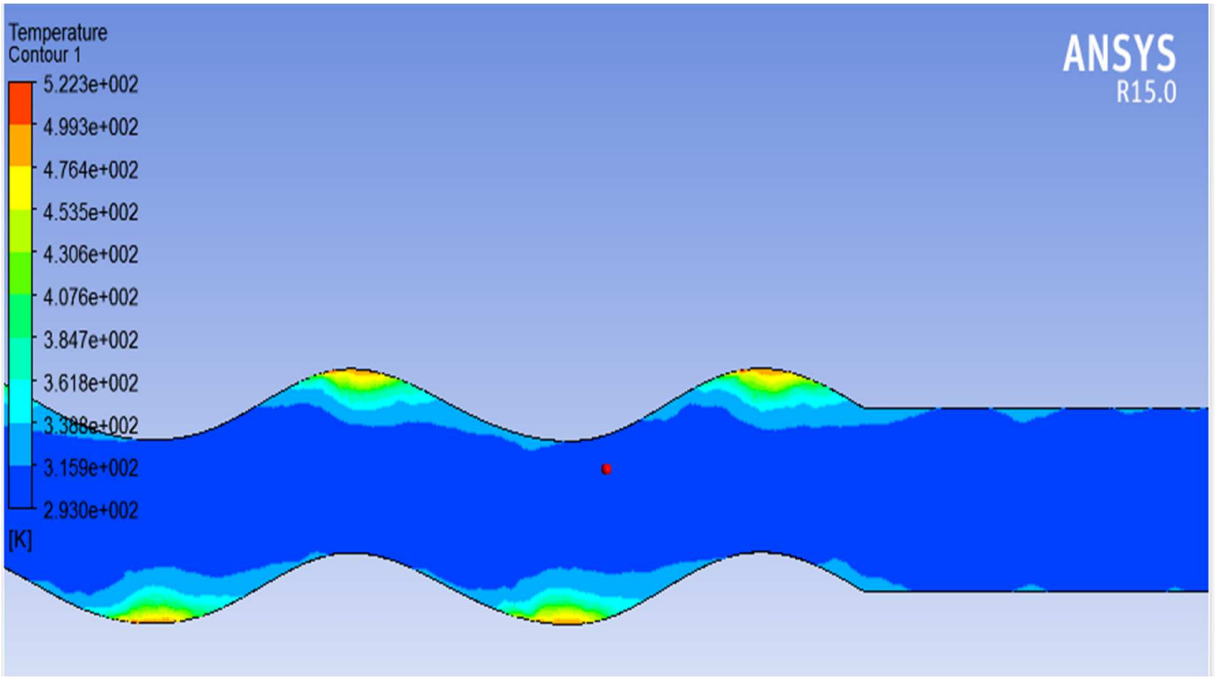

Figure 7.2: Temperature contour at the outlet of channel at Re=400

.

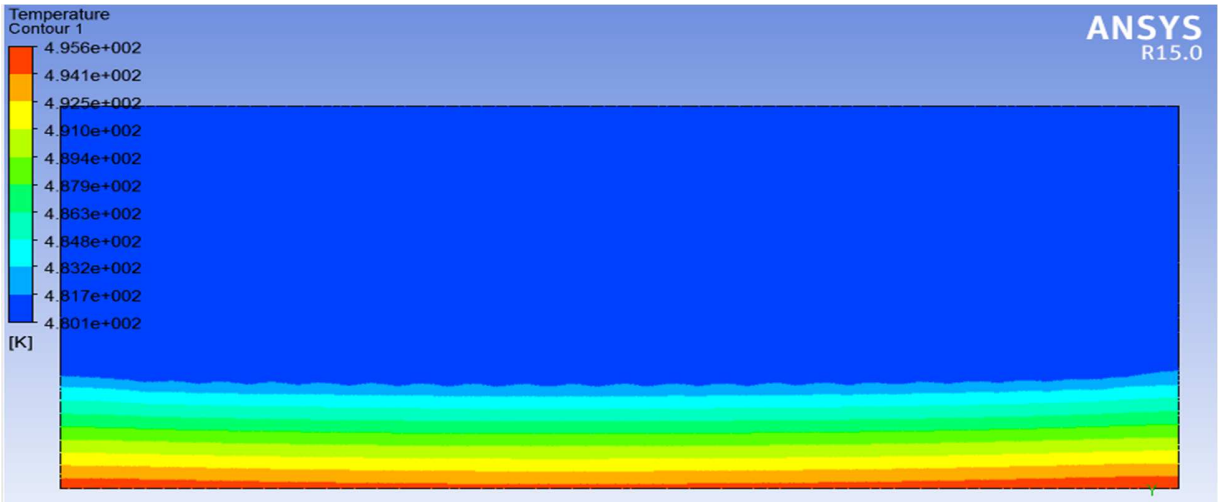

Figure 7.3: Temperature variation along the wall at Re=400

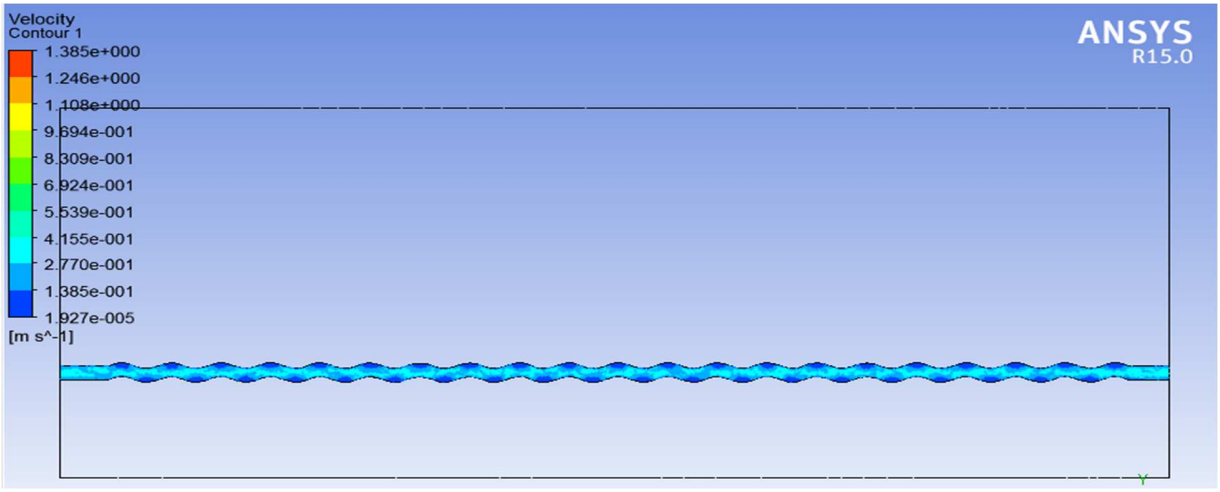

Figure 7.4: velocity contour along wavy channel at Re=400.

In the figures 7.1 to 7.4, the contours for temperature in a wavy edge rectangular channel for Reynolds number value equal to 400 are shown.

- In figure 7.2 temperature at the outlet of the channel is found to be 392 K.
- In figure 7.3 maximum wall temperature is at the bottom wall of the heat sink and is found to be 592 K and further the wall temperature increases in the direction of flow.

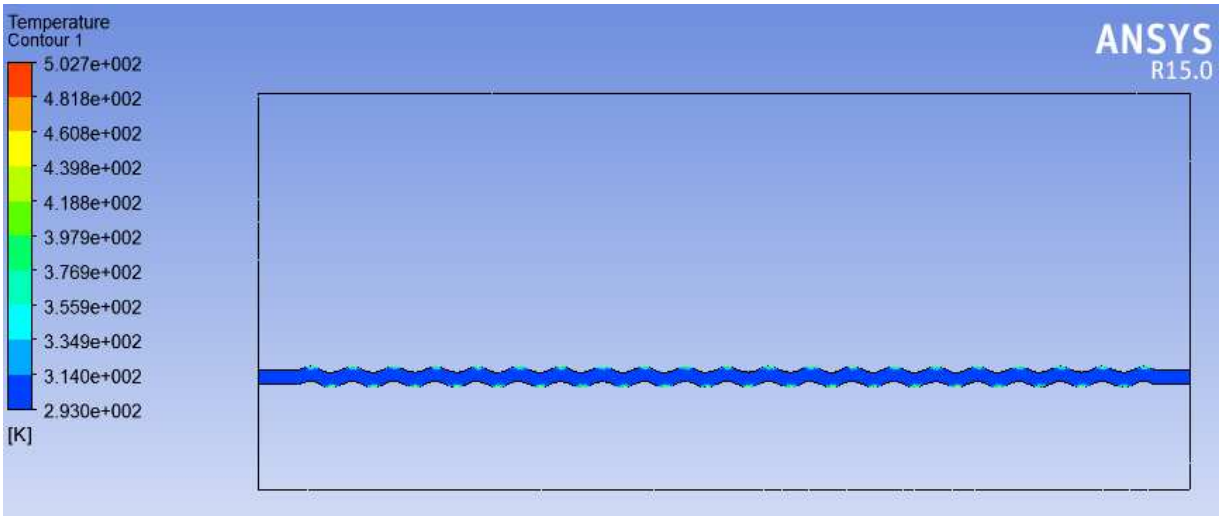

Figure 7.5: Temperature contour along wavy channel at Re=600

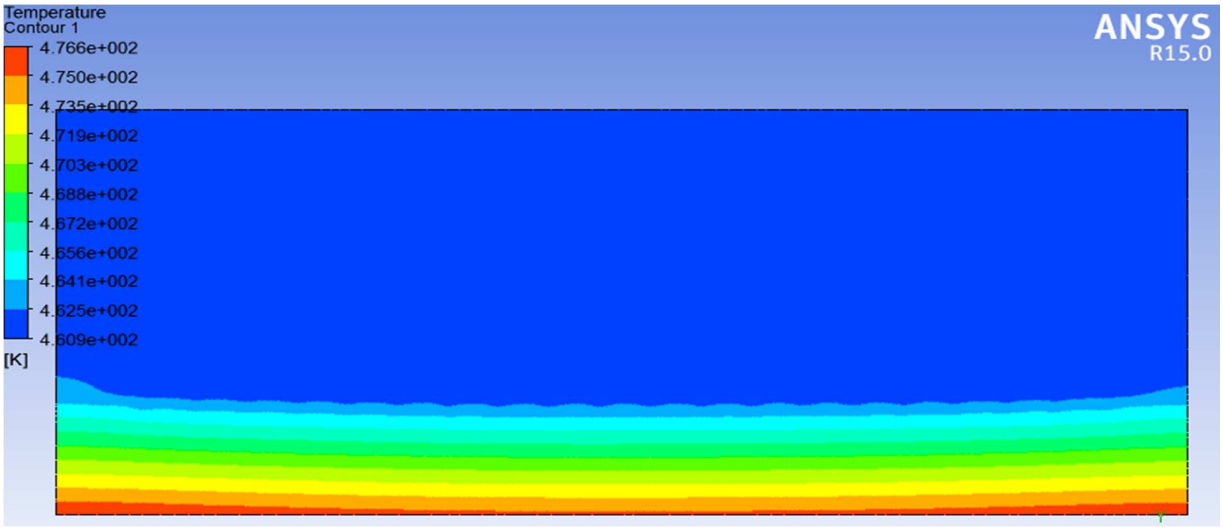

Figure 7.6: Temperature variation along the wall at Re=600

In the figures 7.5 to 7.6, the contours for temperature in a wavy edge rectangular channel for Reynolds number value equal to 600 are shown.

- In figure 7.5 temperature at the outlet of the channel is found to be 379 K.
- In figure 7.6 maximum wall temperature is at the bottom wall of the heat sink and is found to be 502 K and further the wall temperature increases in the direction of flow

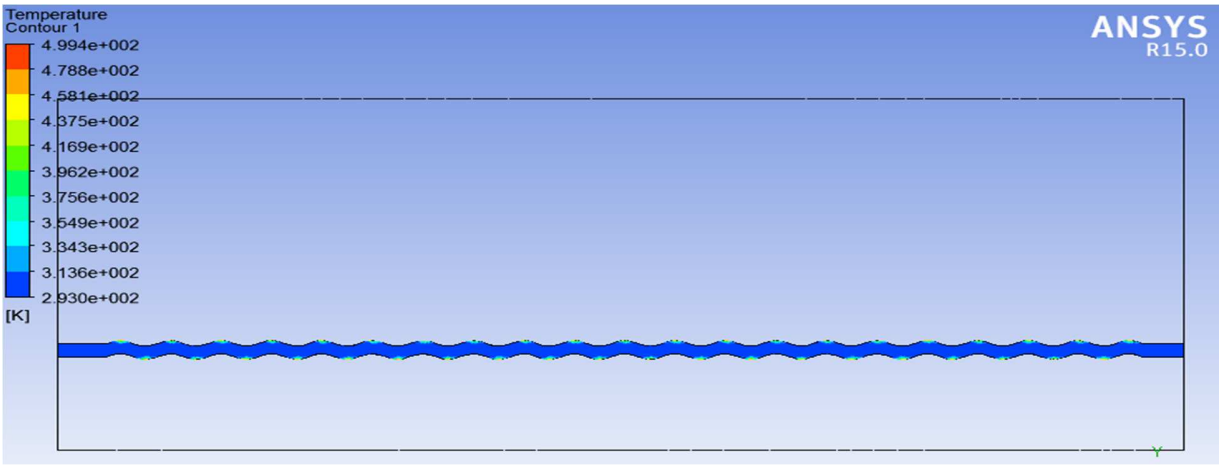

Figure 7.7: Temperature contour along wavy channel at Re=800

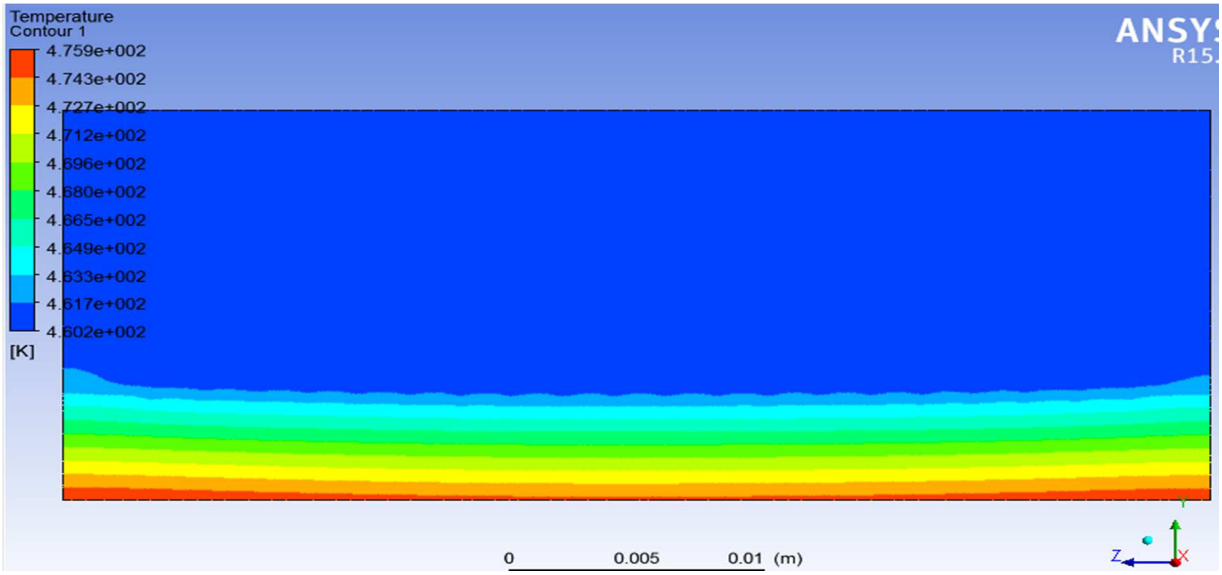

Figure 7.8: Temperature variation along the wall at Re=800

In the figures 7.7 to 7.8, the contours for temperature in a wavy edge rectangular channel for Reynolds number value equal to 800 are shown.

- In figure 7.7 temperature at the outlet of the channel is found to be 377 K.
- In figure 7.8 maximum wall temperature is at the bottom wall of the heat sink and is found to be 499 K and further the wall temperature increases in the direction of flow

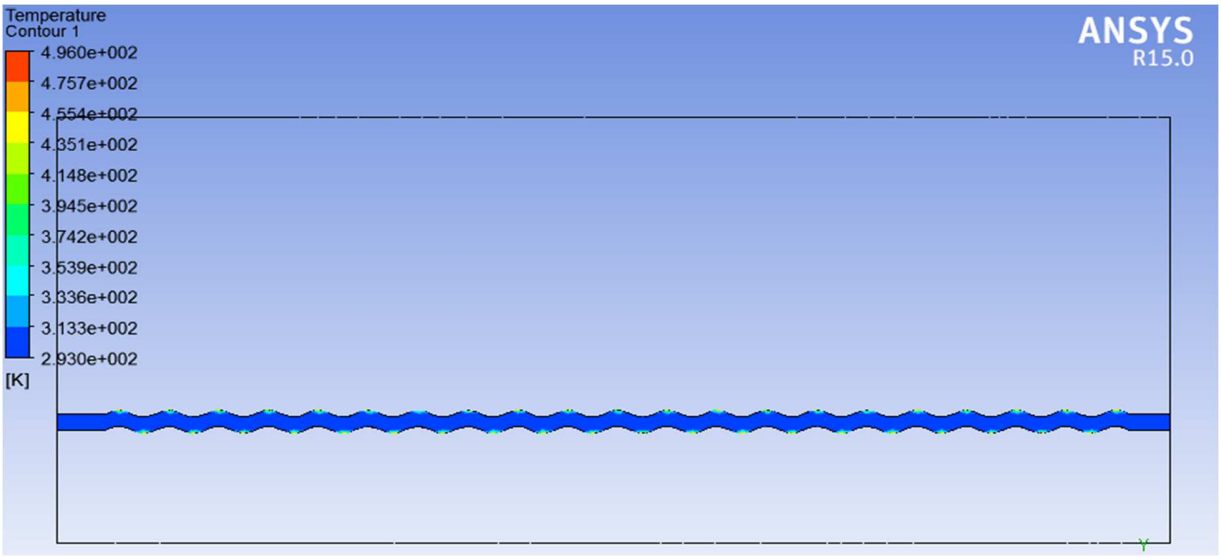

Figure 7.9: Temperature contour along wavy channel at Re=1000

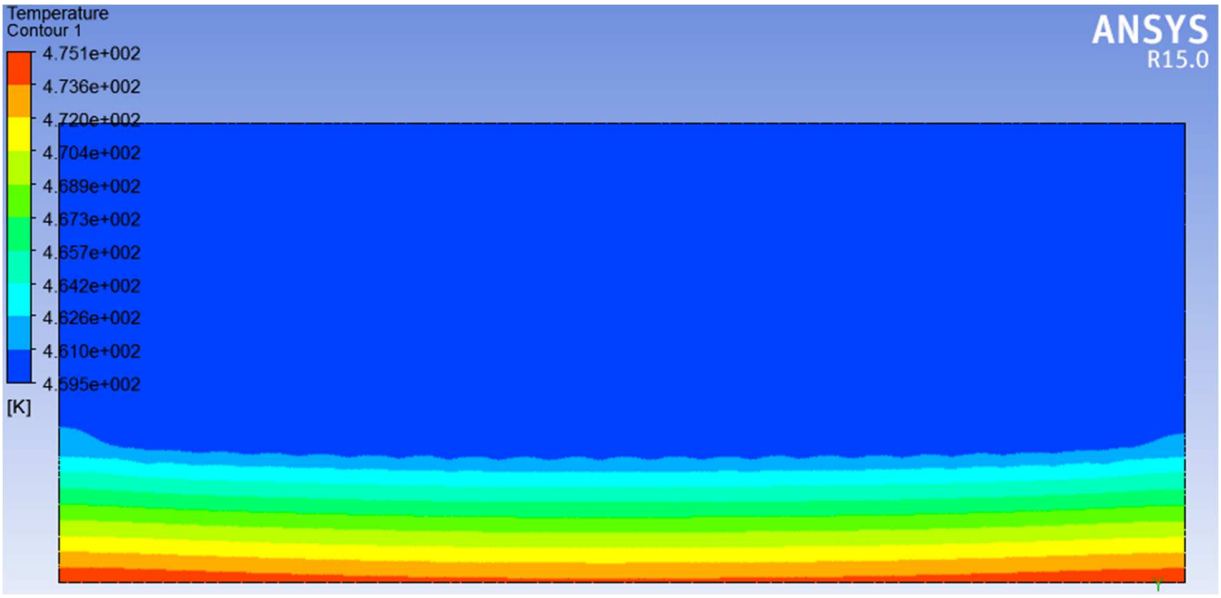

Figure 7.10: Temperature variation along the wall at Re=1000

In the figures 7.9 to 7.10, the contours for temperature in a wavy edge rectangular channel for Reynolds number value equal to 1000 are shown.

- In figure 7.9 temperature at the outlet of the channel is found to be 373 K.
- In figure 7.10 maximum wall temperature is at the bottom wall of the heat sink and is found to be 495 K and further the wall temperature increases in the direction of flow

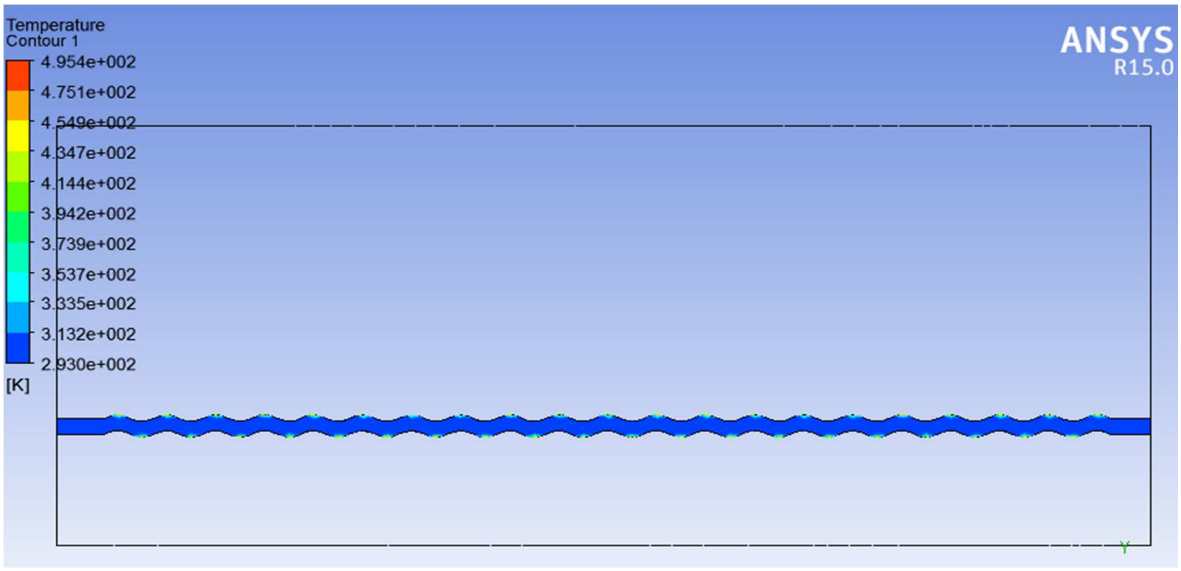

Figure 7.11: Temperature contour along wavy channel at Re=1200

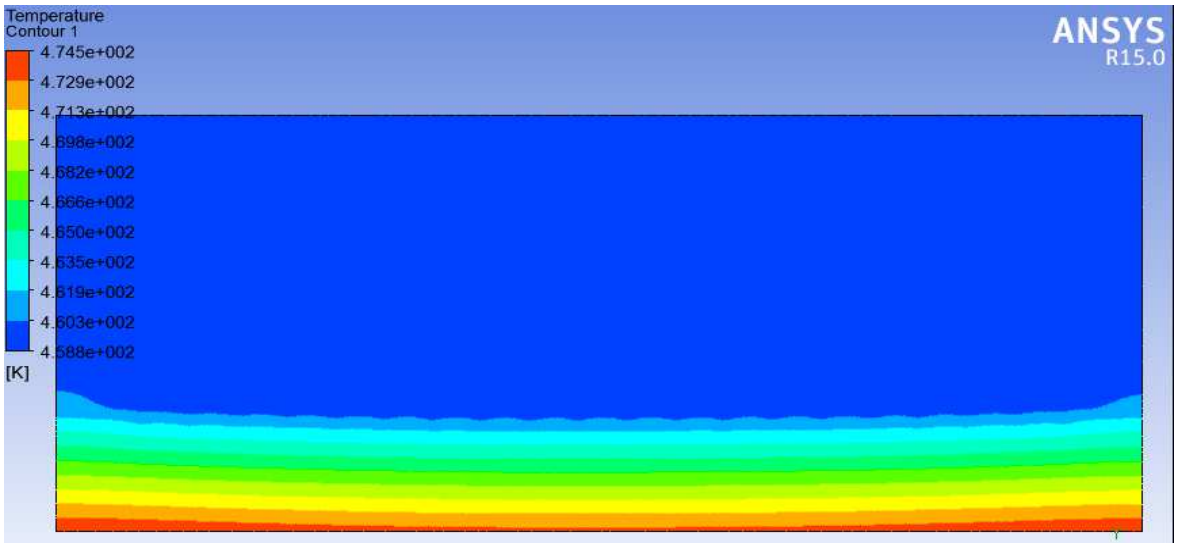

Figure 7.12: Temperature variation along the wall at Re=1200

In the figures 7.11 to 7.12, the contours for temperature in a wavy edge rectangular channel for Reynolds number value equal to 1200 are shown.

- In figure 7.11 temperature at the outlet of the channel is found to be 370 K.
- In figure 7.12 maximum wall temperature is at the bottom wall of the heat sink and is found to be 493 K and further the wall temperature increases in the direction of flow

Results for heat flux of 200 W/cm^2 and different sets of Reynolds number-

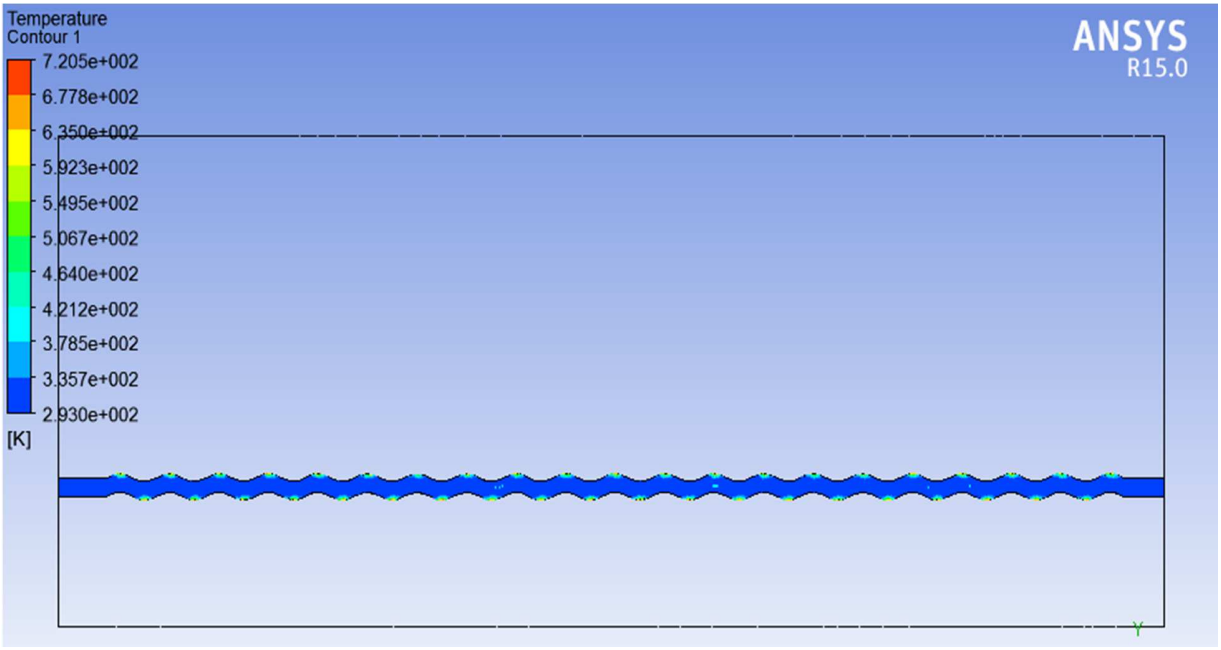

Figure 7.13: Temperature contour along wavy channel at Re=400

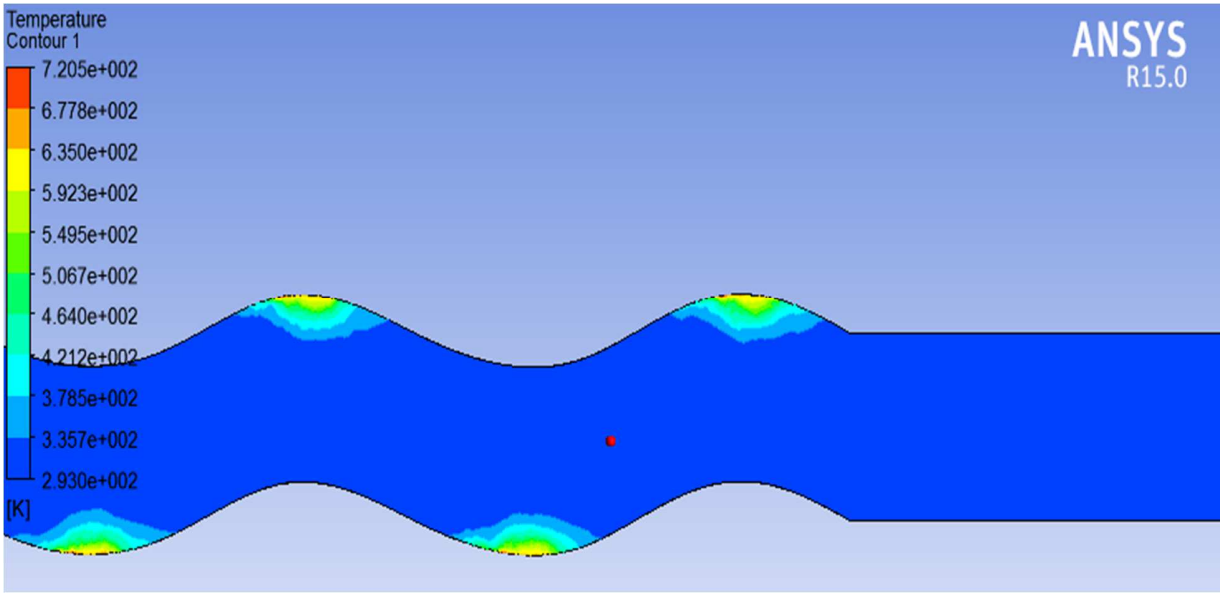

Figure 7.14: Temperature contour closer to outlet of wavy channel at Re=400

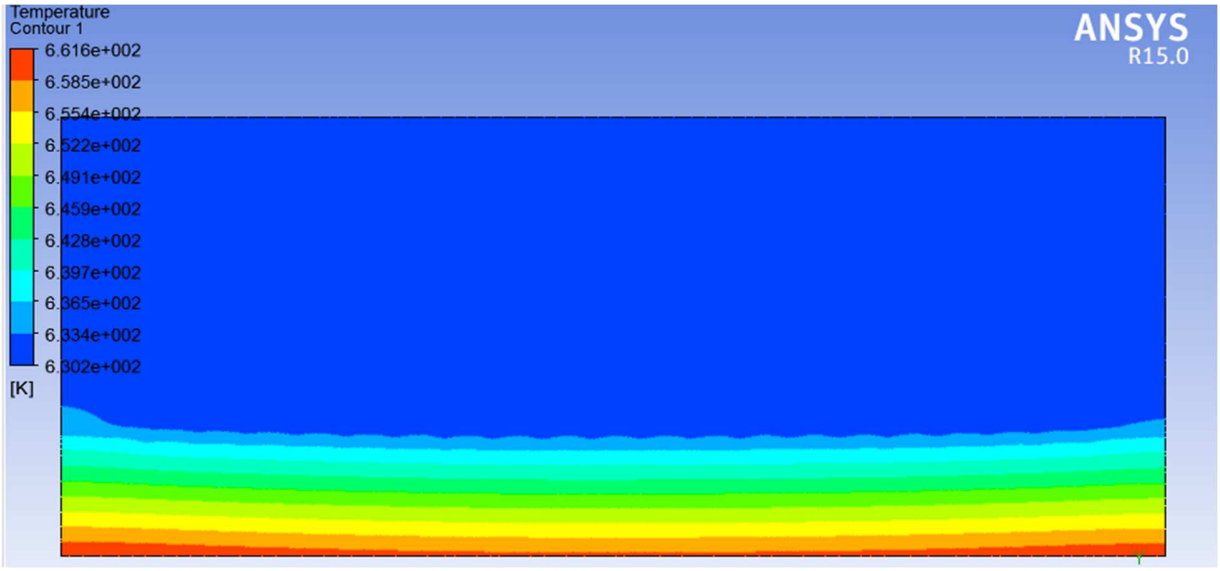

Figure 7.15: Temperature variation along the wall at Re=400

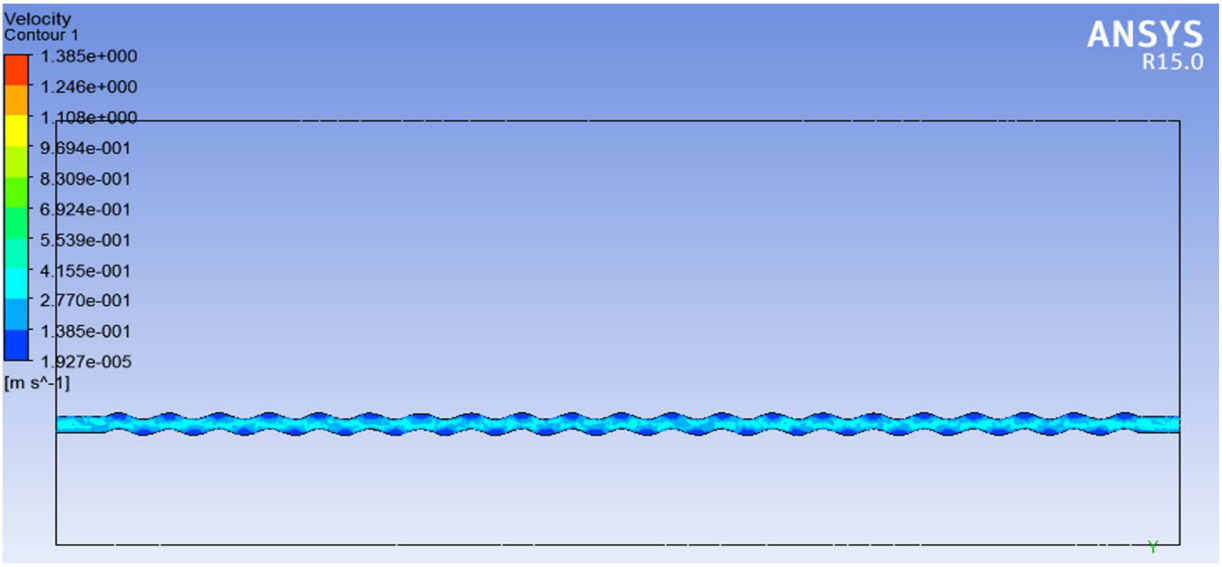

Figure 7.16: velocity contour along wavy channel at Re=400.

In the figures 7.13 to 7.16, the contours for temperature in a wavy edge rectangular channel for Reynolds number value equal to 400 are shown.

- In figure 7.13 temperature at the outlet of the channel is found to be 467 K.
- In figure 7.15 maximum wall temperature is at the bottom wall of the heat sink and is found to be 720 K and further the wall temperature increases in the direction of flow

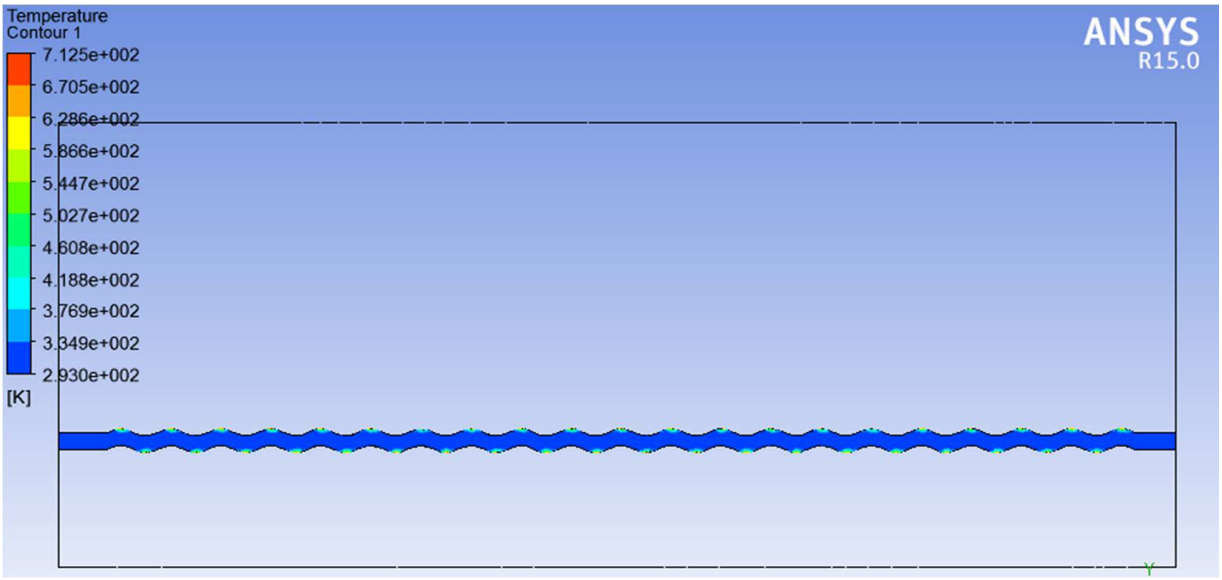

Figure 7.17: Temperature contour along wavy channel at Re=600

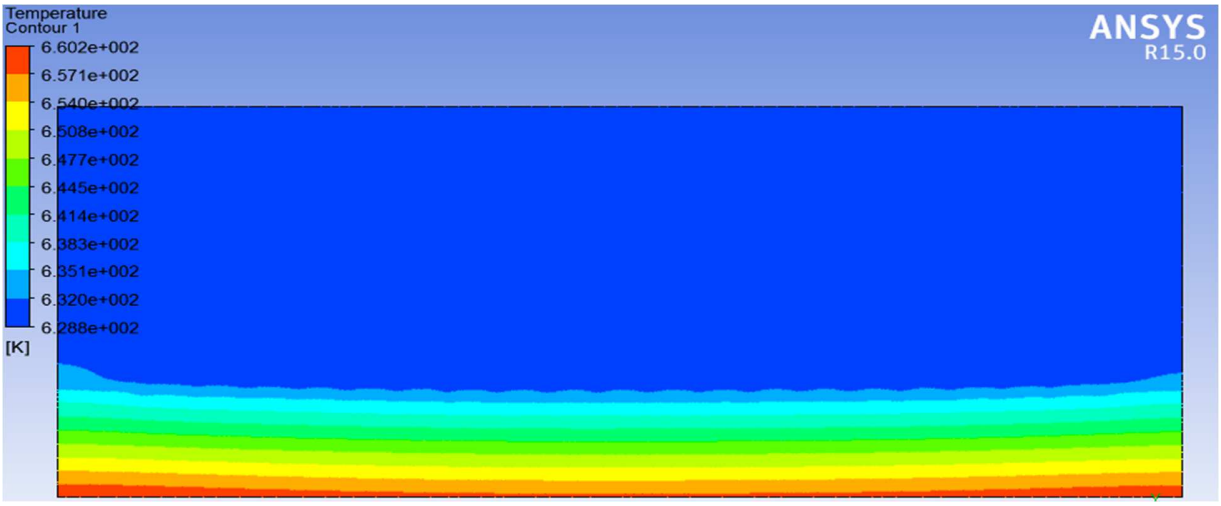

Figure 7.18: Temperature variation along the wall at Re=600

In the figures 7.17 to 7.18, the contours for temperature in a wavy edge rectangular channel for Reynolds number value equal to 600 are shown.

- In figure 7.17 temperature at the outlet of the channel is found to be 466.5 K.
- In figure 7.18 maximum wall temperature is at the bottom wall of the heat sink and is found to be 712 K and further the wall temperature increases in the direction of flow

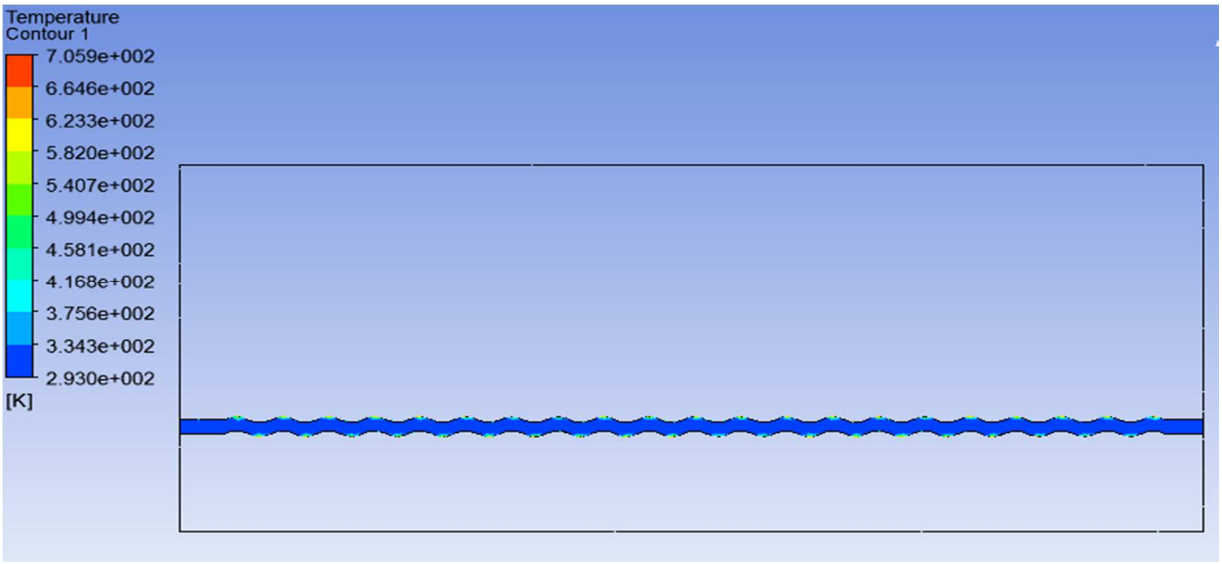

Figure 7.19: Temperature contour along wavy channel at Re=800

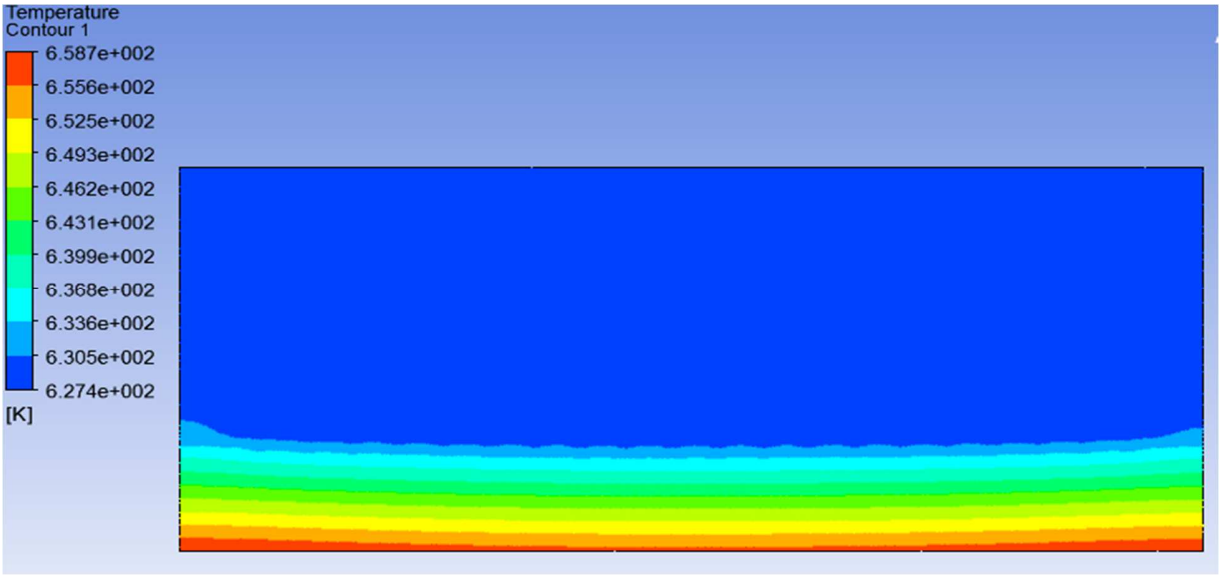

Figure 7.20: Temperature variation along the wall at Re=800

In the figures 7.19 to 7.20, the contours for temperature in a wavy edge rectangular channel for Reynolds number value equal to 800 are shown.

- In figure 7.19 temperature at the outlet of the channel is found to be 466 K.
- In figure 7.20 maximum wall temperature is at the bottom wall of the heat sink and is found to be 705 K and further the wall temperature increases in the direction of flow

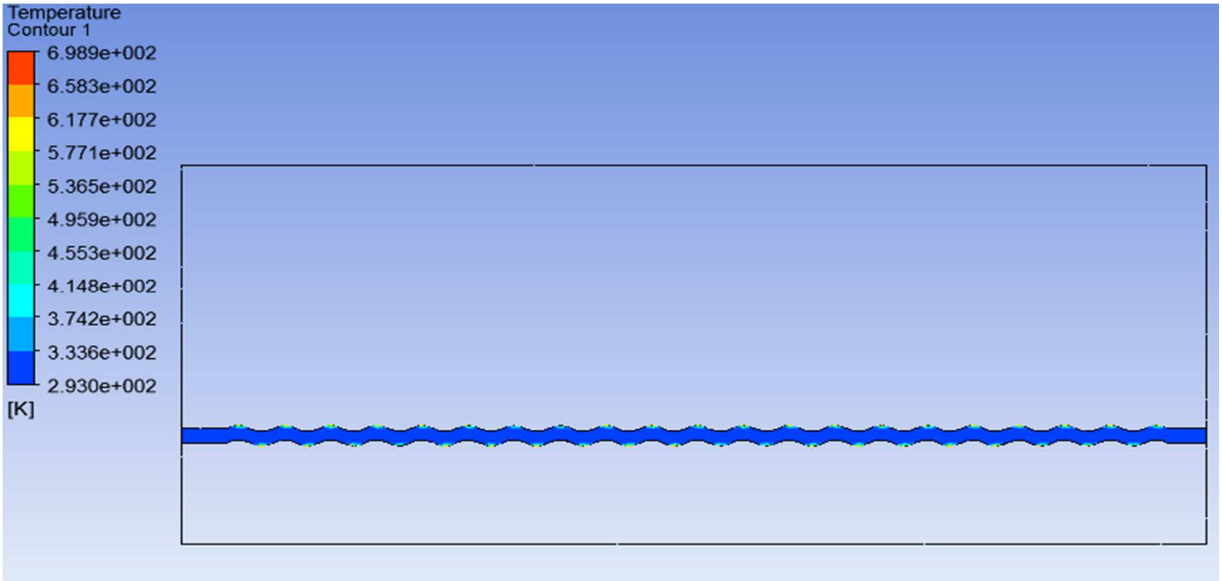

Figure 7.21: Temperature contour along wavy channel at Re=1000

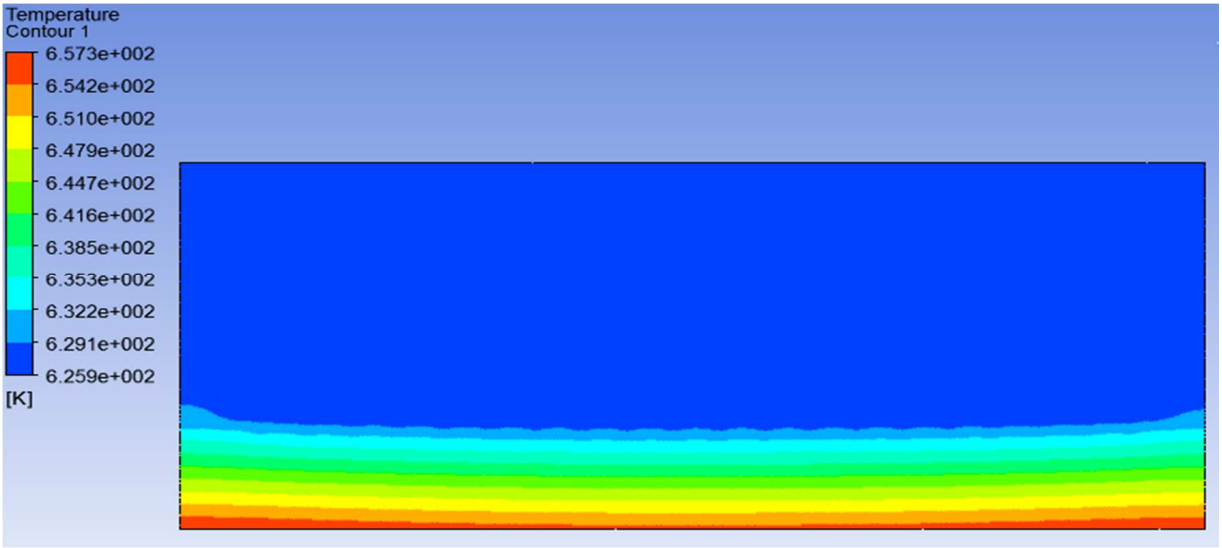

Figure 7.22: Temperature variation along the wall at Re=1000

In the figures 7.21 to 7.22, the contours for temperature in a wavy edge rectangular channel for Reynolds number value equal to 1000 are shown.

- In figure 7.21 temperature at the outlet of the channel is found to be 465.5 K.
- In figure 7.22 maximum wall temperature is at the bottom wall of the heat sink and is found to be 698 K and further the wall temperature increases in the direction of flow

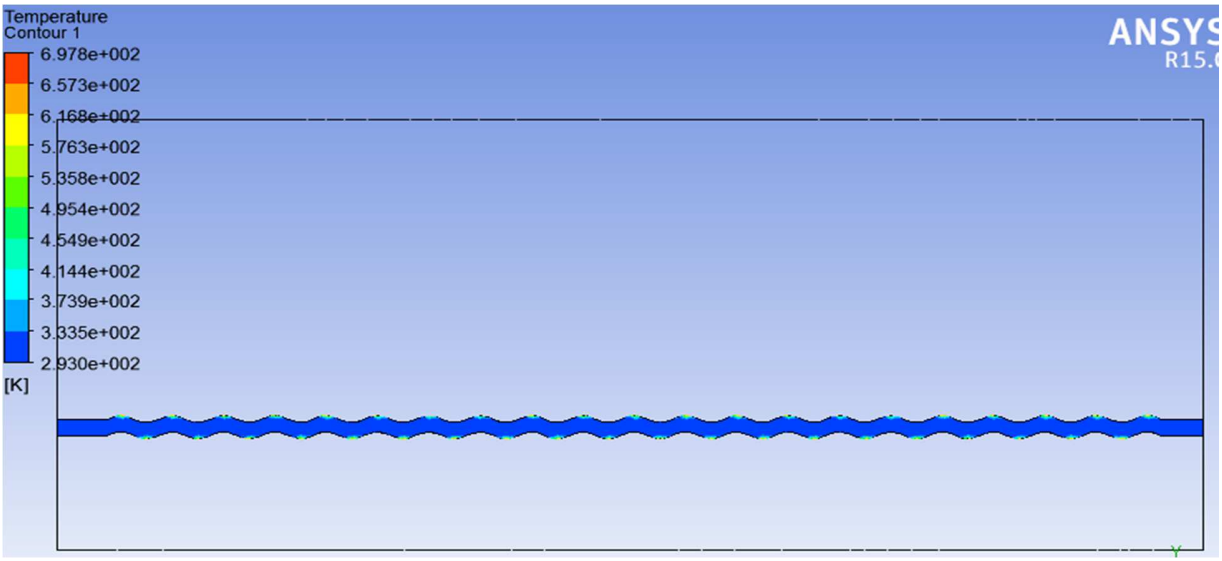

Figure 7.23: Temperature contour along wavy channel at Re=1200

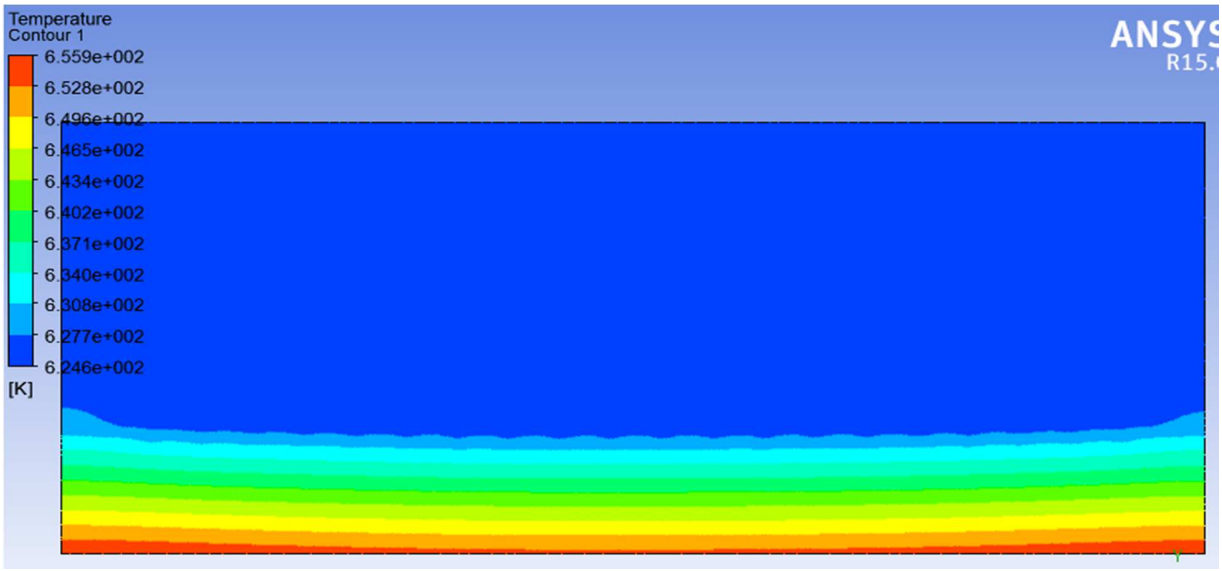

Figure 7.24: Temperature variation along the wall at Re=1200

In the figures 7.23 to 7.24, the contours for temperature in a wavy edge rectangular channel for Reynolds number value equal to 1200 are shown.

- In figure 7.23 temperature at the outlet of the channel is found to be 465 K.
- In figure 7.24 maximum wall temperature is at the bottom wall of the heat sink and is found to be 697 K and further the wall temperature increases in the direction of flow

The computational temperature rise taken from the temperature contours generated for different sets of Reynolds number for 100W/cm^2 bottom wall heat flux are taken from figures 7.1, 7.5, 7.7, 7.9, and 7.11 respectively.

Table 7.2: Temperature rise for different Reynolds number for heat flux=100W/cm^2

Reynolds number	Computational temperature rise(°C)
400	25
600	18
800	16
1000	14
1200	11

The computational temperature rise taken from the temperature contours generated for different sets of Reynolds number for 200W/cm^2 bottom wall heat flux are taken from figures 7.13, 7.17, 7.19, 7.21 and 7.23 respectively.

Table 7.3: Temperature rise for different Reynolds number for heat flux =200W/cm^2

Reynolds number	Computational temperature rise (°C)
400	49
600	39
800	31
1000	26
1200	21

7.2 Graphical result

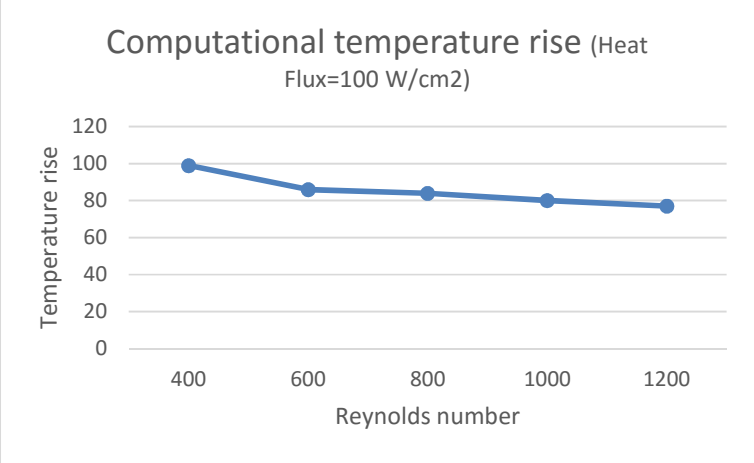

Figure 7.25: Temperature rise vs Reynolds number

Figure 7.25 shows the computational temperature rise results for varying sets of Reynolds number for heat flux =100W/cm^2

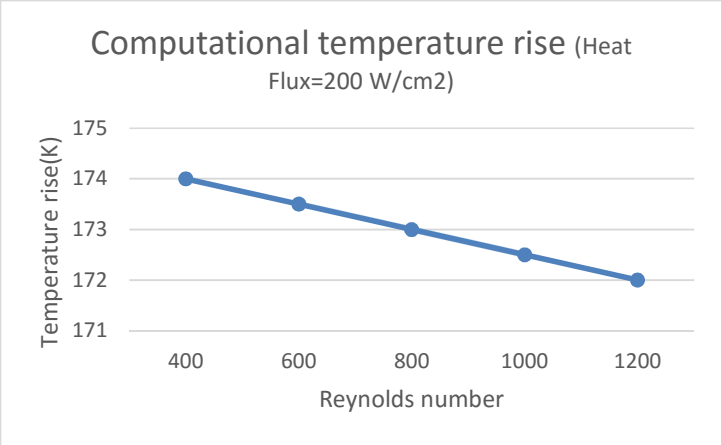

Figure 7.26: Temperature rise vs Reynolds number

Figure 7.26 shows the computational temperature rise results for varying sets of Reynolds number for heat flux =200 W/cm^2

7.3 Comparison of simulation results for temperature rise for problem 2 problem 3

Table 7.4: Temperature rise for different Reynolds number for heat flux=100W/cm^2

Reynolds number	Temperature rise(°C) (water)	Temperature rise(°C) (PF5052)
400	33	99
600	25	86
800	21	84
1000	18	80
1200	17	77

Table 7.5: Temperature rise for different Reynolds number for heat flux=200 W/cm^2

Reynolds number	Temperature rise(°C) (water)	Temperature rise(°C) (PF5052)
400	68	174
600	51	173.5
800	43	173
1000	38	172.5
1200	35	172

7.4 Graphical result

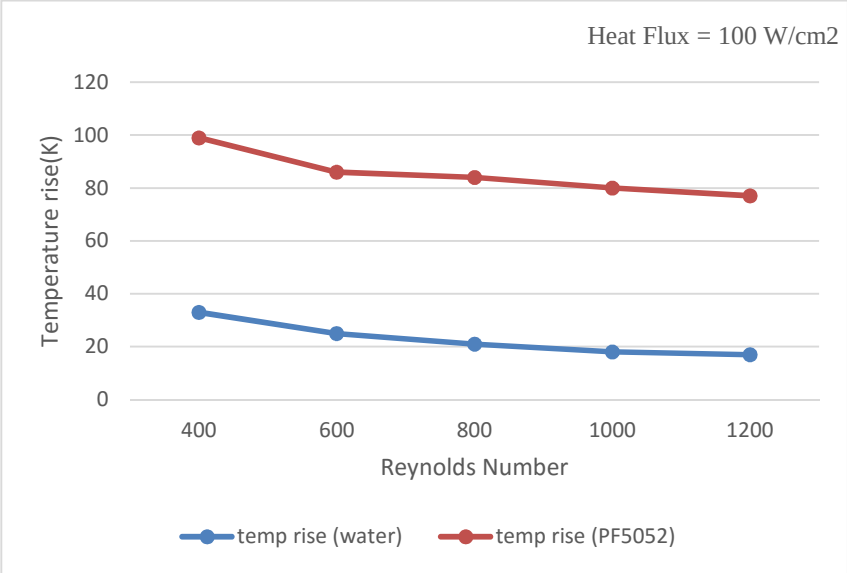

Figure 7.27: Temperature rise vs Reynolds number

In the figure 7.27, comparison of computational temperature rise for the two cases has been shown for the heat flux = 100 W/cm^2 and it clear that temperature rise for the performance fluid is far superior than the water.

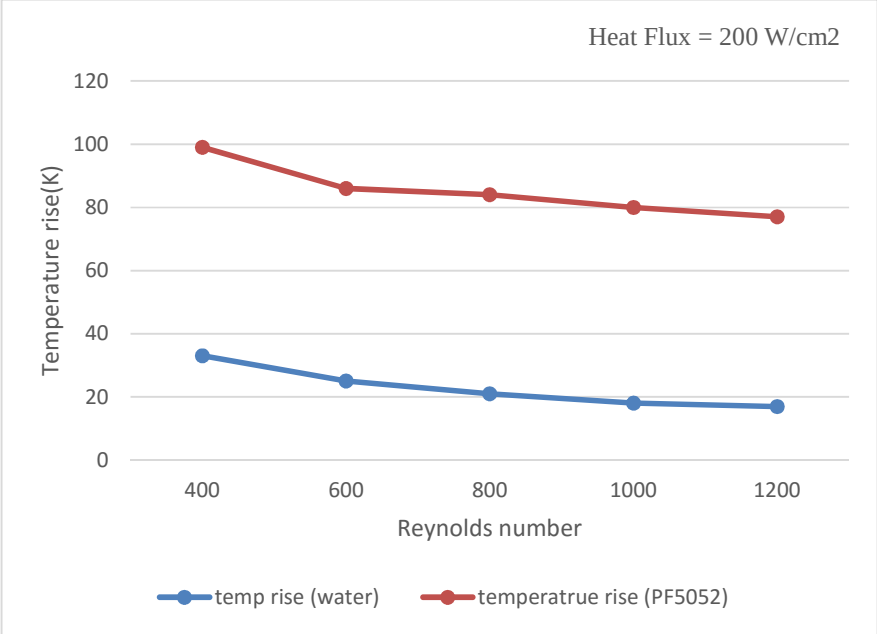

Figure 7.28: Temperature rise vs Reynolds number

In the figure 7.28, comparison of computational temperature rise for the two cases has been shown for the heat flux = 200 W/cm^2 and it clear that temperature rise for the performance fluid is far superior than the water.

CHAPTER 8

CONCLUSION

8.1 Conclusion

Based on the numerical study on both straight and wavy edge type micro-channel with hemispherical obstructions along with problem 2, problem 3, the following conclusions can be made-

- Water temperature rise is more at the outlet of wavy edge type of micro-channels with hemispherical obstructions in comparison to straight micro-channels for same values of Reynolds number and heat flux.
- From the above results both for straight rectangular micro-channel and wavy edge type micro-channel the thermal performance of wavy edge micro-channel is found to be better in comparison to that of straight micro-channel of same hydraulic diameter.
- With the inclusion of hemispherical obstructions in wavy channel, surface area as well as contact time of fluid with heated surface increases due to which thermal resistance decreases which ultimately increases the heat transfer. As a result, we get the higher temperature rise of the fluid.
- Pressure drop is found to be more in wavy edge micro-channels in comparison to that of straight micro-channels, however the loss in pressure is compensated by the better heat transfer characteristics of the wavy micro-channel.
- Velocity of water decreases along the flow direction in wavy micro-channels due to loss in energy of fluid while travelling along wavy channel with hemispherical obstructions.
- As the value of heat flux in wavy type of channel is increased from 100W/cm^2 to 200W/cm^2 there is an increase in the outlet temperature of water, however the pressure drop along the channel decreases. But the difference in pressure drop is very less.
- Temperature rise for performance fluid PF 5052 as compared with water in a wavy microchannel with hemispherical obstructions is quite superior.

8.2 Future scope

- Analysis of rectangular and wavy microchannel with different geometrical shaped obstructions.
- Analysis of Rectangular and wavy microchannel with different performance fluids.
- Analysis of trapezoidal cross-section microchannel with water.
- Analysis of rectangular and wavy microchannel with nano fluids.
- Analysis of rectangular and wavy microchannel with refrigerants.

References

[1] I. Mudawar, W. Qu, Analysis of three dimensional heat transfer in micro-channels, Int. J. Heat and Mass Transfer 45 (2002) 3973-3985.

[2] G.M. Mala, D. Li, J.D. Dale, Heat transfer and fluid flow in micro-channels, International Journal of Heat and Mass Transfer 40 (1997) 3079-3088.

[3] L.T. Yeh, Review of heat transfer technologies in electronic equipment, ASME J. Electron. Packag. 117 (1995) 333–339.

[4] D.B. Tuckerman, R.F.W. Pease, High-performance heat sinking for VLSI, IEEE Electron. Dev. Lett. EDL-2 (1981) 126–129.

[5] I. Mudawar, M.B. Bowers, Ultra-high critical heat flux (CHF) for subcooled water flow boiling —I: CHF data and parametric effects for small diameter tubes, Int. J. Heat Mass Transfer 42 (1999) 1405–1428.

[6] I. Mudawar, W. Qu, Experimental and numerical study of pressure drop and heat transfer in a single-phase micro-channel heat sink, Int. J. Heat and Mass Transfer 45(2002) 2549-2565.

[7] K. Kawano, K. Minakami, H. Iwasaki, M. Ishizuka, Micro channel heat exchanger for cooling electrical equipment, Application of Heat Transfer in Equipment, Systems and Education, ASME HTD-361-3/PID-3, 1998, pp. 173–180.

[8] A. Bejan, A.M. Morega, Optimal arrays of pin fins and plate fins in laminar forced convection, ASME J. Heat Transfer 115 (1993) 75–81.

[9] A.G. Fedorov, R. Viskanta, Three-dimensional conjugate heat transfer in the microchannel heat sink for electronic packaging, Int. J. Heat Mass Transfer 43 (2000) 399–415.

[10] X.F. Peng, G.P. Peterson, Convective heat transfer and flow friction for water flow in microchannel structures, Int. J. Heat Mass Transfer 39 (1996) 2599–2608.

[11] K.K. Ambatipudi, M.M. Rahman, Analysis of conjugate heat transfer in microchannel heat sinks Numer. Heat Transfer A, 37 (2000), pp. 711–731.

[12] Y. Sui, C.J. Teo, P.S. Lee, Y.T. Chew, C. Shu, Fluid flow and heat transfer in wavy micro-channels Int. J. Heat Mass Transfer, 53 (2010), pp. 2760–2772.

[13] P. Gunnasegaran, H.A. Mohammed, N.H. Shuaib, R. Saidur, The effect of geometrical parameters on heat transfer characteristics of micro-channels heat sink with different shapes Int. Commun. Heat Mass Transfer, 37 (8) (2010), pp. 1078–1086

[14] E. Utriainen, B. Sunden, Numerical analysis of primary surface trapezoidal cross wavy duct Int. J. Numer. Method Heat Fluid Flow, 10 (6) (2000), pp. 634–648.

[15] S. Kandlikar, S. Garimella, D. Li, S. Colin, M.R. King, Heat Transfer and Fluid Flow in Minichannels and Microchannels, Elsevier, USA, 2005.

[16] E. Utriainen, B. Sunden, Numerical analysis of primary surface trapezoidal cross wavy duct, Int. J. Numer. Method Heat Fluid Flow 10 (6) (2000) 634–648.

[17] W. Yang, J. Zhang, H. Cheng, The study of flow characteristics of curved microchannel, Appl. Therm. Eng. 25 (2010) 1894–1907.

[18] R.K. Shah, A.L. London, Laminar Flow Forced Convection in Ducts, Academic Press, New York, 1978.

[19] S.G. Kandlikar, W.J. Grande, Evaluation of single phase flow in microchannels for high heat flux chip cooling – thermohydraulic performance enhancement and fabrication technology, Heat Transfer Eng. 25 (8) (2004) 5–16.

[20] S.V. Garimella, C.B. Sobhan, Transport in microchannels – a critical review, Annu. Rev. Heat Transfer 13 (2003) 1–50.

[21] S.V. Patankar, Numerical Heat Transfer and Fluid Flow, Hemisphere, New York, 1980.

[22] J.D. Anderson, Computational Fluid Dynamic: The Basics with Applications, McGraw-Hill, New York, 1995.

[23] Lee, Yong Jiun, Pawan K. Singh, and Poh Seng Lee. "Fluid flow and heat transfer investigations on enhanced microchannel heat sink using oblique fins with parametric study." International Journal of Heat and Mass Transfer 81 (2015): 325-336.

[24] Halelfadl, Salma, Ahmed Mohammed Adham, Normah Mohd-Ghazali, Thierry Maré, Patrice Estellé, and Robiah Ahmad. "Optimization of thermal performances and pressure drop of rectangular microchannel heat sink using aqueous carbon nanotubes based nanofluid." Applied Thermal Engineering 62, no. 2 (2014): 492-499.

[25] Peyghambarzadeh, S. M., S. H. Hashemabadi, A. R. Chabi, and M. Salimi. "Performance of water based CuO and Al2O3 nanofluids in a Cu–Be alloy heat sink with rectangular microchannels." Energy Conversion and Management 86 (2014): 28-38.

[26] Rahimi-Gorji, M., O. Pourmehran, M. Hatami, and D. D. Ganji. "Statistical optimization of microchannel heat sink (MCHS) geometry cooled by different nanofluids using RSM analysis." The European Physical Journal Plus 130, no. 2 (2015): 1-21.

[27] Ebrahimi, Amin, Ehsan Roohi, and Saeid Kheradmand. "Numerical study of liquid flow and heat transfer in rectangular microchannel with longitudinal vortex generators." Applied Thermal Engineering 78 (2015): 576-583.

[28] Chai, Lei, Guo Dong Xia, and Hua Sheng Wang. "Numerical study of laminar flow and heat transfer in microchannel heat sink with offset ribs on sidewalls." Applied Thermal Engineering 92 (2016): 32-41.

[29] Jiang, Pei-Xue, Ming-Hong Fan, Guang-Shu Si, and Ze-Pei Ren. "Thermal–hydraulic performance of small scale micro-channel and porous-media heat-exchangers." International Journal of Heat and Mass Transfer 44, no. 5 (2001): 1039-1051.

[30] Husain, Afzal, and Kwang-Yong Kim. "Thermal optimization of a microchannel heat sink with trapezoidal cross section." Journal of Electronic Packaging 131, no. 2 (2009): 021005.